Investigation of Ultrasonic Neuro-stimulation Effects in Peripheral Axons

Christopher John Wright

A dissertation submitted in partial fulfillment
of the requirements for the degree of
Doctor of Philosophy
of
University College London.

Department of Mechanical Engineering
University College London

July 9, 2016

I, Christopher John Wright, confirm that the work presented in this thesis is my own. Where information has been derived from other sources, I confirm that this has been indicated in the work.

Abstract

Appreciation for the medical and research potential of ultrasound neuromodulation is growing rapidly, with potential applications in non-invasive treatment of neurodegenerative disease and functional brain mapping spurring recent progress. A full understanding of the mechanical interaction of sound waves and neural tissue could allow tailor-made stimuli to produce different effects or specifically stimulate separate tissue types, adding great value to an already promising technique. Despite this worthy goal, little progress has been made in our understanding of the nature of the ultrasound-tissue interaction. The current study forms part of a long term goal to tackle this issue by isolating and characterising the effects of, and sensitivity to ultrasound for all the different structures found in nervous tissue. A simple, well characterised model of nervous transmission is therefore used along with a tightly controlled acoustic environment so that the characteristics of direct US stimulation effects can be investigated. Experiments are performed that demonstrate the capability of ultrasound to directly stimulate unmyelinted peripheral axons, characterise the stimulus response dynamics and determine the responsible ultrasonic force mechanism. A Passive Cavitation Detector (PCD), unimpeded ultrasound path and wavelet acoustic analysis techniques are used to detect different modes of cavitation with high sensitivity which are then tested for correlation to nerve responses. In the present case, direct ultrasound stimulation of peripheral axonal tissue is found to require either stable or inertial cavitation. The lowest intensity at which stimulation is observed is 25 W/cm^2, similar to previous neuromodulatory thresholds found in peripheral nerves. This study therefore represents a significant advance in our understanding of the mechanisms behind the ultrasound neurostimulation phenomenon.

Acknowledgements

I would like to thank all those who made this PhD project possible and to those that helped me out in the lab. Thanks to Professor Martin Koltzenburg for use of his lab space and stimulation and recording equipment, to Professors Hugh Bostock and David Holder for advice and guidence through the project. Thanks to Peter Kelly and the whole MEng workshop for discussions about the mechanical aspects of my designs, as well as manufacturing my equipment so well. Thanks to Dr. James Phillips and his research team for colaborating on the cell construct work. Finally, thanks to my supervisors Professors Nader Saffari and John Rothwell for making this project possible and constant guidance throughout.

Contents

List of Figures

List of Tables

Acronyms

AFM Atomic Force Microscopy.

AP Action Potential.

BOLD Blood Oxygen Level Dependant.

CAP Compound Action Potential.

CNS Central Nervous System.

CW Continuous Wave.

dB Decibels.

DC Duty Cycle.

DCS Decompression Sickness.

FFP Fixed Focal Point.

FFT Fast Fourier Transform.

FWHM Full Width Half Maximum.

HIFU High Intensity Focused Ultrasound.

ICD Inertial Cavitation Dose.

KZK Khokhlov-Zabolotskaya-Kuznetzov.

MFP Moving Focal Point.

MI Mechanical Index.

MS Mechanosensitive.

PCD Passive Cavitation Detector.

PNS Peripheral Nervous System.

PRF Pulse Repetition Frequency.

RMS Root Mean Square.

SCD Stable Cavitation Dose.

SLS Selective Laser Sintering.

SNAP Sensory Nerve compound Action Potential.

STFT Short Time Fourier Transform.

TSD Total Stimulus Duration.

US Ultrasound.

VP Varying Permeability.

Glossary

ρ	Density.
α	Acoustic attenuation coefficient.
γ	Bubble surface tension.
σ	Standard deviation.
τ	Retarded time.
β	Nonlinearity Coefficient.
δ	Diffusivity of Sound.
ω	Ultrasound driving frequency.
κ	Heat capacity ratio.
ω_0	Resonant frequency of a bubble.
δ_{tot}	Total damping constant of bubble oscillation.
E	Young’s modulus.
F_{abs}	Radiation force due to the absorption of acoustic energy.
F_{bub}	Primary radiation force on a microbubble.
F_{ref}	Force on a surface due to reflection of acoustic energy.
H	Mean bubble curvature.
I_{SPPA}	The spatial peak, pulse average intensity.

I_{SPTA} The spatial peak, temporal average intensity.

I_{SPTP} The spatial peak, temporal peak intensity.

PD Maximum particle displacement.

P_0 Hydrostatic pressure.

P_a Ultrasonic pressure.

P_b Bubble Pressure.

P_{rad} Radiation Pressure.

P_v Vapour pressure.

R Pressure reflection coefficient.

R_0 Bubble radius.

Z Specific acoustic impedance.

c Speed of sound.

f Wave frequency.

r Radial dimension of the propagating ultrasound wave.

v Poisson's ratio.

y Frequency dependence coefficient.

z Axial coordinate.

Chapter 1

Introduction

This chapter will begin by giving the background knowledge of ultrasound mechanics and nerve structure necessary for an understanding of the subject. A brief introduction to the field and applications of neurostimulation will then be given, summarising the strengths and weaknesses of current techniques and thus outlining the niche that ultrasound neurostimulation can fill. An evaluation of the technique thus far will be provided followed by the motivation, aims and original contributions of the current work.

To understand the state of Ultrasound (US) neurostimulation literature and the introduction to the current study, a basic understanding of both US mechanics and the physiology of nervous tissue is recommended. The following sections 1.1 and 1.2 are intended to bring readers up to this basic level and should be skipped if not required.

1.1 Overview of Ultrasound

Ultrasound is a longitudinal pressure wave consisting of periods of compression and rarefaction in a fluid. Particle motion is parallel to the axis of wave propagation, not perpendicular. The frequency of this wave must be above 20 kHz, the upper limit of human hearing to be considered ultrasonic. Piezoceramic materials are most commonly used to generate US, transducing an oscillating electrical voltage to oscillating shape change which creates the pressure wave. These devices are known as US transducers.

1.1.1 Ultrasound Transducers

Single element piezoelectric bowl shaped transducers are the most prevalently used in the literature for US neuromodulation. High Intensity Focused Ultrasound (HIFU) transducers usually have a very tight bandwidth so that production of the desired frequency is efficient and specific, allowing them to be driven at high intensities. Although an in depth understanding of US generation is not required for interpreting this report, there are some transducer properties that will be useful to know:

- Resonant (or centre) frequency
  - The frequency at which transduction to ultrasound energy is most efficient. Also known as the fundamental or driving frequency.
- Efficiency
  - The particular transducer's efficiency of conversion from electrical to acoustic energy.
- Damping factor
  - The rate at which the oscillations of the piezoelectric material die down once the driving signal stops.
- Bandwidth
  - Defines the frequency range that can be produced by the transducer. This determines how far from the centre frequency the transducer can be driven, and the subsequent reduction in transduction efficiency.
- Focusing
  - All the transducers used in the current study are spherically focused to increase the amplitude of the acoustic field in a specific area known as the focal point or zone.

1.1.2 Acoustic Output Parameters

The ultrasound that a transducer outputs can have many different variants and parameters. The terms that will be used in this study to describe US stimulation protocols are listed and explained here:

- Pressure

  - Defined as the Force per unit area that the wave exerts on the medium, as a deviation from the ambient pressure, usually described by peak (instantaneous) pressure.
  - Root Mean Square (RMS) pressure is the mean of squares of the instantaneous values of the pressure waveform, square rooted.
  - The pressure variation of US can be measured by a hydrophone in water as opposed to intensity which is much more difficult to measure directly.

> Intensity

  - Defined as the acoustic energy per unit area normal to the direction of beam propagation at a particular instant. For measurement purposes the instantaneous intensity can be linked to pressure by the equation:

$$I_{SPTP} = \frac{{P_a}^2}{\rho c}, \tag{1.1}$$

where I_{SPTP} is the spatial peak, temporal peak intensity, P_a is instantaneous US pressure, ρ is the density of the medium and c is speed of sound in the medium. Since the instantaneous intensity does not give any information about how intensity varies over time, there are three commonly used measures of intensity for ultrasound pulses:

> Spatial Peak Temporal Average Intensity (I_{SPTA}).

  - The mean of the instantaneous intensity over a time period at the location of maximum intensity in the acoustic field. For the purposes of this study high intensity will be defined as anything above 720 mW/cm^2, which is the FDA limit for diagnostic imaging [of Ultrasound in Medicine Clinical Standards Committee, 2015]. This measure combined with the absorption/attenuation characteristics of a medium is most relevant to predicting heating for long exposure times.

> Spatial Peak Temporal Peak Intensity (I_{SPTP})

  - The greatest instantaneous intensity value reached both in space and time,

I_{SPTP} has a maximum limit for obstetric examination of 310 W/cm^2 [Preston et al., 1988].

- > Spatial Peak Pulse Average Intensity (I_{SPPA})
  - The same as the temporal average intensity but over just the pulse ”on” duration. I_{SPPA} has a maximum limit for obstetric examination of 190 W/cm^2 [Preston et al., 1988].

Though some of the above US intensities may seem high compared to other non-destructive medical exposures, most of the ultrasonic energy is efficiently transmitted through the tissue with very little energy being absorbed. Attenuation of US energy by tissues is dependent on their attenuation coefficient α (Equation 2.4) which is a combination of absorption, reflection and scattering effects. More mechanisms of US-tissue interaction will be discussed in section 2.3.

- > Pulsing
  - intermittent US generation is known as pulsing, as opposed to constant US which is known as Continuous Wave (CW).
  - Pulsing is often used to reduce total energy deposition and associated heating rates while maintaining mechanical effects.
  - Pulse length is the length of time of the pulse ”on phase”, producing a certain number of cycles of the fundamental frequency.
  - Pulse period is the time from the start of one pulse to the start of the next.
  - Pulse Repetition Frequency (PRF) is the inverse of the pulse period.
  - Duty Cycle (DC) gives the ratio of pulse ”on time” to pulse period.
- > Total Stimulus Duration (TSD)
  - Total length of time during which the stimulus protocol is applied.

1.1.3 Material Acoustic Properties

How the ultrasound wave interacts with the medium it is travelling through is dependant on the properties of that medium, these determine the combination of mechanical and thermal effects that are produced. The properties and concepts which are likely to be new to the reader are described below:

> Specific acoustic impedance

  - The ratio of driving force to particle velocity response of a specific medium. For a plane wave this ratio can be determined as a product of the density and speed of sound in a medium and is known as the characteristic acoustic impedance [Kinsler et al., 1982]. As speed of sound in any medium does not vary much, specific and characteristic acoustic impedance can be approximated as frequency independent.

> Attenuation coefficient

  - The rate at which ultrasound energy is dissipated within a transmission medium, summing the effects listed below. This is usually used for biological tissue or other complex media where the individual mechanisms are difficult to quantify. The attenuation coefficient is therefore experimentally determined for different tissues.
  - Scattering
    - ∗ If a complex medium such as soft tissue contains objects smaller than the ultrasound wavelength, the object will scatter the wave in all directions, known as Rayleigh scattering. Larger, irregularly shaped objects can also scatter the sound in a similar manner.
  - Reflection
    - ∗ This occurs where a wave passes through the interface between two media with different acoustic impedances causing a portion of the wave's energy to be reflected. Planar reflection is governed by Snell's law (Equation 4.2).
  - Absorption
    - ∗ As ultrasound propagates through a medium, it periodically displaces particles (or points in a medium) which relax back to their original position at a rate dependant on the material properties. If the media's

natural relaxation time is longer than the period of the US wave and is still returning when the next compression arrives, it will require more energy to reverse it's direction. This can cause the tissue to absorb more energy though the effect becomes negligible at very high or low frequencies compared to the relaxation time. This is usually the dominant mechanism of ultrasound energy loss in soft tissue Shung et al. [2012].

> Non-Linearity

- Perfectly linear wave propagation would result in a received wave, some distance from a source, maintaining the exact same waveform (frequency components) as when it was produced. However, the higher temperature and speed of sound in the compressed regions of the wave cause the peaks to travel faster than the troughs. This is known as non-linear transmission and all compressible media are to some extent non-linear, though the effect greatly increases at high pressure amplitudes.
- As the wave travels, the sinusoidal wave profile will change because of this effect, shifting towards a sawtooth profile which introduces higher harmonics of the fundamental frequency when analysed. This can alter the interaction with the transmission media, such as increasing absorption and in extreme situations causing shock waves.

1.1.4 Radiation forces

Ultrasonic radiation force is caused by the pressure gradient of the waveform between a peak and a trough, and is therefore a time oscillating force for any point or particle in the transmission media. The net force should be zero in a time-averaged linear scenario but acceleration of suspended particles is always observed in the direction of propagation. This time-averaged forward force results from non-linearity in the wave propagation and can be estimated using equation 2.2, the result of which is usually orders of magnitude smaller than the linear, harmonic oscillating force, though unidirectional and therefore able to create much greater displacement and stretch.

Radiation forces can also be caused by reflections as the momentum of the wave changes, transferring kinetic energy onto the reflecting surface. The difference in impedances between a gas or vapour bubble and water is very high which means that bubbles reflect and scatter a large proportion of the US energy, propelling them in the direction of propagation. This is known as the primary radiation force on bubbles.

The oscillation of bubbles can also cause secondary radiation (Bjerknes) forces as they re-radiate energy from the initial driving wave which can have significant effects in bubble agglomeration over short distances [Crum, 1975, Leighton, 1994].

1.1.5 Cavitation

Cavitation is defined here as the formation, collapse or stable oscillation of gas or vapour cavities. These cavities can form or grow during the negative pressure phase of the ultrasound wave by reducing the pressure below the partial pressure of dissolved gas and vapour pressure in the fluid. Practically speaking this will not occur without nucleation points, which are inhomogeneities such as hydrophobic crevices on which gas phase can form and grow, or pre-existing gas bubble nuclei. Once of a sufficient size, bubbles will compress and expand under pressure oscillations much more than the surrounding fluid [Young, 1999], creating direct forces on nearby structures or microflows in the fluid.

> Stable cavitation
    - Bubble oscillation that does not result in breakup or collapse of the bubble, acting much like a spring under oscillating compression. Growth or shrinkage due to rectified gas/vapour diffusion across the bubble surface may occur.

> Inertial cavitation
    - Violent bubble collapse resulting in very high localised temperatures and forces.

the likelihood of inertial cavitation in soft tissue is most often qualified by the Mechanical Index (MI), which relates to the peak negative pressure of an US exposure protocol via the equation [of Ultrasound in Medicine Clinical Standards Committee, 2015]:

$$MI = \frac{PNP}{\sqrt{F_c}}, \tag{1.2}$$

where PNP is the Peak Negative Pressure and F_c is the centre frequency of the ultrasound wave. This is only an approximate measure as the probability of inertial cavitation is highly unpredictable, especially in complex environments such as soft tissue and depends on factors such as dissolved gas pressure, ambient pressure, cavitation nuclei, tissue non-linearity and other factors.

1.1.6 Cavitation Signal Analysis

To the author's knowledge, no US neurostimulation study thus far has analysed acoustic signals during stimulation protocols, though the use of a PCD is common practice for detection and characterisation of cavitation in other fields. This section will give the reader an introduction into acoustic cavitation detection and characterisation techniques, highlighting their relative strengths and weaknesses for this application.

In order to understand what kind of cavitation may be occurring, several methods have been developed to identify and quantify the different acoustic emissions by which different bubble behaviours are characterised. These fall into the categories of passive and active cavitation detection. Active cavitation detection [Roy et al., 1990] measures the backscattered signal from an emitted pulse and is not used in this study as it does not easily differentiate between inertial and stable caviation, and the interrogation pulse can affect the cavitation that it is trying to measure [Hsieh et al., 2011]. Passive cavitation detection, which is used in the current study, measures the emission spectra of the cavitating bubbles using a focused or planar US transducer called a PCD.

Passive cavitation detection takes advantage of the different acoustic emissions that bubbles can produce when collapsing (inertial cavitation) or oscillating (stable cavitation) to identify types of bubble activity present. Inertial cavitation will usually cause a high amplitude, short duration signal that has a very broad frequency range as the bubble implodes and fractures. In contrast, stable cavitation is characterised by a signal containing multiple harmonics of the driving frequency or the bubble's natural resonant frequency.

Cavitation resulting from ultrasound usually creates a bubble cloud instead of a single oscillator, which complicates the signal. This is especially true in situations with heterogeneous cavitation nuclei as many different inertial events and oscillation modes will be occurring simultaneously with overlapping frequency spectra and often vastly different amplitudes. Furthermore, there are sources of confounding noise and other oscillation modes such as bubble surface oscillations, forced and unforced bubble oscillations, non spherical bubble geometries and non-linear US propagation [Leighton, 1994], making differentiating individual events and determining the causative event a difficult task.

To analyse the frequency components of a signal over a specified time period, a Fast Fourier Transform (FFT) algorithm is used and often analysed in isolation to determine cavitation activity [Chen et al., 2003, Tu et al., 2006]. This however will not give any information on how the frequency spectra will change over time. In order to solve this problem, the time window can be shortened and repeated over the total time of interest, known as an Short Time Fourier Transform (STFT). The spectra of every interval is then combined to create a spectrogram of the acoustic emission frequencies over time which is often interpreted qualitatively after digital signal filtering for cavitation detection [Farny et al., 2009, McLaughlan et al., 2010a,b]. STFTs and other time-frequency analysis techniques such as wavelet transforms [Graps, 1995] and Bilinear distribution functions [Janssen, 1994, Semmlow, 2011], analyse both the temporal and spectral information of a signal in a continuous manner which is more suited to time varying signals such as cavitation.

The fundamental limitation of an STFT is fixed resolution. Increasing the size of the time window increases the frequency resolution but decreases the temporal resolution and vice versa. In contrast, wavelet analysis techniques are multi-resolution and can give good time and frequency resolution simultaneously, enabling accurate detection and time location of both inertial, short duration events and long duration, low frequency patterns [Graps, 1995]. In other words, the wavelet transform analyses the signal at different frequencies with different resolutions as opposed to resolving each spectral component equally as was the case with the STFT. This is ideal for complex signals with a broad frequency range such as those produced by cavitation clouds. The technique has been used for cavitation detection in several applications already [Haqshenas and Saffari, 2015, Yujin Zong, 2006]. Wavelet is also preferred over Bilinear distributions as these create unwanted cross-terms when analysing complex signals [Cohen, 1995], arising in distributions which are a non-linear function of the signal [Papandreou-Suppappola, 2002].

1.2 Overview of the Nerve Fibre

This section is intended as a brief overview of relevant biological structure and function to facilitate understanding of US-tissue interaction theories which will be posed in this report. More in depth information about these topics can be found in text books [Alberts et al., 2002].

A typical mammalian peripheral nerve bundle consists of afferent sensory, and efferent motor neurons as well as sheath tissue and myelination cells call Schwann cells. The nerve cells will all have dendrites, a cell body containing the nucleus and machinery for protein production and folding, a long axon and a synaptic terminal. A basic example of these major features is shown in figure 1.1(a), though individual nerve cells in the Central Nervous System (CNS) can be significantly more complicated in structure, involving thousands of input and output connections.

Neurons are cells that have highly electrically polarised membranes, at rest their interior is highly negative with respect to the positive outside (Figure 1.1(a)). This electrical gradient is maintained by using trans-membrane proteins and energy to pump charged ions in opposite directions against their concentration gradients. The ions involved in this electrical polarisation along the peripheral nerve axon are sodium and potassium (Figure 1.1(b)), whose distribution inside and outside the cell is also controlled by several other types of trans-membrane proteins.

Within the axonal membrane are many trans-membrane proteins that form channels for the ions to pass through, facilitating passive diffusion of ions down their electrical and chemical gradients. These channels are entropically stabilised in the membrane by hydrophobic sequences in the protein structure that create an outwardly hydrophobic layer in the middle of the protein, shown in orange in Figure 1.1(b), which is approximately the same thickness as the hydrophobic membrane. Most of these rest in a closed state and are gated by local changes in membrane voltage, known as voltage gated ion channels. This means that once a certain threshold voltage is reached the channels will change conformation and open, allowing passage of sodium and potassium ions down the electro-chemical gradient to depolarise or hyperpolarize the membrane respectively. This in turn will alter the local membrane potential and open more voltage-gated channels, propagating the depolarisation down the axon in a wave. If multiple axons in close proximity generate action potentials synchronously, the combined ionic flux creates a negative potential wave in the extra-cellular environment which can be measured by electrodes and is known as a Compound Action Potential (CAP).

Upon the action potential reaching the pre-synapse (Figure 1.1(c)$_1$), a cascade of events occurs that leads to release of chemical messengers (neurotransmitters) which are received by and cause a response in the second cell. The incoming action potential will cause voltage gated calcium channels to open in the pre-synaptic terminal, initiating a rapid influx of calcium into the cell (Figure 1.1(c)$_2$). The primary effect of this is to initiate fusion and docking machinery, causing primed synaptic vesicles (bags of neurotransmitter) in contact with the pre-synaptic membrane to fuse and release their neurotransmitter into the synaptic gap (Figure1.1(c)$_3$). This signal is detected by the receptor proteins in the post-synaptic membrane which transmit the signal inside the cell by changing their conformational shape (Figure 1.1(c)$_4$). The effect that this has on the post-synaptic cell can vary greatly depending on the cell type, position of the input on the cell, type of neurotransmitter and many other factors.

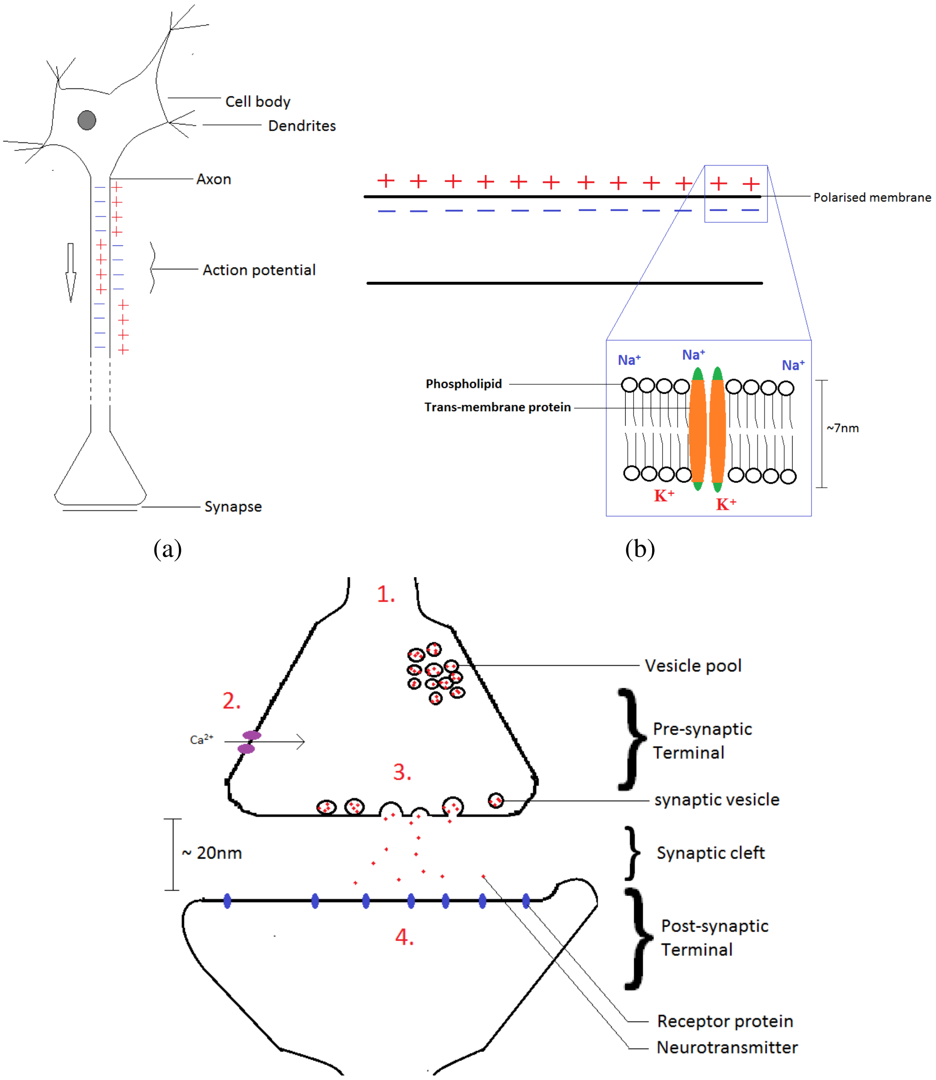

(a) (b)

(c)

Figure 1.1: Example diagrams of nerve structure and function (a) a Diagram of a typical motor neuron cell showing membrane polarisation and unidirectional action potential propagation from the cell body located in central ganglia to the axon terminal in peripheral muscle tissue. (b) More detailed diagram of the structure of the nerve membrane at rest, showing the majority of potassium ions in the nerve lumen and the majority of sodium ions outside. An example trans-membrane protein is shown with the hydrophobic thickness in orange and hydrophilic sections in green. (c) Diagram of the axon terminal and synapse including functional structures involved with a simplified process of synaptic transmission.

These basic mechanics of nervous transmission are conserved between many types of nerves and even between distant species such as crabs and humans. However, most mammalian peripheral nerves are myelinated (some are not), whereas invertebrate axons are not. Myelination involves a modified fatty Schwann cell, wrapped around the axon to electrically insulate, aiding faster nervous transmission. Myelinated action potential transmission also works slightly differently, where the depolarisation jumps between nodes (not covered by myelin) where ion channels are densely clustered.

1.3 Background and Motivations

Diseases and dysfunction of the nervous system, both central and peripheral, are common causes of morbidity and mortality around the world. Despite huge investment into pharmaceutical solutions for some of the more prevalent problems, progress has been slow. For a few of these diseases, successful new treatments have been found in neurostimulatory medical devices. Examples include deep brain stimulation for Parkinson's disease, Vagus nerve stimulation for epilepsy and depression as well as Sacral neuromodulation for incontinence. The gold standard for all of these are implantable electrodes, which themselves are associated with much morbidity from the need for highly invasive surgery, regular battery replacements and immunosuppression.

Though implants are improving, techniques that allow non-invasive neurostimulation such as Transcranial Magnetic Stimulation and Direct Current Stimulation are gaining favour since they avoid the complications mentioned above. However, neither of these techniques can replicate the location specificity, reliability, or stimulation depth that implants can achieve.

US, through the development of HIFU for ablative surgery and blood-brain barrier disruption, has demonstrated its ability to overcome both of these targeting issues, reaching anywhere in the brain and other body areas with millimetre precision. Pioneering studies have demonstrated its capability to elicit neurostimulation at low intensities *in vitro* [Tyler et al, 2008] and in small animal models [Tufail et al, 2010, Yoo et al, 2011a, Younan et al., 2013]. Despite the short time that has passed since these studies, the same techniques have already been demonstrated to be effective for neuromodulation in primates and humans [Deffieux et al., 2013b, Hameroff et al., 2012, Lee et al., 2015, Legon et al., 2012, 2014].

As with the preceding wave of HIFU research, new medical treatments and devices have facilitated academic research into US neurostimulation and paved the way for rapid uptake into the clinic. HIFU devices used in hospitals specifically, as well as potentially other ultrasound devices, can be adapted to produce neurostimulation protocols potentially allowing rapid transition from the lab bench to the clinic.

As well as medical applications in the diseases mentioned above and many others, non-invasive, highly specific neural stimulation has huge diagnostic and research potential for probing brain function. No other technique as yet can safely affect the function of different brain areas in awake humans and the availability of such a technology may revolutionise many areas of diagnosis, treatment and research.

Despite the recent progress in the application of the technique, still very little is known about the mechanisms at work behind the observations. Understanding in this regard has been hampered by poor characterisation of the ultrasound field, especially in small animal models where small cranial volumes make reflections a significant problem [Younan et al., 2013]. Combined with the variety of tissue and animal models used, very little consensus has been achieved on successful US parameters, exemplified by occasional directly conflicting or negative findings [Colucci, 2009, Gavrilov and Tsirulnikov, 2012].

This mechanistic and parametric confusion in the literature highlights the need for more rigorous approaches involving well characterised ultrasound, which have in fact recently started to emerge. The most recent studies in primates and humans require much less complex modelling to achieve accurate predicted intensity values due to the larger brain volumes and there has been some acknowledgement and work towards fixing the small target volume problems [Kamkin and Kiseleva, 2009, Mehic et al., 2014, Younan et al., 2013]. However, though the field is moving in the right direction, studies with a focus on accurate ultrasound characterisation are still low in number.

On the biological side, the complexity of the brain tissue targets makes it impossible to know whether any observed effects, such as motor activity, occurred through inhibition or enhancement of existing activity, or by generation of entirely new action potentials. Though there have been many *in vitro* studies in the past that have simplified the biological targets, only one of these achieved a simultaneously well controlled US field [Colucci, 2009], though this group was investigating the inhibitory, not stimulatory effect.

In order to address these issues, the current study uses a controlled *in vitro* environment, directly stimulating and recording CAPs from excised crab nerves. The aim of this approach is to create an environment where both the biological and ultrasound environment can be measured and modelled accurately to identify reliable thresholds and subsequently gain insight into the mechanism by which mechanical forces are transduced into propagating electrical activity in nerve fibres.

1.3.1 Experimental Rationale

The axon, cell body and synapses of a single neuron may have different responses to mechanical action, affected by the varying structural geometry, ion channel expression and other factors. Reducing the structural variation and potential cellular mechanisms at play is therefore critical to fully understand how cells respond to ultrasonic forces. Consequently, the current study examines the US effects on solely axonal tissue and support cells.

An *ex vivo* rat Saphenous nerve and then crab leg nerve model were chosen as simple, robust and well characterised examples of axonal tissue [Horridge and Chapman, 1964, Janicak et al., 2010, Selvín-Testa and Urbina-Vidal, 1975] that are easy to source, handle and record CAPs from. An *in vitro* model was essential in providing the primary novelty and aim of this study, in its degree of accuracy of US pressure and intensity measurement. As well as allowing more reliable comparisons with quantitative acoustic models, the simpler US field and lack of any tissue depth allows more accurate measurements of the acoustic noise at the stimulation site than *in vivo* experiments, helping identification of cavitation activity. Secondarily, as well as being representitive of unmyelinated nerves in humans, the response of this axonal transmission model system to US has not yet been investigated.

The simplicity of these models at the current stage means that US effect on biological structures such as synapses and cell bodies cannot be investigated as they are not present in the extracted tissue. The current report will therefore only concern itself with the action of ultrasound on the structures of nerve axons.

1.4 Objectives and Novelty

The current work aims towards the much highlighted necessity in the literature for a basic mechanistic understanding of the US-neurostimulation phenomena, which will be essential in separating the different effects that US can have on nervous tissue and for finding novel applications. The ultimate contribution of this fundamental understanding will be in discovering and optimising US neurostimulation protocols for medical or research applications.

Within the general remit of understanding the US force mechanism and US-tissue interaction, using the experimental procedures detailed in section 3.1 and 4, the authors aim to answer these specific questions:

- Can peripheral axonal tissue alone be directly stimulated by ultrasound?

  Does the stimulation protocol cause damage?

- What is the intensity or pressure threshold?

  Is the response success determined by either US radiation force, or cavitation?

Chapter 2

Literature Review

This chapter will review the literature around the subject of ultrasound neurostimulation, with a specific focus on giving the reader an understanding of the progress and current understanding of its mechanism of action. A short summary of the history of the technique will first be given, followed by a critical appraisal of more recent key papers in central and peripheral US neurostimulation. A discussion of the evidence for involvement of different bio-structures and US force mechanisms in the US-nerve response will then be given. To conclude, a summary of where the weight of mechanistic evidence lies in the literature will be given, and a hypothesis proposed.

2.1 History

The use of US for neuromodulation has been investigated sporadically for over 80 years but is only recently gaining significant momentum as a viable research area. Initial studies by Harvey and then later by Fry and others showed a variety of different US effects on neural tissue including potentiation and inhibition [Fry et al., 1950, Harvey, 1929, Wall et al., 1953]. After the initial study in 1929 by Harvey, it wasn't until Gavrilov et.al. in 1975 that ultrasound stimulation was achieved independently of electrical stimulus again, although their initial focus was on specifically Mechanosensitive (MS) neuronal structures such as the skin or inner ear [Gavrilov, 1984, Gavrilov et al., 1977, 1975]. the first recent indication that US could stimulate non-specifically mechanosensitive structures came from stimulation of the auditory nerve in cats [Foster and Wiederhold, 1978] in 1978 later confirmed by Gavrilov et.al in frog models with destroyed labyrinth structures [Gavrilov, 1984]. In both studies the thresholds for stimulation were a lot higher than with an intact labyrinth, or on other known mechanosensitive structures. Activity was observed in the midbrain auditory centres in response to the focused ultrasound, and histological analysis showed activated auditory nerve fibres.

In keeping with these findings of auditory nerve stimulation, in 1993 an effect was seen in humans during ultrasound Doppler imaging procedures where subjects heard high frequency tones, equating in pitch to the PRF and in amplitude to the intensity [Magee and Davies, 1993]. However it is possible that this is a direct effect on the cochlea rather than any nerves as the characteristics of the stimulation are different as well as seemingly being a lot more reliable than typical neurostimulation observations.

There are also many observations of US inhibiting nerve firing [Colucci, 2009, Foley et al., 2008, Juan et al., 2014, Young and Henneman, 1961] instead of, or as well as stimulating it, which is being used by some groups to develop treatments like suppression of epileptic seizures [Min et al, 2011b, Tufail et al, 2011, Yoo et al, 2010]. To try and combine the observations of stimulation and inhibition, often seen in the same studies [Mihran et al., 1990, Muratore et al., 2009, Tsui et al., 2005, Velling and Shklyaruk, 1988], Muratore et al. suggested an intensity dependent interaction between the two mechanisms summed up in figure 2.1. Due to the focus of the current study on neurostimulation rather than inhibition, discussion of inhibitory mechanisms and observations in the literature will largely be omitted.

Before 2008, exploratory studies almost all focused on examining effects on peripheral nerves [Dalecki et al., 1995, Foley et al., 2008, Fry, 1968, Gavrilov et al., 1977, Lele, 1963, Mihran et al., 1990, Sheltawy and Dawson, 1966, Tsui et al., 2005, Wright et al., 2002, 2015, Younan et al., 2013] with a few targeting central nervous structures [Tsirulnikov et al., 1988, Wall et al., 1953]. This preference shifted dramatically towards the central nervous targets after 2008 when Tyler's group demonstrated that hipocampal slices could be stimulated at much lower intensities than those used on peripheral nerves (Figure 2.2) [Tyler et al, 2008]. Subsequent to this, studies on the effects of low intensity US in the living brain have yielded a range of exciting results, such as stimulating motor activity [Tufail et al, 2010], affecting GABA release [Yang et al., 2012], reversibly inhibiting epileptic activity [Min et al, 2011b] and eliciting somatosenory sensations [Lee et al., 2015].

This difference in sensitivity, first identified by Dr. Tyler's group, is a general

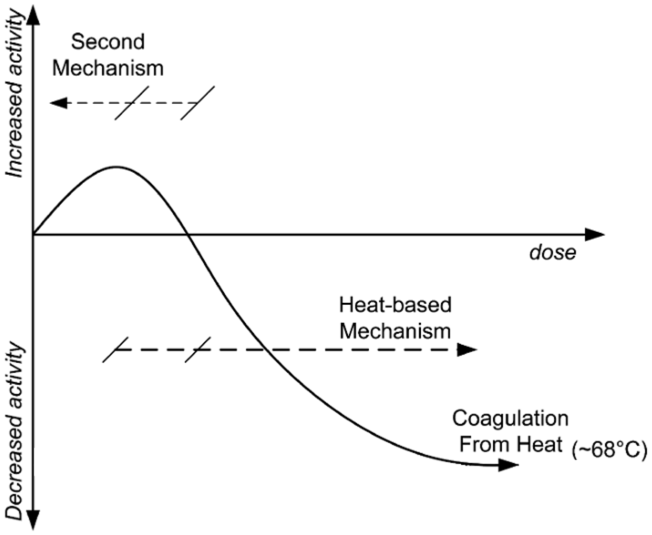

Figure 2.1: Concept graph of an ideal nerve's response to US dose. The dose and activity axis intersect at the threshold intensity on the horizontal and the basal activity level, pre-sonication on the vertical axis. Stimulatory effect at low doses is labelled as an unknown "second mechanism". The higher dose mechanism is assumed to be heat based inhibition alone. Image taken and modified from Muratore et.al., 2012.

theme in the literature, showing that Peripheral Nervous System (PNS) tissue is less sensitive to US stimulation than CNS tissue. The dramatic difference can be seen in figure 2.2 although it should be kept in mind that unreliable US reporting standards make comparisons difficult. As such figure 2.2 is a comparison of the time averaged Intensity (I_{SPTA}) which is the most widely reported standard. It is likely be that the pulse average intensity is more important for mechanically induced bio-effects as this will determine the peak mechanical forces. A comparison of I_{SPPA} or peak pressures instead of I_{SPTA} for example may correct for some of the difference as the primarily *in vivo* CNS studies tend to use protocols with short pulses a lot to avoid potential heating which significantly lowers the resultant I_{SPTA} values. However, given that this cannot account for a difference so large, the information can be used to guide investigation into the likely biological target structure as some of the numerous differences between CNS and PNS tissues are likely to be the cause of the differing sensitivity and therefore key to the mode of action. For ease of identification and comparison therefore, the remainder of this section will be split into CNS and PNS sub sections.

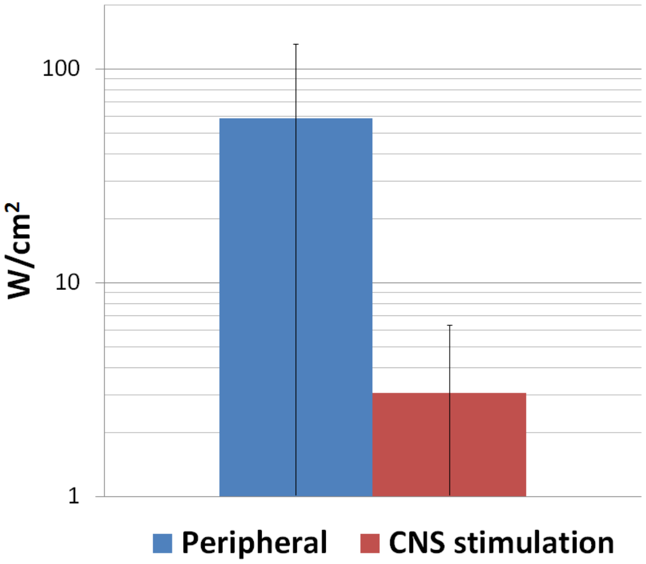

Figure 2.2: Comparison of aggregated threshold intensity data (Spatial peak temporal average) from past literature on peripheral versus central nervous US induced modulation or stimulation. Error bars denote standard deviation. In studies where a range of intensities were investigated, the highest value was used. All studies with successfully demonstrated effects and well reported stimulus parameters were included [Dickey et al., 2011, Fry et al., 1950, Hu et al., 2011, Lee et al., 2015, 2014, Legon et al., 2012, 2014, Menz et al., 2013, Mihran et al., 1990, Min et al, 2011a, Tsirulnikov et al., 1988, Tych et al., 2013, Tyler et al, 2008, Yoo et al., 2013, Yoo et al, 2011a, Younan et al., 2013].

2.1.1 Central Nervous System

Tyler's paper, as mentioned in section 2.1, was the first of a recent trend in demonstrating and investigating US neurostimulation effects in CNS neurons at low intensities [Tyler et al, 2008]. As well as demonstrating the existence of a direct stimulation effect on CNS neurons, they found that both sodium and calcium flux and exocytosis of synaptic vesicles could be detected in response to US stimuli in mouse hippocampal slice cultures. As both of these ionic flux effects could largely be blocked by TTX (a sodium channel blocker), it was claimed that the mechanism of stimulation was primarily the direct effect of membrane stretch on sodium channels. However, the same observation would have held true for activation that was initiating further upstream than the involvement of sodium channels in the signalling pathway. This was later acknowledged and the same group expanded their hypothesis to include many more possible mechanisms of action [Tyler, 2010].

The direct US stimulatory effect was then demonstrated *in vivo* in the brain of a living anaesthetised mouse in both the motor cortex and hippocampus in the absence of significant temperature rise [Tufail et al, 2010]. As with Tyler's study before, the intensities used in these experiments were remarkably low, staying around or often well under 100 mW/cm^2, much lower than previous peripheral nerve investigations [Dalecki et al., 1995, Mihran et al., 1990, Wright et al., 2002]. In this first study by Tufail et al., an ”US collimator” 2-4.7 mm in diameter was used to deliver the stimulus to the rat's head, which is less than or close to the wavelength of US (4.6mm at 0.35MHz used in their study). This would have acted like a point source, radiating US in all directions through the mouse's head rather than focusing onto the motor cortex as was claimed. The same issue would also have been present in a similar study, also stimulating mouse brains [Moore et al., 2015]. Despite these issues, many of the findings of both papers remain valid and intriguing, demonstrating that US is able to differentially target and stimulate different functional brain regions [Tufail et al, 2010].

A more acoustically controlled study followed in 2011 stimulating rabbit brains in a similar manner but with a phased US array, a craniotomy of the intervening skull layer, and real time MRI monitoring of the US focal position [Yoo et al, 2011a]. The US was shown to induce increases in the Blood Oxygen Level Dependant (BOLD) signal of the somatomotor cortex, which are often associated with brain region activity, and elicit forepaw movement from the anaesthetised animal. The BOLD signal increase was observed at amplitudes lower than the threshold for forepaw movement [Yoo et al, 2011a]. Although it is tempting to attribute this to low level neurostimulation effects, it could be due to other factors such as vasodilation caused by nitric oxide release induced by low intensity ultrasound [Altland et al., 2004, Iida et al., 2006], temperature rise or possibly by activation of more sensitive MS channels in the endothelium of blood vessels [Olesen et al., 1988, Schmidt et al., 2012]. This means that a BOLD signal cannot be used to prove US stimulation success but could have the advantage of allowing useful guidance feedback while at sub-stimulatory intensities.

In the same study however, sonication of the visual cortex using slightly different parameters did not produce any BOLD response and in fact reversibly reduced the amplitude of visual cortex responses to light stimulus applied to the rabbit's eye, thus demonstrating a region specific, opposing effect of US neuromodulation. Along with other differences in parameters, the stimulatory pulse average intensity threshold in this study was much larger than in previous examples by Tyler and Tufail in mice (12.6 W/cm^2 compared to 23-163 mW/cm^2), though in later studies by the same group the intensity of stimulation was dropped to 1-6 W/cm^2 [Kim et al., 2014a], probably due to optimisation of their other stimulation parameters such as pulsing and frequency.

A potential problem with the MRI guidance technique is that static magnetic fields are known to affect ion channel activity, especially mechanosensitive ones [Hughes et al., 2005] as well as bio-membrane phospholipids. This raises questions about stimulation results from studies combining US stimulation and MRI observation like Dr. Yoo's. Tissue motion generated by US radiation forces in a magnetic field may also be generating current via Lorentz forces [Fry, 1968, Norton, 2003].

The third group to examine the mouse twitch response, essentially repeating studies by Tufail and Yoo [King et al., 2013], confirms Tufail's original findings that US can stimulate motor reflexes and that lower frequencies are more effective. The scope of this study was much broader, testing and reporting on a number of different ultrasound variables including 8 different frequencies at 3 different intensity levels in three mice tested per point (Figure 2.6). Although contradictions with other studies are posed such as a preference for CW protocols here, this paper and others not mentioned here in detail add to the finding of a robust US neurostimulatory effect in the CNS [Choi et al., 2013, Menz et al., 2013, Min et al, 2011a, Muratore et al., 2009, Yang et al., 2012, Younan et al., 2013].

Reflections within the head of small animal models or *in vitro* setups are a major confounding factor both for brain region targeting and the accuracy of intensity measurements made by a hydrophone in free water, which has been the standard in the literature. This was only acknowledged and accounted for in 2013 by Younan et al., who found through modelling and acoustic phantom experiments that sub-wavelength peaks were created within a rat skull with a factor of 3.6 times greater acoustic intensity (I_{SPTP}) than measurements in free water would predict [Younan et al., 2013]. As the first study to take good account of acoustic reflections by modelling the wave propagation within the rat's head, Younan's experimental data has added significant evidence for US's neurostimulatory effect in the brain and has provided the first reliable threshold data ($I_{SPPA} = 17.5 \pm 7.5$ W/cm^2 using 0.32 MHz US).

Also addressing the problems of small volume brains, several recent studies have simply started applying US stimulation to larger brain models [Deffieux et al., 2013a,b, Hameroff et al., 2012, Lee et al., 2015, Legon et al., 2014]. In both monkeys and humans, these studies have observed successful modulation of activity in various brain areas and although they can provide useful threshold data for effect observation, they shed little light on the biological mode of action due to the tissue complexity present. It is difficult to even claim if stimulation or inhibition occurred given the possibility for inhibition or stimulation of inhibitory pathways, resulting in the ubiquitous use of the term ”neuromodulation”.

Although larger brain volumes solves one problem it also opens up another. The greater soft tissue depths and skull transition is more likely to generate significant non-linearity in the beam propagation, which has not been factored into intensity or pressures measurements in any of these studies [Deffieux et al., 2013a,b, Hameroff et al., 2012, Lee et al., 2015, Legon et al., 2014]. Although the low intensities of these studies reduce the possible influence of non-linearity, the often very short pulse lengths can increase its effect and for ensuring accurate metrology, it should always be considered.

Another vital piece of information that the most common live animal studies cannot bring is the timescale of the US stimulation cellular response. The latency between CNS stimulation and motor response involves many different processes making it impossible to measure the time contributions of the US reception mechanisms at work. Response latency in such studies also varies by an order of magnitude (approximately 20-200 ms [Kim et al., 2012, Tufail et al, 2011, Tyler et al, 2008, Yoo et al, 2011a]), possibly depending on the level of anaesthesia. Very little information can therefore be gained from the measurements and the involvement of slow mechanisms of change such as long cell signalling pathways cannot be ruled out, again highlighting the advantage of experimenting with simpler biological systems such those used in the current study.

2.1.2 Peripheral Nervous System

US stimulation attempts made on the PNS have been shown to be successful primarily when targeting the specifically mechanosensitive structures in the skin [Gavrilov and Tsirulnikov, 2012, Lee et al., 2014, Legon et al., 2012, Muratore et al., 2009]. Whereas attempts at inducing *de novo* action potentials by targeting the nerve trunk have hitherto been mostly unsuccessful except for one recent study [Kim et al., 2012], instead resulting in inhibition only [Juan et al., 2014, Lele, 1963]. Modulation of Action Potentials (APs) stimulated electrically though, is easily observed [Mihran et al., 1990, Tsui et al., 2005, Young and Henneman, 1961].

The existence of mechanosensitive receptor structures means the mechanism of US stimulation in the skin is likely to be very different from stimulation of a nerve axon or of areas within the brain. Many of these sensitive receptors may be stimulated in a straight-forward manner by the forces in US that they were adapted to detect, for example, the radiation force of US is likely to be detected by Meissner's corpuscles just like any physical pressure exerted on the skin [Dickey et al., 2011]. Some of these receptors, however, may be stimulated by non-conventional aspects of the US-tissue interaction. The most recent study targeting human skin found patients reporting a cooling sensation, opposed to the small amount of heating that would have occurred [Lee et al., 2014], which they put down to activation of mechanosensitive sodium channels.

Though the stimulation of skin *in vivo* with US demonstrates a useful tool for assessing peripheral nerve function, the complex tissue structures and uncontrolled acoustic environment make it a poor model to investigate the US mode of action.

Experiments on excised amphibious (frog) sciatic nerves [Mihran et al., 1990, Tsui et al., 2005] are some of the closest biologically to the crab leg nerve model used in the current study. The earliest of these investigated single 0.5 ms pulses of 2, 4 and 7 MHz US at 100-800 W/cm^2 and noted enhancement and suppression of electrically induced CAPs [Mihran et al., 1990]. Tsui's work in contrast was on long exposures (5 minutes) of CW ultrasound with 1,2 and 3W driving powers, similar to Mihran's work [Mihran et al., 1990] or Fry's even earlier [Fry et al., 1950], saw both enhancement and suppression [Tsui et al., 2005]. The existence of an enhancement effect in these papers provides support for the existence of a stimulatory interaction of US in peripheral nerve trunks.

Even closer to the nerves used in the current work is the crayfish vertebral nerve chord used by Fry et al [Fry et al., 1950]. They used a much lower intensity of 35 W/cm^2 and 1 MHz CW ultrasound, also finding a slight enhancement of electrically stimulated CAPs followed by inhibitory effect as the exposure went on longer. The agreement of these findings despite vastly different protocols serves to strengthen the evidence for a robust US induced effect that is conserved across different models of axonal tissue. However, despite that these studies were specifically aiming to investigate the mechanism of action as well as just demonstrate an effect, again, US reflections in the test environment were not accounted for.

The only study to report successful de-novo generation of CAPs by US in a peripheral nerve bundle did so using a live anaesthetised rat model, targeting the abducens nerve [Kim et al., 2012]. Unsuccessful stimulation of neck and leg muscles was attempted before successfully stimulating the abducens nerve (measured by abductive movement of the eyeball) using the same US parameters (0.35 MHz, 8.6-20 W/cm^2 I_{SPPA}, 1.5 kHz PRF, 0.36 ms pulse duration, 54% DC and a TSD of 200 ms). 0.65 MHz was attempted but found ineffective. Although other parameters vary slightly the intensity used is in the same range used by Yoo et al., for CNS stimulation (12.6W/cm^2 I_{SPPA} [Yoo et al, 2011a]). However, the pressure values stated were solely derived from a characterisation of the focal point of the transducer in free water by a previous study [Yoo et al, 2011a]. As with most *in vivo* studies, no attempt was made to stop reflections within the rat skull. This oversight is particularly important in this study as the abducens nerve target is located very close to the skin, which is an air-tissue interface and will cause strong reflection and associated radiation forces. Combining these points with the fact that the US was focused onto the abducens nerve through brain tissue and that no direct measurement of abducens nerve activity was made, leads the author to question the claimed specificity of stimulation.

Technically demonstrating US stimulation of peripheral nerves is a recent paper studying the effects of US and cavitation on the behaviour or nematodes with sensory neurons engineered to express TRP-4, a specifically mechanosensitive ion channel [Ibsen et al., 2015]. As well as genetically sensitising the neurons of the animals, microbubbles were introduced in the vicinity of the animals which were necessary for successful neurostimulation. With these added factors, it is unclear whether the mechanism of neurostimulation will be the same as in other US neurostimulation studies but it does demonstrate the principal of US mechanical forces, sensed by mechanosensitive ion channels, eliciting neurostimulation in a biologically controlled environment. Only once investigations are undertaken to quantify the exact mechanical forces acting to achieve each observation of neuromodulation such as this, will a combined mechanistic understanding be possible.

2.1.3 Overview of the Literature

A consistent problem with the literature so far remains the patchy reporting of acoustic parameters, making it difficult to make direct comparisons between reported pressures, intensities or input voltages. Acoustic intensity is most usually quoted as the spatial peak time average (I_{SPTA}), however, as the effect of the US is considered to be mechanical, the important intensity value will be the pulse average (I_{SPPA}) or the equivalent RMS or peak negative pressure.

On top of the often inconsistent reporting, many studies have been guilty of poor control of the US environment itself in both *in vivo* and *in vitro* experiments, on CNS and PNS structures. The primary problem is that US is not given any path to dissipate or absorbent material put in place, meaning that the target (animal head or test chamber) will be flooded with reflections or even standing waves, making the resulting ultrasound field highly unpredictable. This problem is almost universally ignored in studies investigating US neurostimulation with one exception [Colucci, 2009] even after the problem was highlighted by Younan et al., in 2013 [Younan et al., 2013]. Progress is being made in the right direction though. A recent study has demonstrated the possibility of using a high carrier frequency, modulated at 0.3-1 MHz to achieve neurostimulation in small animal models with much higher spatial resolution [Mehic et al., 2014]. Improving control of ultrasound through measurement, modelling or better experimental design, throughout the field of US neurostimulation will be an essential step towards consensus on successful stimulation thresholds and understanding the mechanisms at play.

Added to this, the sporadic use of different animal models and US parameters in the literature has led to many results which are difficult to compare and are often in disagreement. The mixed findings in the literature have even on occasion called into question the existence of the stimulatory effect itself [Colucci, 2009]. For example Gavrilov wrote in his 2012 review that his group were unable to stimulate local impulse activity or propagating excitation in any brain material in several separate vertebrate animal studies (frog, rat, rabbit, and cat) by the use of focused ultrasound [Gavrilov and Tsirulnikov, 2012]. More recently, Chu et al. reported no neuromodulation when using a higher mechanical index exposure in the somatosensory cortex than studies by dr

Yoo's group [Chu et al., 2015], only finding successful short and long term suppression when microbubbles were introduced. Even the studies which do observe successful neurostimulation find the response to be unreliable [Kamimura et al., 2015, King et al., 2013, Younan et al., 2013] which raises the possibility that there is a lot more negative response data that remains unreported.

For a full understanding of how US interacts with biological tissues, there is a wide range of other observed US induced bio-effects that should be considered because, if they are not caused by neurostimulation which seems possible in many cases, they may share underlying mechanisms. Much like the US-nerve interaction, most of these findings are very new and as yet have very poorly understood mechanisms. For example, in humans alone when applied to the tongue US can produce sensations similar to weak current [Gavrilov et al., 1977], it can aid in bone and tendon repair and re-growth [Della Rocca, 2009, El-Bialy, 2007], can alter stem cell differentiation [Ebisawa et al., 2004], and can induce foetal movement, even at diagnostic intensities [Fatemi et al., 2001].

If non-human studies are included the list goes on, improving nerve regeneration through NGF expression in rats [Chen and Grinnell, 1995, Crisci and Ferreira, 2002], enhancement of bone regeneration in rats [Jung et al., 2015], enhancing tooth repair and formation of new dental tissue [El-Bialy, 2007, Patel et al., 2015, Scheven et al., 2009] and electroreceptor stimulation in sea skates [Broun et al., 1980]. US even has non-thermal effects at molecular levels, altering gene expression and enzyme activity [Johns, 2002]. This wide range of effects has prompted the search for a unified theory such as proposed by Krasovitski et al., in 2011 [Krasovitski et al., 2011] where a single mechanism may account for all of the observed bio-effects of US, not just neurostimulation.

It is clear from the literature that US can, in certain circumstance modulate action potentials or activate motor functions. However it is not clear what all the steps or mechanisms are between the US energy being absorbed and the action potential firing. The key information that should unlock this black box is determining the point in the chain of events where the non-biological, mechanical forces are transferred into, and alter the state of a key biological process. This will hopefully involve a dominant effect on a single identifiable structure that senses or is altered by the direct US force that begins events leading towards action potential firing. Towards finding such a structure, in section 2.2 the author will discuss the evidence for and against the involvement of different cellular components.

2.2 Biological Target Structure

The preference in recent US stimulation literature for *in vivo* models and Central Nervous System (CNS) tissue targets leaves little way of knowing which neuronal cell types or which parts of those cells are responding to ultrasound, if indeed the effect is region specific. This wide variety of potential structures makes it difficult to predict exactly how the ultrasound energy is being transduced into a cellular response. What follows is a section on the evidence and reasoning behind several hypotheses on the cellular effect of US, focusing on the candidate structures that may be directly affected by US induced mechanical forces.

2.2.1 Transmembrane Ion Channels

As the direct effector of a nerve depolarisation response, ion channels are expressed ubiquitously in the membranes of neuronal cells, with different species and subtypes performing different functions in different cells or cell-regions. Opening or closing of ion channels involves a change in the protein conformation which alters their radius or hydrophobic thickness, meaning that all of them will be to some extent sensitive to mechanical forces through the surrounding membrane or other sources [Morris and Juranka, 2007, Ursell et al., 2007]. The simplest theory for US neurostimulation therefore is that ion channels are both the only structure sensitive to the mechanical US force and the only biological effectors involved in the AP initiation. Given the variety of channel types, functions, distributions and force thresholds, this explanation is sufficient account for the wide range of US bio-effects reported in past literature, mentioned in section 2.1.3.

There are several ion channel types that could initiate action potentials, or promote/enhance existing activity in response to US such as sodium, calcium and potassium channels which have all been implicated [Dinno et al., 1989, Hu et al., 2011, Mortimer and Dyson, 1988, Tyler et al, 2008], though the evidence for their relative importance in the response to US is thin. This is most likely due to the difficulty in separating the US induced ionic flux from the action potential ionic flux that follows, the electrical or chemical characteristics of any pre-threshold depolarisation is easily obscured by subsequent AP events.

Calcium channels are used to propagate potential in the dendrites of neurons (Figure 1.1(a)) and trigger synaptic vesicle fusion and NT release into the synapse between nerves (Figure 1.1(c)), whereas sodium and potassium channels are the main driver for axonal action potential propagation. This means that if the effect is ion channel specific it may also be location specific.

Effects on calcium ion flux in response to US has some support from several different sources including fibroblasts *in vitro* [Dinno et al., 1989, Mortimer and Dyson, 1988, Otter and Salmon, 1985], during neuritic growth [Hu et al., 2011], calcium influx induced apoptosis in HIFU exposures [Dai et al., 2014, Lee et al., 2013], calcium transients in rat cardiomyoblasts [Fan et al., 2010] , although it remains unclear whether this is through the direct action of the US on calcium ion channels or via some upstream mediator. It could also be speculated that the increased importance of calcium signalling for dendritic APs and in synapses is a reason for lower intensity thresholds for US stimulation in the CNS (Figure 2.2).

The sensitivity of these channel types to US forces may vary on sub-type as well as the surrounding mechanical environment, meaning that a calcium, or other ion channel in the synaptic terminal will have very different properties to one located in the dendrites of a nerve for example. The result of the cellular response to the ion in question will also vary depending on the cell or tissue type. Indeed this tissue/cell region specificity of response is observed in the literature [Bachtold et al., 1998, Yoo et al, 2011a], as is the force windowing of effects that different sensitivity channels would predict [Fry et al., 1950, Muratore et al., 2009, Tsui et al., 2005, Velling and Shklyaruk, 1988]. This makes determining the affected channels very difficult in any experiments with multiple exposed cell regions or tissue types and illustrates why less complex models such as in the current study will be essential for determining the key biological sensors of the US. Even in simple tissue models with multiple channel types, if force windowing like this occurs with US then it will add to the complexity of observations and the difficulty of eliciting specific effects.

Figure 2.3 demonstrates this variability of force thresholds in channel types found within a single neuron. These types of differential force detection mechanisms are known to be important in many areas of the body, for example in epithelial cells of arterioles it is known that several stretch sensitive ion channels respond to membrane tension with opposing effects at different force amplitudes[Lansman et al., 2011, Olesen et al., 1988]. Channels described as mechanosensitive will likely have much lower mechanical force thresholds for opening than the sodium, potassium and calcium channels directly involved in AP transmission.

2.2.2 Mechanosensitive Ion Channels

There exists a subset of ion channels that are specifically mechanosensitive, that have a structure particularly sensitive to certain mechanical forces. It is the direct influence of US on MS ion channels that is the basis for one of the most prevalent theories on how US neuromodulation is brought about.

Exactly how these channels detect mechanical forces is not well established and varies between individual examples, even some TRP channels usually cited as archetypal MS ion channels are still in question as to whether they sense the force directly or indirectly, i.e. they could be part of the immediate downstream signalling from the actual force sensor [Christensen and Corey, 2007, Lin and Corey, 2005].

It is thought that MS channels are present in all cell and tissue types as some of their functions are universal such as regulation of cell volume [Hua et al., 2010] or cell motility and growth [Sukharev and Anishkin, 2004]. Interestingly US has recently been shown to have an effect on neurite growth in the brain which required the presence of stretch sensitive ion channels [Hu et al., 2011], suggesting that some MS ion channels may only be present in juvenile stages of cell growth. Similarly, a recent paper has demonstrated a direct US neurostimulatory effect in *C.Elegans* which was greatly enhanced by the presence of transfected mechanosensitive pore-forming TRP-4 channel subunits [Ibsen et al., 2015].

Potentially explained by MS ion channels' universal presence, several studies have discovered that low intensity US, even at imaging levels, can cause alteration of ionic membrane permeance in non-neuronal structures [Chapman et al., 1980, Dinno et al., 1989, Mortimer and Dyson, 1988, Velling and Shklyaruk, 1988]. Of course MS channels will have other, non-universal functions in the body and their distribution and type will vary between tissues, defining or at least contributing to any tissue specific effects of US.

One persuasive argument for MS ion channel density being the determining factor in nerve sensitivity comes from observations made by clinicians and researchers that neuropathic tissues or damaged nerve fibres, which recruit MS ion channels as part of the inflammation process, have a much higher mechanical and chemical sensitivity [Rivera et al., 2000] which corresponds to a higher sensitivity to US stimulation [Chen et al., 2010, Tych et al., 2013]. This work was furthering Gavrilov's initial idea to apply US to diagnose and locate neuropathies in peripheral nerves [Gavrilov and Tsirulnikov, 2012].

Differences in MS ion channel types and concentrations can also explain the much lower US sensitivity of the PNS compared to the CNS. Evolutionarily, PNS neurons would encounter significantly more outside mechanical forces and therefore are adapted to be mechanically insensitive, whereas CNS neurons would not require this insensitivity to mechanical forces. This of course excludes sensory nerve endings in the PNS, which have a high concentration of MS ion channels and are easily stimulated with US [Dalecki et al., 1995, Dickey et al., 2011, Lee et al., 2014, Legon et al., 2012].

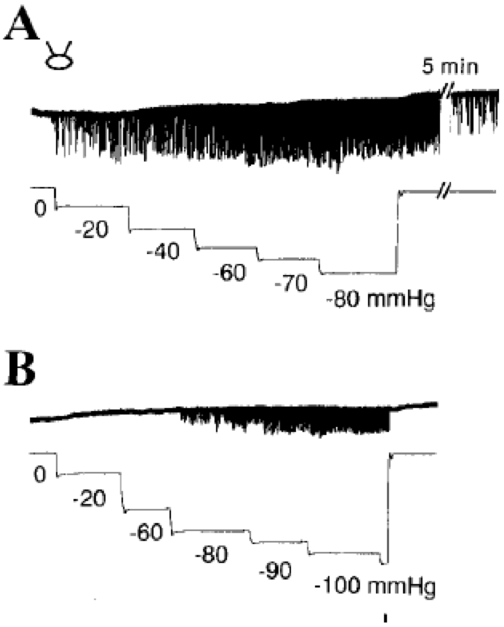

Figure 2.3: Two separate MS channel types identified in dorsal root ganglion neurons cultured from a neonatal rat measured using a whole cell patch clamp technique showing increased conductances as pressure is increased. A) Low threshold MS channel B) High threshold MS channel [Cho et al., 2002]

Ion channels shown to exhibit sensitivity to mechanical stimulation include non-selective cation superfamily, two pore domain potassium channel superfamily, amiloride sensitive sodium channel superfamily and voltage gated ion channels [Hamill, 2011, Morris and Juranka, 2007], though all ion channels will be to some extent mechanosensitive. Of these, the peripheral axon models used in this study contain two pore potassium leak channels that help maintain resting potential and are constitutively active, as well as voltage gated sodium and potassium channels.

Given the evidence, it seems highly likely that MS ion channels have an important role to play in sensing and responding to the stimulatory US forces, though this role may be alongside other potential mechanisms which must be considered.

2.2.3 Direct Membrane Effects

It is possible that ultrasound forces could be stimulating neuronal tissue through mechanisms that just involve the lipid membrane itself. For example, if US generates sufficient localised forces to cause small ruptures/pores in a cell membrane, the general ion flux would cause depolarisation and an action potential in nerves. This is a well documented phenomenon called sonoporation which requires cavitation [Zhou et al., 2008] and is often used for DNA or therapeutic compound delivery [Carugo et al., 2015]. Universally, sonoporation protocols use microbubbles which have not been employed for neurostimulation with one exception [Ibsen et al., 2015] and generation of cavitation in soft tissues without these nuclei would require significantly higher intensities than are used in neurostimulation studies [Gateau et al., 2011]. Sonoporation should therefore be considered where cavitation is implicated, but is unlikely to be involved in low pressure protocols. Even if cavitation effects involving nanobubbles are involved as is discussed in section 2.3.4, collapse and jetting of these bubbles requires shock waves [Choubey et al., 2011] which are not produced in any example of US neurostimulation.

Altering the charge distribution on the membrane as its thickness increases in one location or as the membrane flexes is known as a flexo-electric current. This has been demonstrated as an effective driving force for ion transport through membrane channels [Petrov et al., 1993, Plaksin et al., 2014], and could subsequently initiate action potentials. Minor capacitive currents have been demonstrated in synthetic membrane without proteins in response to US [Prieto et al., 2013] radiation force which is probably a flexo-electric effect. However, although this study represents a step in the right direction for control of the biological environment, their acoustic environment included water surface reflections that, although later accounted for, contributed most of the observed membrane flexure. Artificial vibrations would also have been introduced to the membrane through the highly impeding structures that held the bilayer in place, which is not accounted for. Thirdly, flexure would only be created in this scenario because of movement relative to the fixed membrane holding apparatus, which does not reflect the *in vivo* tissue environment where cells are not held at fixed points and will be moving simultaneously with those around them. Combining these concerns with two similar previous studies that found no effect of US on bilayer electrical properties [Pohl et al., 1993, Rohr and Rooney, 1978], either the flexo-electric or capacitive current effects are considered an unlikely mechanism.

2.2.4 Vesicular Fusion

Other than direct action on sensitive ion channels, there are other possible ways that US could be eliciting a direct stimulatory response, some of which have had support in the literature, and some less so. In the CNS, one possibility is the direct induction of vesicle fusion with the pre-synaptic membrane. There is a pool of NT containing vesicles that are held very close to the surface of the pre-synaptic membrane (Figure 1.1d), where it is conceivable that the US might induce premature fusion of these primed vesicles, though this or other effects within the synapse have not been directly investigated yet.

Vesicle fusion induced by ultrasound is a documented phenomenon although in the studies that have successfully demonstrated it, the vesicles were orders of magnitude larger (50 μm polymer vesicles), and the US was continuous wave US of a higher power and lower frequency than reported stimulatory parameters [Zhou and Yan, 2005]. As the mechanisms behind this observation were not investigated it is also not known if or how the effect would scale to relevant sizes (10-50 nm) [Alberts et al., 2002]. As there is not yet any data on the mechanical properties or sensitivity of these ”kissing” vesicles, a quantified idea of mechanistic feasibility is difficult to come by.

Although this theory and other synapse specific interactions have merit for investigation, they cannot account for all the recent battery of data in the literature since neuromodulation has been observed in tissue samples involving no synapses whatsoever in peripheral nerve studies [Foley et al., 2008, Gavrilov et al., 1977, Young and Henneman, 1961] or unconnected cells in culture [Muratore et al., 2009]. Also Menz et.al.'s work on retinal stimulation seemed to demonstrate that if any synaptic effect occurred in their study, it was at or before the ca2^+ influx step (Figure 1.1d) [Menz et al., 2013].

Although US may not cause immediate stimulation in this way, it seems likely that it will at least induce more subtle effects at the synapse which could alter function over the medium to long term and needs to be investigated for a full understanding of US-nerve interaction. For example it has been shown that mechanical forces such as presynaptic membrane stretch can increase synaptic vesicle clustering and exocytosis probability [Chen and Grinnell, 1995, Siechen et al., 2009]. However, as the current study is concerned only with the direct induction of potentials, longer timescale effects won't be discussed further.

2.2.5 Less Prevalent Theories

In addition to membrane stretch effects it has also been suggested recently that intraneuronal microtubules could be resonating at specific US frequencies to elicit varied neurological effects [Hameroff et al., 2012]. These structures regulate spine, synapse and neuron morphology as well as being used as tracks for transport within the cell. While this has no obvious way of causing rapid excitatory responses in neurons, it could play a role in the slow inhibitory or other neuromodulatory effects.

Other aspects of the cytoskeleton could also have a significant effect on both immediate and downstream effects of the US. Actin filaments for example are thought to act as tension sensors, playing an active role in signal transduction [Galkin et al., 2012]. They could also serve as membrane anchoring points, inhibiting the free movement of one or both leaflets of the membrane at specific points thereby possibly increasing membrane tension. Deformation of cells in culture by amounts up to 2 μm and membrane contraction resulting in cell volume decrease have even been observed in responses to low power levels of ultrasound [Hu et al., 2014, Muratore et al., 2009], although the simple metrology of stimulus intensities and resultant forces of the Muratore study has been disputed as it is surprising that such low intensities are able to generate large effects [Gavrilov and Tsirulnikov, 2012].

A new theory based around differential impedances of organelles has been proposed where the difference in forces acting on different parts of the cell may be setting up resonant effects in the 10-100kHz range that could be having impact on cell function through repetitive strain and fatigue-like effects [Or and Kimmel, 2009]. From the current perspective though this theory seems unlikely as the authors only predicted strains of 0.5% at frequencies much lower than those typically used in successful US neurostimulation.

One way to explain the mechanosensitivity of nerve axons generally and in response to ultrasound could be the Soliton model. This is an alternate to the standard Hodgkin-Huxley model of axonal signal conduction where instead of a propagating electrical potential and voltage gated ion channels, the signal is conveyed by a compression wave along the axonal membrane, much like a sound wave [Andersen et al., 2009]. In fact mechanical waves in the axon are well established to travel along with the propagating action potential [El Hady and Machta, 2015, Tasaki et al., 1989], causing local changes in volume, pressure [Barry, 1970] and optical properties [Tasaki and Byrne, 1993]. Though the Soliton model alone cannot explain many observations of nervous conduction (such as collisions [Tasaki, 1949]), it is clear that there is a mechanical component to axonal transmission which is usually ignored in the literature and as such, is still poorly understood. More research into this area will have to be performed before it is clear if and how the mechanical component is connected to signal transmission and how ultrasound might interact with it.

As well as axonal transmission, there are several other mechanical processes and events that occur in neurons where US's effect have never been assessed such as spine twitch [Crick, 1982] or actin mediated conformation changes [Star et al., 2002] either or both of which may be affected by US stimulus [Tyler, 2012] and which are inter-linked with each other and other cellular processes and structures such as ion channels. This builds the idea that US may be producing many simultaneous, combinatorial effects in any one cell that will need to be dis-entangled at some stage to fully understand and utilise the individual phenomena. The hope is that there will be one dominant effect of the US that can be understood and manipulated easily such as immediate axonal depolarisation.

2.3 Energy Transduction Mechanism

Understanding how the US wave generates the key causative forces required for neurostimulation is essential for a full comprehension of the US-nerve interaction and is very closely tied in with determining the affected biological structure, as answering one question will certainly contribute to our understanding of the other.

The 5 influences of US propagation through living tissue are outlined by Wulff et.al. in 1951 as: ”(1) heating caused by absorption of acoustic energy;’ (2) periodic pressure changes; (3) radiation pressure; (4) streaming or flow in viscous media; and, (5) inertial and stable cavitation”. These serve as a complete list of the possible, broad mechanisms through which US elicits neurostimulation. In this section, the logic of, and evidence for the involvement of each in US neurostimulation will be discussed.

The first point mentioned, heating, is discounted as a stimulation mechanism in the literature and in this study due to the low average intensities or short pulse durations making the predicted heating negligible (<0.1°C) in most examples of neurostimulation [Kim et al., 2012, Lee et al., 2015, Tyler et al, 2008, Yoo et al, 2011b].

Despite the passage of more than 60 years it has still not been determined which of the remaining mechanisms is the primary source of bio-effects in nerves. Of course all of them may be occurring to some extent but the importance of each will change based upon the parameters of the US stimulus being applied and the structure of the tissue. Hence the community must focus on a tight set of parameters which are optimum for eliciting certain desired effects so that its effect in different tissues can be determined, or vice versa. In the case of neurostimulation no ”optimum” or desirable characteristics of the US stimulus have been arrived at by any consensus in the past literature which leaves the conjecture about the mode of action and method of energy transduction very open.

It is likely that there are multiple ways of bringing about an excitatory effect using US. By using sonication parameters or a particular tissue environment that maximises compression due to radiation force (e.g. nerves against bone) or by causing cavitation or even direct pressure effects on proteins, excitatory effects could be produced. This multiplicity of different possible stimulation routes is largely ignored in the literature but could go a long way towards explaining the wide range of successful parameters as well as seemingly contradictory trends and proposed mechanisms, which highlights the need for a concerted effort aimed at isolating and characterising the full range of possible US-tissue interactions at a fundamental level.

Radiation force, or the radiation force envelope has been widely implicated in past studies, mainly based on observations of stimulation occurring at the beginning and ends of pulses [Dalecki et al., 1995, Gavrilov et al., 1977, Gavrilov and Tsirulnikov, 2012, Menz et al., 2013] which is when tissue motion will occur. This may explain the prevalence and success of rapid trains (PRF>1kHz) of very short US pulses, popular in recent protocols for neurostimulation [Kim et al., 2014a,b, Legon et al., 2012, Moore et al., 2015, Tyler et al, 2008, Yoo et al, 2011a, Younan et al., 2013] as they maximise the tissue movement due to radiation force. Shorter pulses also create higher harmonics with greater absorption and tighter beam paths from non-linear propagation [Rudenko et al., 1996] which increases radiation forces and steepens force gradients and resultant tissue sheer stresses. However, some recent studies have challenged the importance of pulsing, reporting that pulse length does not have an effect when averaged power is kept constant [Colucci, 2009, King et al., 2013, 2014, Menz et al., 2013, Vartanyan et al., 1990] and it is the author's opinion that radiation force cannot account for recent studies in the CNS which will be discussed in the next section.

2.3.1 Radiation Force

Within soft tissue, radiation force will produce forward motion in the focal area until the elastic tissue reaches an identical counter force or until the pulse ends, and the reverse motion occurs when the force stops. This motion will be acting at the beginning and ends of each US pulse and repeated at the PRF. When using a focused transducer, tissue displacement will create static compression at the front, stretch at the rear and shear stress around the focal area, the gradients of which will depend on the intensity profile of the US focus.

It has long been known that mechanical pressure on nerves can either have stimulatory or inhibitory effects depending on the force applied [Julian and Goldman, 1962a]. It therefore may be possible that short pulses are applying a ”flick” to neural matter, which could cause action potentials to fire in the ways discussed in section 2.2. If sufficient radiation force can indeed be produced by US stimulation, it is most likely to have been the dominant factor in early observations by Gavrilov's group where much higher intensity exposures were used (up to 4000 W/cm^2, [Gavrilov, 1984]), as well as other groups showing effects in the skin [Dalecki et al., 1995, Gavrilov et al., 1996, Lee et al., 2014, Wright et al., 2002], since it is known that skin structures (which represent a reflective phase change from the water transmission path) are sensitive to minute pressures of less than 4 mN applied by Von Frey hairs [Garrison et al., 2012]. However it is not clear if the same force is responsible for more recent neurostimulation studies in the CNS as these tend to use much lower focal intensities on structures that are not specifically mechanosensitive.

Of the US effects mentioned in section 2.3, radiation force is the easiest to model and understand and therefore predict its influence on tissues. Estimates of forces generated in previous studies successfully demonstrating neurostimulation can even be made. The acoustic radiation force acting in Tyler et.al's paper (2008) can be calculated by the equations [Duck, 1990, Nightingale et al., 2001]:

$$I_{SPPA} = \frac{P_a^2}{\sqrt{2}Z}, \qquad (2.1) \qquad\qquad F_{abs} = \frac{2\alpha I_{SPPA}}{c}, \qquad (2.2)$$

where I is the spatial peak, pulse average intensity, P_a is the temporal peak US pressure, Z is the characteristic acoustic impedance of brain tissue (1.6e^6 Rayls), F_{abs} is the radiation force due to the absorption of acoustic energy, α is the attenuation coefficient of neural tissue in nepers per meter calculated from equation 2.4 and c is the speed of sound in soft tissue at room temperature (1562 m/s) [Roy, 1991]. These equations assume plane wave and linear propagation. Equation 2.2 is a linear approximation based on a derivation of the Navier-Stokes equation [Doherty et al., 2013, Nowicki et al., 1996] which does not take into account the non-linear waveform, scattering or boundary reflection effects.

Calculating the pulse averaged spatial peak force that should be present in Tyler's study using the values, α = 5.7 nepers/m measured at 1 MHz [Roy, 1991], c = 1562 m/s [Duck, 1990], I = 2.9 W/cm^2 (I_{SPPA}) [Tyler et al, 2008] yields a volume force of 0.19 mN/cm^3.

Given that some mechanosensitive and voltage sensitive tissues have been identified with shear stress force thresholds at 0.01 mN/cm^2 or lower [Cho et al., 2002, Olesen et al., 1988] (Figure 2.3 (1 mmHg = 13 mN/cm^2)) it is possible that sufficient membrane stretch or cellular deformation could be generated to affect them. However, these shear stress forces are not quantified in the literature and cannot be easily modelled without more accurate quantification of the experimental ultrasonic field and tissue properties.

A simpler more comparable measure to this calculated US radiation force would be those collected by Rivera et al. [Rivera et al., 2000], measuring the bulk mechanical force threshold for stimulation of a rat peripheral nerve neuroma by application of a blunt glass rod (1.2 mm diameter). Though the inflammation associated with a neuroma makes this model more sensitive than a natural peripheral axon, the threshold range they found was 3.90-30 mN or 86-670 mN/cm^2, significantly above the radiation force estimates presented here but similar to the findings for skin [Garrison et al., 2012] or tongue receptor sensitivity [Trulsson and Essick, 1997]. Though the nerve model and test environment differ, with more than a factor of 10 difference between these and Tyler's estimated forces, radiation force is not expected to have been the source of the excitation in their study but may be in studies using much higher intensities or frequencies.

Though the membrane stretch forces or shear stresses produced in previous studies cannot be modelled with any confidence, the shape of the tissue displacement profile as a result of US exposure can be understood by modelling radiation force as a point force in a fully elastic solid using the equation [Nightingale et al., 2001]:

$$PD = \frac{P_{rad}(1+v)(4z^2(v-1)+r^2(4v-3))}{8E\pi(r^2+z^2)^{\frac{3}{2}}(v-1)}, \tag{2.3}$$

where PD is the maximum particle displacement, z is the distance along the force axis from the point force, r is the radial distance away from the axis (Figure 2.4), v is Poisson's ratio, E is the Young's modulus of the material and P_{rad} is the applied force [Nightingale et al., 2001].

The point force assumption means that the maximum displacement at the location of applied force is infinite but assuming a tightly focused ultrasound beam (ideally sub millimetre diameter), the displacement field predictions are informative. Using values from the literature of v = 0.469 [Soza et al., 2005] and E = 9 kPa [Soza et al., 2005] and a radiation force of 10 mN, we can see from figure 2.5 that displacement

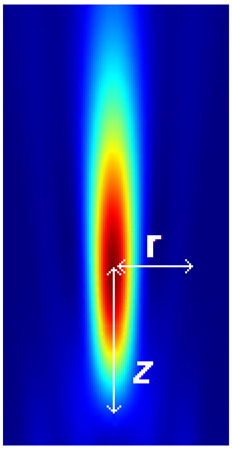

Figure 2.4: Conceptual distribution of tissue displacement as a result of radiation force from a focused ultrasound transducer. Geometry of r and z used in equation 2.3.

reduces exponentially away from the area of force application, dissipating to negligible levels 0.2 mm away from the point force. Shear stress in soft tissues will therefore be concentrated in very close proximity to the beam axis in the areas of steep US intensity (radiation force) gradient, with the shear maximum forming a hollow cylinder shape around the beam axis.

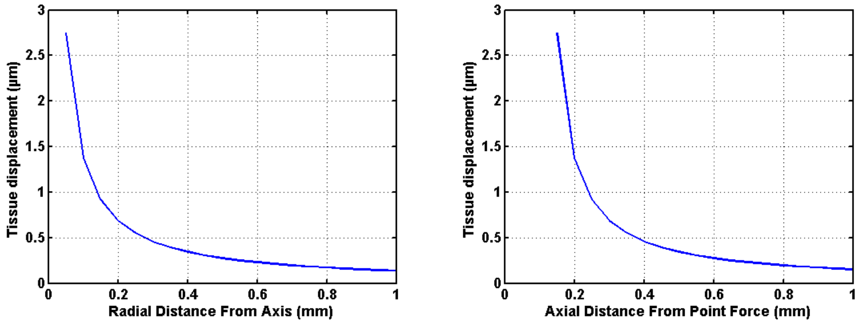

(a) (b)

Figure 2.5: Theoretical calculations using equation 2.3 for tissue displacement in the direction of beam propagation (a) at radial distances away from the beam axis and (b) at axial distances away from the point force.

Accurate analysis of the spatial geometry of US stimulation using focused transducers may therefore be an excellent way of characterising the key mechanism within any radiation force neurostimulation. Current attempts to map the stimulated area [Kim et al., 2014b, Yoo et al, 2011a] in the brain do not have high enough resolution to identify the geometry of activation around the focal region and no reports have yet suggested particular distributions. A study by Kim et al., in 2014 in fact found that the area of stimulation was actually smaller than the focal area of the transducer (measured by Full Width Half Maximum (FWHM)) [Kim et al., 2014b]. As the radiation force gradient is still high at the half maximum amplitude, this result could indicate that shear stress is not the cause. However, the group's findings are likely to have been confounded by the complex US field reflections and standing waves within the rat's head which produce unpredictable intensity patterns, opposing radiation forces from reflections and sub-wavelength peaks [Younan et al., 2013].

From this simple modelling of radiation force and displacement it seems unlikely that the direct radiation force produced in recent low intensity ($<$10 W/cm^2) nerve stimulation protocols will reach thresholds known to affect or open mechanosensitive ion channels through tissue compression, tension or shear forces. Though of these possibilities, the effect of sheer stress warrants further investigation.

As mentioned at the start of this section, studies targeting peripheral nerves more often use protocols that produce potentially stimulatory, super-threshold radiation forces and have found response dynamics consistent with a radiation force mechanism [Dalecki et al., 1995, Gavrilov et al., 1977, Legon et al., 2012, Mihran et al., 1990, Wright and Davies, 1989]. Gavrilov et al. in particular found tactile stimulation force thresholds in a very similar range to the bulk force thresholds reported by Rivera et al. (13-16 mN/cm^3, estimated from reported intensity thresholds) [Gavrilov et al., 1977]. There have also been a few studies on the CNS with sufficiently high intensity thresholds to warrant further investigation into the importance of radiation force in the observations of each study [Choi et al., 2013, Legon et al., 2014, Menz et al., 2013], though these high intensity exposure protocols ($>$10 W/cm^2) are certainly in the minority.

Considering the bulk of the CNS stimulation literature, if radiation force was a significant mechanism then shorter wavelengths would be more effective (as they generate greater absorption forces and therefore greater pressure gradients) whereas the prevailing observation is that longer wavelengths (lower frequency) have a lower stimulation threshold and higher success rates in both central and peripheral nervous studies (Figure 2.6) [Gavrilov and Tsirulnikov, 2012, King et al., 2013, Lee et al., 2014, Mona, 2007, Muratore et al., 2009]. Although one study has shown success at the much higher frequency of 43 MHz carrier signal modulated at 15 Hz to 1 MHz [Menz et al., 2013].

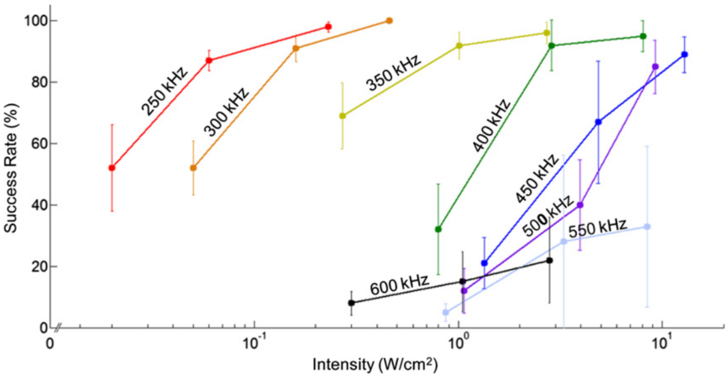

Figure 2.6: Adapted from King et.al., 2013 [King et al., 2013] showing an extensive study performed on 3 mice where the effect of frequency and intensity were tested on the response reliability of US neurostimulation. All data points were averaged over the 3 animals. Error bars represent the standard-error of the mean. Intensities were measured using a hydrophone.

Though the modulation frequency was similar to fundamental frequencies used in the neurostimulation literature, they found as long as the average power was kept the same the modulation frequency actually had no effect. If the same calculations applied earlier in this section to Tyler's study are applied to the intensities and frequencies used in Menz's work, the resultant radiation force would be 0.88 N/cm^{-3}, easily over the bulk force thresholds expected to cause stimulation [Rivera et al., 2000]. This large difference results from the attenuation coefficient (α) of soft tissue, which varies with frequency according to a power law as shown by the equation:

$$\alpha = \alpha_0 f^y, \tag{2.4}$$

where f is frequency and y is the frequency dependence exponent. A frequency dependence exponent of 1.3 and α_0 of 8.6 (Estimate for brain tissue for brain tissue [Duck, 1990]) were used to model the attenuation at different frequencies and resultant radiation forces in the current work.

The findings of Menz et al., together with earlier literature [Dalecki et al., 1995, Gavrilov and Tsirulnikov, 2012, Lee et al., 2014, Mihran et al., 1990, Wright et al., 2002] suggests that US radiation force is capable of reaching stimulatory thresholds and may therefore be the dominant force mechanism when high frequency or high acoustic intensities are implemented. These observations of radiation force stimuli are characterised by observations of activation on pulse onset and offset when tissue motion would occur [Dalecki et al., 1995, Gavrilov and Tsirulnikov, 2012, Mihran et al., 1990]. However, in the main body of recent CNS studies, the nature of the observed stimulation, the low intensities and low frequencies used, make primary radiation force unlikely to be a dominant factor in these.

2.3.2 Acoustic Streaming

Typically acoustic streaming refers to bulk flow set up in viscous media by the time averaged radiation force. This cannot occur in structured tissue such as in the brain but could appear in *in vitro* experiments with larger free fluid volumes. However, regarding its importance to stimulation observations in the literature, given the short stimulus durations used in US neurostimulation and usually very short unrestricted fluid volumes used *in vitro*, bulk fluid streaming is not a possible mechanism *in vivo* and unlikely to contribute *in vitro*.

Acoustic streaming can also be referred to as micro-streaming, where higher localised forces and liquid flow on the micro-scale are created, usually from stable cavitation. This can cause membrane deformation, shear stress in the extra-cellular matrix or even perforation of a membrane. This mechanism was in fact a major part of Tyler's continuum mechanics hypothesis for ultrasonic neurostimulation [Tyler, 2010]. Others claim that bubbles of a sufficiently large size to elicit micro-streaming are not expected to be present within soft tissue under normal conditions [Leighton, 1994]. With the absence of large microbubbles in tissue the author believes that this is not likely to contribute to neurostimulation in the CNS but should be considered in experiments where microbubbles may be present such as those performed *in vitro*. Further evidence for the presence and involvement of bubbles and cavitation will be discussed in section 2.3.4.

2.3.3 Pressure Oscillation

As the US pressure wave travels, tissue will be subject to alternate positive and negative pressure cycles, compressions and expansions will be caused according to the compressibility of the tissues in question. The compressibility of soft tissue is similar to that of water [Cowin and Doty, 2007] and will therefore not change volume more than 1% at the pressures involved. Oscillatory tissue motion or strain from compression at PRF or fundamental frequencies are therefore deemed not to be a significant factor in neurostimulation.

2.3.3.1 Molecular Effects

Though bulk compressibility of soft tissue is low, individual proteins are often very sensitive to pressure [Mozhaev et al., 1996]. Ultrasound can therefore interact with individual molecules and cause conformational change, affect solvent interactions and hydration [Caruso et al., 2009] or hydrophobic thickness.

The research field of static pressure effects on proteins [Mozhaev et al., 1996], cells [Frey et al., 2008] and other biological systems or molecules is large and this section is not intended to be a comprehensive review but should serve as an illustration of the scope of the field.

Static pressure is known to have several effects on the kinetics of voltage gated ion channels which is studied as an important factor in the effects of deep sea diving and in the physiology of marine animals like the crabs used in the current study [Macdonald, 2002]. For example, high pressure is specifically known to activate some large conductance potassium channels which, alone, would hyperpolarise and inhibit nerve firing given potassium's Nernst (equilibrium) potential of approximately -90 mV [Alberts et al., 2002]. More generally, all water soluble domains of proteins can be affected by pressure as well as altering the ordering of hydrocarbon chains in a membrane, changing the fluidity properties or causing phase transition [Kato et al., 2002]. Affecting lipid membranes in this way can also affect the membrane thickness, and change the properties or state of the proteins (including ion channels) within them.

When sufficient non-linear acoustic propagation occurs during transmission through a fluid, the compressional US peak pressure will be higher than the rarefactional for a focused beam. This difference will increase in tissues with higher non-linear propagation effects and for larger travel distances, resulting in a time-averaged positive pressure which could have effects analogous to static pressure. However, studies on lipid membrane phase transition tend to use much higher static pressures ($>$10 MPa) and timescales in the range of seconds to demonstrate effects [Winter and Jeworrek, 2009], whereas peak pressures used in neurostimulation are usually far below this (Table 4.2) and time averaged pressures even lower. Total stimulus durations are also typically under a second. The effect should therefore be considered more closely in protocols with high intensity, longer exposure time or a high degree of non-linearity, but is not expected to be a major factor in currently successful US neurostimulation protocols.

It is possible that some known static pressure effects on channel conduction can translate to a microsecond timescale, transiently affecting sensitive ion channels or other structures periodically with the pressure waveform, thus altering the time averaged conductance of the channels. Studies have shown that ion channels can indeed change conformation within the timescale of a single compression or rarefaction phase [Bjelkmar et al., 2009], and that many MS ion channels also have a negative pressure threshold in the range of kPa [Hamill, 2011], well within the range of pressures that are used in US neurostimulation protocols and later in this study. There is also a growing area of research into the effects of ultrasound in DNA damage for intensities of 10-42 W/cm^2 [Chandran et al., 2015], or albeit at lower frequencies, on the structures of proteins for food processing applications [Chandrapala et al., 2011, O'Sullivan et al., 2016].

In terms of correlation with the literature, a direct pressure oscillation mechanism does not fit with observations of stimulus occurring at beginning or end of pulses [Dalecki et al., 1995, Gavrilov and Tsirulnikov, 2012, Mihran et al., 1990], the unreliable response dynamics [Kamimura et al., 2015, King et al., 2013, Younan et al., 2013], or apparent usefulness of pulsing itself [Dalecki et al., 1995, Gavrilov et al., 1977, Lee et al., 2015, 2014, Menz et al., 2013]. However, this mechanism does provide an alternate explanation for the observed frequency dependence of the neurostimulatory effect (Figure 2.6).

There is currently not enough information on the effects of US on the compressibility of relevant biological proteins and the transient or permanent conformational changes that it can cause. Therefore, given imperfect fit with current observations in the literature, oscillating pressure effects on molecular conformation is not expected to play a significant role in the immediate US stimulation effect but warrants further investigation as the research progresses.

2.3.4 Cavitation

Cavitation, as defined in section 1.1.5, is most often brushed aside as a potential mechanism in the literature due to the low intensities used to elicit neurostimulation [Deffieux et al., 2013b, Lee et al., 2015, Tufail et al, 2010, Yoo et al, 2011a], below the FDA recommended MI limits for soft tissue ultrasound [Duck, 2007]. The limitations with this claim however are firstly that the MI limit is concerned only with preventing inertial cavitation of sufficiently large bubbles to cause significant damage, and secondly, that MI is only a guide and cannot be used to truly predict the occurrence of cavitation as this will depend on the tissue type, bubble nuclei, dissolved gas content and other factors. Though some studies have reported very high pressure thresholds for *in vivo* cavitation in the brain [Gateau et al., 2011], others have found significant non-inertial cavitation at much lower intensities (240 mW/cm^2) [ter Haar et al., 1982, Ter Harr et al., 1986]. Though these two studies had much longer duration exposures of over a minute, the finding does indicate that bubble nuclei can be affected in some way by low intensities over much shorter durations.

Several studies have failed to detect cavitation by light microscopy during US exposure [Tyler et al, 2008], and afterwards to detect tissue damage [Tyler et al, 2008], through MR imaging [Yoo et al, 2011a], or changes in animal behavioural tests after 7 days [Tufail et al, 2010]. Combined with the high pressure requirements it seems reasonable to conclude that large scale tissue damage from inertial cavitation is not a contributing factor in any study showing successful stimulation in the CNS, though this is less certain for PNS studies. However, in these same studies, non-inertial or even non-resonant stable cavitation could play a critical role. In the current study, for the first time, a PCD is used to detect cavitation simultaneously with US neurostimulation protocols. High sensitivity is achieved because acoustic emissions from bubbles are unimpeded by overlaying tissue layers and a novel, sensitive method of analysing these signals is employed to detect and characterise cavitation (Section 4.7.2).

The evidence thus far for cavitation as a mechanism comes entirely from the strong preference in many studies towards low fundamental frequency [Gavrilov and Tsirulnikov, 2012, King et al., 2013, Lee et al., 2014, Muratore et al., 2009, Tych et al., 2013] which also detracts from radiation force as a mechanism, leaving cavitation to be a likely factor in these studies. However, the implication of cavitation is contravened by conventional bubble mechanics, which predicts that it should not occur without pre-existing stable bubbles or bubble nuclei within the tissue, which are not present in normal tissue at a suitable size [Leighton, 1994]. According to the Laplace-Young equation:

$$\Delta P_b = 2\gamma H, \tag{2.5}$$

where ΔP_b is the pressure difference across the bubble surface, γ is the surface tension and H is the mean curvature. At atmospheric external pressure a 10 nm bubble would have to have an internal pressure of 144 atmospheres to sustain itself. This simple mechanics predicts spherical bubbles in liquid media smaller than 1 µm will dissolve into the liquid unless the media is super-saturated with gas. Despite this, nanobubbles are observable in gelatin and distilled water [Yount et al., 1984] and nuclei must be present in some form for observations of bubble growth in tissue under US [ter Haar et al., 1982, Ter Harr et al., 1986] or static pressure (such as from Decompression Sickness (DCS)) to occur. The questions of what these nuclei are, where they might be located and how they might respond to US raise themselves. If pre-existing bubbles do exist in tissues *in vivo*, then finding their location may be key to determining the specific effects of US in the tissue.

One explanation for the existence of bubble nuclei within tissues is the Varying Permeability (VP) model, the essence of which is that small bubbles ($<1\ \mu$m) are able to resist collapse through a skin of amphiaphilic molecules that provide compression strength [Leighton, 1994, Yount, 1997]. These bubbles could potentially exist in solution both inside and outside cells. The model has been used to create diving tables for humans to avoid DCS [Yount, 1982]. Bubbles may also be occurring in hydrophobic crevices, though neither theory has been experimentally verified as yet [Papadopoulou et al., 2013]. The random occurrence, number or size of these nuclei within the ultrasound focus may well explain the variable response reliability seen in the literature [King et al., 2013, Younan et al., 2013], which is not satisfactorily accounted for by any of the other proposed force mechanisms.

Though there is still much that conventional mechanics cannot explain about nanobubble behaviour [Weijs et al., 2012] and what form *in vivo* cavitation nuclei take, much progress is being made in this field. Research using Atomic Force Microscopy (AFM) measurements has shown that their stiffness is much lower than conventional mechanics predicts, similar in fact to measurements from microbubbles [Walczyk and Schönherr, 2014, Zhao et al., 2013], potentially due to charged particles or solutions on their surface [Duval et al., 2012, Jin et al., 2007]. Nanobubbles have also been shown to respond to transient pressures [Andersen and Mørch, 2015] and to be effective cavitation nuclei [Belova et al., 2010]. Given these new nanobubble insights, low intensity ultrasound may well be significantly interacting with them to elicit neurostimulation through one of the above proposed mechanisms.

Another recent theory in the neurostimulation literature is that nanobubbles can form in the intra-membrane space of a lipid bilayer [Krasovitski et al., 2011, Plaksin et al., 2014, Rappaport et al., 2013] (Figure 2.7) which would apply a modified form of the VP model. Despite the highly hydrophobic environment, usually ideal for gas phase formation there is an entropic force as well as Van der Walls and charged ion attraction and repulsion [Ohshima, 2010] that normally prevent any gas phase from nucleating in the intra-membrane space and the leaflets from coming apart. If bubbles are formed within a continuous bilayer the surfactant skin would not provide the same compressive strength as in the standard VP model because the bubble formed would be lens shaped [Rappaport et al., 2013], not spherical. However, tension between the two leaflets may occur in specific places such as at cytoskeletal attachment points or in areas where there is hydrophobic mismatch between the membrane and trans-membrane proteins. Hydrophobic mismatch is where lipid bilayer thickness does not match with the hydrophobic transmembrane region of a protein, such as an ion channel. This creates an entropically unstable state. Some proteins are permanently in this mismatched state, which may result in the membrane leaflets being held apart around the protein. The latter of these possibilities would place the bubbles in direct contact with the ion channels themselves, possibly allowing the minute changes in bubble radii to have significant effect on the channel kinetics.

Critical evidence for this theory comes from one of the long-range attractive forces acting between the two hydrophobic surfaces at the scale of several hundred nanometers. This was first suggested by Parker et.al. in 1994 [Parker et al., 1994] to be due to the entropic attraction of bubbles that had formed on both hydrophobic surfaces [P., 2003]. This finding has been confirmed recently using AFM to directly observe flat nanobubbles which have formed spontaneously on hydrophobic surfaces, going on to propose that these may act as the nuclei for DCS bubble formation [Arieli and Marmur, 2011].

Krasovitski et.al were the first to make this potential link between intra-membrane bubbles and neurostimulation, using destructive intensities of US to demonstrate generation of large, observable cavitation related damage predominantly associated with membranes [Krasovitski et al., 2011]. They claimed these were evidence that the nucleation points for bubble formation must be associated with the biological membrane, and furthermore that bubble nucleation was occurring between the 2 leaflets of the membranes. It was concluded that these bubbles were the primary site and mechanism of action for many non-temperature US induced bioeffects, not just neurostimulation.

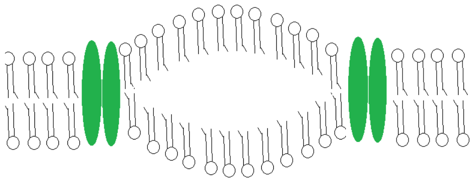

Figure 2.7: Schematic diagram of how intra-membrane bubbles might exist as lens shaped expansions of the bi-layer lipid membrane between trans-membrane protein anchoring points.

The reasoning for such a hypothesis is immediately apparent as even very small bubbles forming intramembranously could result in forces acting on ion channels and other structures sufficient to cause conformational changes. With different membrane properties and tissue types and the huge variety of proteins that this mechanism might be affecting it is easy to see how it might account for the range of different US induced bioeffects described in section 2.1.3. One of the most likely forces that this would cause on transmembrane proteins especially is hydrophobic mismatch, where the altered membrane thickness would result in a hydrophobic membrane thickness that did not match up with the fixed hydrophobic thickness of an adjacent protein (Figure 1.1(b)). This has been shown to change the free energy state of proteins, resulting in an altered probability of being in an open state, even with very small thickness changes [Marsh, 2008, Ursell et al., 2007, Yefimov et al., 2008].

An alternate theory on how these intra-membrane bubbles may cause stimulation is through the flexo-electric current phenomena described in section 2.2.3. A capacitive current would also be generated as the membrane changes thickness.

Krasovitsky's model and other bubble based mechanisms will increase their generated forces proportionally to the pressure amplitude and inversely proportional to the square root of the frequency. This means higher pressure and lower frequency would be desirable for creating strain on the membrane and therefore the ion channels which is again largely consistent with observations (Figure 2.6) [Krasovitski et al., 2011, Lee et al., 2014, Rappaport et al., 2013]. Further modelling in 2013 revealed that if intramembrane bubbles do exist, their behaviour and predicted US threshold parameters are seemingly in good agreement with the literature [Plaksin et al., 2014]. However, the main conceptual issue with this theory at the moment remains the nucleation of the bubbles.

The models proposed by these studies also do not take into account the non-spherical bubble shape or the tension in the membrane both of which will increase the surface tension making bubbles of this nature less likely. Without a solution to this, nor an explanation of how the initial conditions occur, the simple nanobubbles proposed in the VP model seem closer to reality and have been observed by multiple sources. The VP model therefore is considered by the author the more likely candidate for cavitation nuclei that may be excited to elicit US neurostimulation.

A third hypothesis for US-bubble interactions affecting nerve excitability can be drawn from a model for ion channel gating that involves bubbles within the channel itself [Roth et al., 2008]. These bubbles are proposed to exist within the pores of specific channel types to explain universal but unexplained observations of ion channel open state instability [Eisenberg, 2008]. The instability of these bubbles would make it highly likely that the pressure differences induced by US would have an effect on them and directly influence the channel open probability. This gating theory is a result of predictions of ion channel behaviour by computational models and not yet linked to any experimental data. Due to the minute physical and time scales in question, the model's predictions have proved so far impossible to test or prove experimentally. To the author's knowledge no further investigation into this channel gating model has been made.

2.3.4.1 Rectified Diffusion

Rectified diffusion is an averaging of the diffusion processes over the course of a bubble's oscillation towards expansion or shrinkage of the cavity, which may affect the size distribution of a population of bubbles over the course of an US exposure. If tension is considered in a bubble with a surfactant shell, such as proposed in the VP model, then permeability during rarefaction increases as surfactant molecules are pulled further apart, and decreases during compression thus allowing more gas to diffuse in during rarefaction and less to diffuse out during compression [Yount, 1982]. VP skins can even become impermeable to gas if exceeding just 0.8 MPa pressure [Yount, 1997], below the peak positive pressures generated in the present study. Surface area will also be higher during rarefaction, allowing more gas to diffuse in than out.

Modelling work on unbounded bubbles suggests that inertial cavitation thresholds are below the thresholds for rectified diffusion in bubbles smaller than 400 nm [Church, 1988, Louisnard and Gomez, 2003]. This raises the possibility that the US is actually causing collapse rather than growth of pre-existing nanobubbles to produce cellular effects, though all bubbles in the VP model and intra-membrane bubbles are surfactant bound. The smallest bubbles modelled by Church were 100 nm radius and these had thresholds for positive rectified diffusion of 0.6-0.8 MPa which is within the range of pressures used in US neurostimulation, and close to the predictions of the VP model.

Rectified diffusion has less of an effect with shorter timescale exposures and will be reduced by using lower DC pulses, both of which are relatively small in successful neurostimulation studies [Tyler et al, 2008, Yoo et al, 2011b]. The size distribution of any population of bubbles is therefore not likely to be significantly affected by rectified diffusion in most stimulation protocols but may change due to inertial collapse of some fractions.

Though there are still many questions to be answered, from the fit with the successful neurostimulation protocols in the literature, some form of *in vivo* cavitational mechanism strikes the author as the most prominent mechanistic option.

2.4 Summary

In terms of the mechanism behind US neurostimulation, the weight of evidence currently implicates ion channels as the critical force sensor, although upstream mediators cannot be ruled out. How these channels are activated by the US is less clear, with significant evidence both for radiation force in some cases and cavitation in others being the critical factor. It is the author's opinion that neurostimulation will be possible using protocols favouring either of these dominant forces to affect the same or similar biological targets.

With this view, it seems likely that multiple modes of action are at play with US exposure, the balance of which determines the overall short and long term effects on the cells. These will vary between different tissues due to the presence of different biological structures being affected and different dynamics of US absorption/transmission/reflection. The combination of these variables is fully capable of giving the wide variety of responses to US seen in different tissues as well as seemingly contradictory results in some studies. With a better understanding of exactly how the US interacts with tissue on a cellular and molecular scale, a much greater range of successful stimulus options may become possible as the optimum pulse parameters for different US force mechanisms could be determined for any given tissue composition and location, allowing adaptation of the technique to different roles with trade-offs between specificity, tissue depth, reliability, safety and other factors.

Chapter 3

Rat Saphenous Nerve

Initial experiments were conducted to test for the existence of a directly stimulatory effect of US exposure in mammalian nerves. The phenomenon identified in these experiments and its mechanism of action was then investigated in a crab leg nerve model in two separate experiments. The design and protocol of each experiment is described in the section.

3.1 Experimental Protocol and Apparatus

3.1.1 Design and Justification

This experiment was developed to test for the presence of an US neurostimulatory effect in mammalian peripheral nerves, using well known and tested electro-physiological methods [Maurer et al., 2007]. Peripheral nerves were opted for over CNS neurons or an artificial membrane model to provide the best tradeoff between simplicity and relevance and the best capability for creation of a simple acoustic environment. Population recordings were chosen over a single unit approach to give greater chance of detecting low probability cellular level stimulation events.

In order to maintain a liquid US transmission path between the HIFU transducer and the target, a solid coupling cone was designed that also allowed the transducer to be submerged and turned over, ensuring the absence of bubbles on any surface. The second function of the cone was to aid the targeting of the ultrasound beam.

3.1.2 Equipment Details

The equipment used in the current setup shown in figure 3.2 is detailed here. US stimulus waveform was produced by an Agilent 33220A function generator amplified by

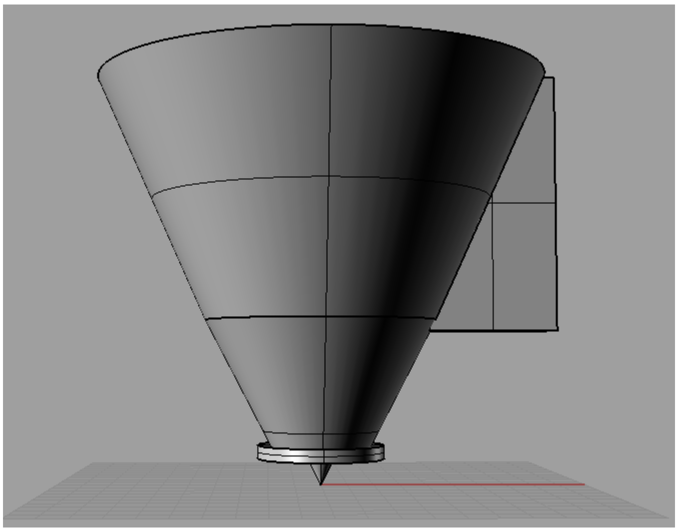

Figure 3.1: 3D CAD image of the transducer holder and projected focal point. Image taken in Rhino-ceros 3D NURBS modelling for windows.

Model	Manufacturer	CF (MHz)	Focal Length (cm)	Aperture (cm)	LFA (cm)	WFA (cm)
PA409	Precision Acoustics	0.67	7.2	6.0	4	0.5
H-101-MR	Sonic Concepts	1.1	6.3	6.4	1	0.14
H-106	Sonic Concepts	2	6.3	6.4	0.6	0.08

Table 3.1: HIFU transducer reference table. CF = Centre Frequency, LFA = Length of Focal Area, WFA = Width of Focal Area. Focal area dimensions are given according to the FWHM.

an E&I 1020L 200 W class AB linear power amplifier with 55 dBm gain. The transducer used for 0.88 MHz ultrasound generation was a Sonic concepts HIFU transducer, Model H-101-MR (Table 3.1.2) with an impedance matching network for fundamental resonance, specifically tuned to 858 kHz and 1.180 MHz. Electrical recordings from the nerve were taken using a Krohn-Hite 3945 - bandpass filter with upper limit of 2 kHz and lower of 2 Hz and a CED 1902, Cambridge Electronic Design isolated differential amplifier. Electrical data was plotted on a LeCroy 9304 oscilloscope and saved on a PC. The coupling cone (Figure 3.1) was designed in Rhino-ceros 3D NURBS modelling for windows and built by Selective Laser Sintering (SLS) out of PA2200, a lightweight powder sintered polymer.

The ultrasound transmission path was modelled and the proportions of the coupling cone designed so that the transducer's focal point would lie exactly along the cone axis, 1 cm from the truncated apex. Low targeting error (±0.1 mm) relative to the predicted focal point was expected as this was the resolution of the rapid prototyping technique.

To keep the path of the ultrasound free of bubbles, the inside surface of the coupling cone was smoothed. The ridge at the end of the truncated apex (Figure 3.1) facilitated attachment of a latex bag (hanging length - 10 mm), providing an adjustable focal height and completing the water path to any target. Both the cone and latex membrane were found to have no effect on the amplitude or frequency spectrum (measured by differential FFT, where an FFT of the US signal with and without the coupling cone and latex bag was subtracted.) of the ultrasound at the focal point (Table 3.1.2) at two different driving frequencies. The minor amplitude differences shown in table 3.1.2 are thought to be due to minor shifts in the clamped transducer position as the sheath or cone was removed.

Frequency (MHz)	Transducer alone	With cone	With latex sheath
0.86	1	0.97	0.98
1.1	1	1.05	0.98

Table 3.2: Normalised amplitude values at the transducer focal point with and without the transducer holder in place and with and without the latex sheath.

Acoustic intensities were measured in degassed and deionised water using a plane tipped fibre optic hydrophone (Precision Acoustics) at smaller than -2 MPa pressures and extrapolated to greater pressure amplitudes using KZK modelling. More information on this technique can be found in section 4.6.

3.1.3 Nerve Preparation and US Stimulation Protocol

The skin and saphenous nerve were removed from the hind limb of a male adult Sprague-Dawley rat. The skin and nerve were then mounted with the inside of the skin facing up in a custom built nerve bath. This was filled with synthetic interstitial fluid consisting of (in mmol): 108 NaCl, 3.48 KCl, 26 $NaHCO^3$, 3.5 $MgSO^4$, 1.5 $CaCl^2$, 9.6 sodium gluconate, 5.55 glucose, 7.6 sucrose and 10 HEPES, titrated with NaOH to a pH 7.40. This fluid was maintained at 32°C and continuously cycled through the chamber and gassed with oxygen. The proximal end of the nerve was placed in a separate chamber, isolated from the main chamber by liquid paraffin. The nerve end was de-sheathed and attached to a gold wire electrode, the reference electrode was placed in the main chamber. A simplified diagram of this setup is shown in figure 3.2.

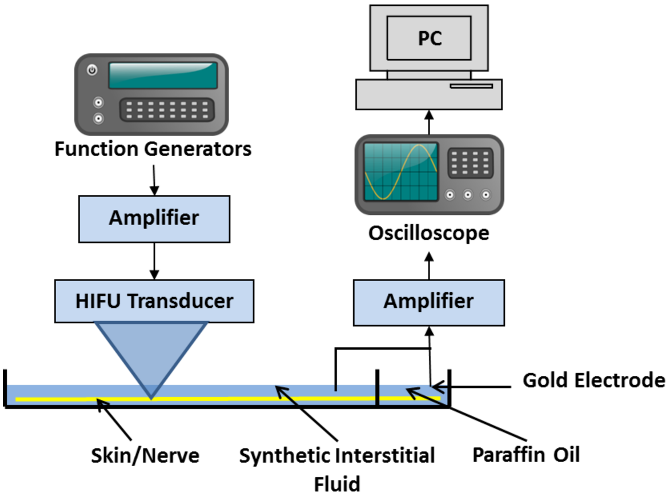

Figure 3.2: Schematic diagram of the experimental setup used to generate US stimuli recordings in the rat saphenous setup.

The transducer and cone apparatus were clamped above the nerve bath, exactly 10 mm from the surface of the nerve bundle (measured by a physical spacer, 10 mm in height, that was subsequently removed) and approximately 5 mm along the nerve bundle from the distal terminus that innervates the skin, measured by eye.

The preparation was stimulated with single US pulses with a PRF of 0.5 Hz at 858 kHz. Pulse length was originally fixed at 1 ms to analyse the effect of changing amplitude (Table 3.3) followed by an analysis of pulse length using a fixed amplitude of 1216 W/cm^2 (Table 3.4). For both the amplitude and pulse length experiments, 3 skin-nerve preparations in total were each exposed to the range of intensities or pulse lengths, repeated 30 times. 1 minute of recording preceded the beginning of each set of stimuli to act as a negative control to detect the rate of spontaneous Sensory Nerve compound Action Potentials (SNAPs). Aβ and C-fibre SNAPs were recorded with an isolated amplifier using a low pass filter of 2 kHz and a high pass filter of 2 Hz. After the end of each minute stimulus regime, the nerve bundle was mechanically stimulated with a blunt glass rod at the distal end where the fibres innervate onto the skin.

3.1.4 Data Analysis

The voltage traces were subject to ”spike2” CAP analysis software (Cambridge Electronic Design), for locating compound action potentials within the trace. SNAP templates were taken from responses to mechanical stimuli (blunt glass rod), administered to the distal portion of the nerve bundle after each set of exposures, and used to search the rest of the data for similar patterns in each recording. Response reliability was quantified through the counting of SNAPs that occurred during, or within 5 ms of the end of the US stimuli pulses, out of the 30 stimuli per nerve experiment. SNAPs detected within 5 ms of each other were regarded as one event. Significance of observations compared to null hypotheses were calculated using a Pearson's Chi Squared Test.

3.2 Results

In this *ex vivo* set up it was found that single US pulses can stimulate propagating action potentials (Figure 3.3). Received stimulation responses were multi-unit when received (involving the activation of many axons) but often entirely absent. These potentials were low latency (<5 ms after US exposure), giving an average conduction velocity of 12.4 m/s measured from the peak of the SNAP assuming instantaneous stimulation, AP initiation centrally within the US focus and no change in CAP waveform as it travels. Modelling using a Bio-heat transfer equation (Section 4.6) found that heating was under $0.1°C$ in all protocols.

3.2.1 Amplitude analysis

Examination of the effect of US intensity on response reliability (Table 3.3) shows a strong positive correlation. Of the measures that intensity also affects (temperature, radiation force and pressure), peak negative pressure values predicted by KZK modelling were seen to display the same, almost linear trend, as SNAP response reliability. It can be seen from these results that even at very high intensity values the response to ultrasound stimuli is only 80% reliable (24/30 US pulses resulted in SNAPs), declining to 40% at 1216 W/cm^2 and 23% at 284 W/cm^2 (Table 3.3).

3.2.2 Pulse Length Analysis

Pulse length was also found to have an effect on response reliability in the range of lengths tested using the highest amplitude exposure from section 3.2.1 (Table 3.4, figure 3.4). A plateauing was rapidly observed, with lengths above 10 ms providing no improvement to response reliability. Longer pulse lengths than 50 ms were not tested to avoid exceeding a $0.1°C$ temperature rise.

Spontaneous nerve activity was observed in every recording during the 1 minute

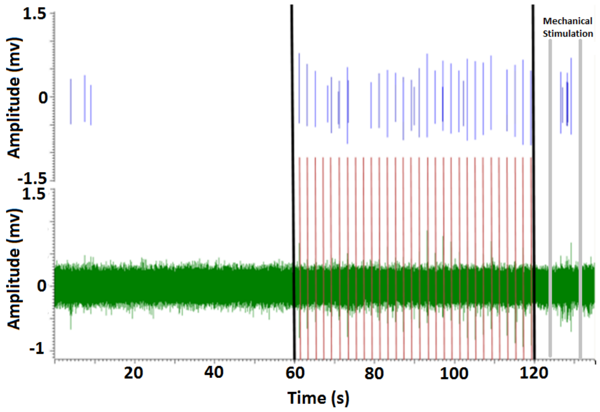

Figure 3.3: Recorded voltage trace from *ex vivo* Saphenous nerve of adult Sprague-Dawley rats stimulated with ultrasound. Recordings were taken for 1 minute without US. Ultrasound stimulus was then applied every 2 seconds for 1 minute with 0.86 MHz, 1 ms, 1216 W/cm^2 US pulses (indicated by vertical red lines), followed by a mechanical stimulus. SNAP amplitudes, detected using Spike 2 analysis software, are displayed above the voltage trace (indicated by the blue vertical lines). The start and end of the stimulus regime are marked by vertical black lines.

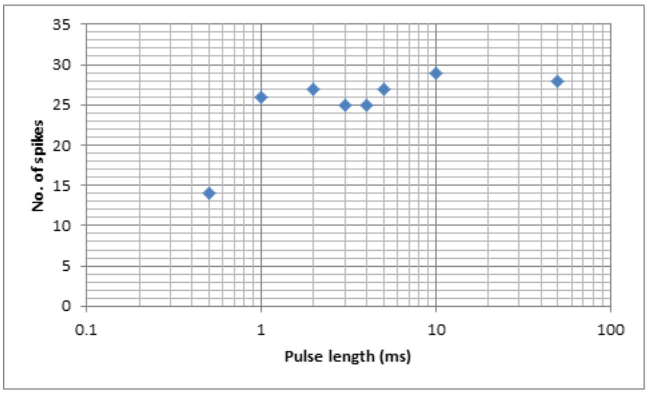

h

Figure 3.4: Mean count of SNAPs resulting from US stimulation, recorded from the *ex vivo* Saphenous nerve of adult Sprague-Dawley rats stimulated with ultrasound.

Intensity (I_{SPPA}, W/cm^2)	284	1216	6139
Peak negative pressure (MPa)	2.7	5.1	9.0
Force generated (mN)	3	11	56
Response reliability (%)	23	40	80

Table 3.3: Reliability of the SNAP response to varying ultrasonic exposure intensities. Reliability values are the mean of three separate nerve experiments. Calculated force amplitudes and pulse average negative pressure values are also displayed.

pre-stimulus recording and in between US exposures (Table table 3.4). Activity due to the US stimulus significantly exceeded this background rate at all pulse lengths tested ($P<0.005$). The background firing rate (not due to US) during the period of US firing was significantly reduced across all pulse lengths compared to the pre-stimulus rate ($P<0.005$) (Table 3.4).

Pulse length (ms)	spikes pre stimulus	spikes due to stim	spikes between stimulus
0.5	5	14	2
1	3	26	4
2	5	27	2
3	5	25	5
4	4	25	4
5	3	27	6
10	8	29	5
50	7	28	4

Table 3.4: Detailed mean count of SNAPs recorded from the *ex vivo* Saphenous nerves of adult Sprague-Dawley rats occurring in the pre stimulus recording, in response to US stimulus of different pulse lengths, and detected between the US stimului.

Chapter 4

Crab Walking Leg Nerve - Experimental Protocol and Apparatus

4.1 Design and Justification

The switch to an excised crab walking leg nerve model from the experiments described in section 3.1 was made primarily to cut out the potential involvement of the skin's mechanoreceptors in reception of the US stimulus. An unmyelinated axonal tissue model was chosen to be as simple as possible, but also has direct comparability with other unmyelinated nerves in humans such as noiceptive C-fibres and many central nervous axons [Kandel et al., 2000]. Though there are differences in lipid and protein composition of the crab leg nerve compared to mammalian unmyelinated neurons, basic nerve conduction principals are well conserved [Page, 1971, Sheltawy and Dawson, 1966].

To reduce the effect of reflections to the pressure field at the focal point and to fulfil this study's aim of a well controlled US field, the nerve bath was re-designed to include an acoustic window with a water bath and US absorbers underneath shown in figure 4.1. The nervous tissue was cooled via the bath underneath to slow down its rate of conduction which separates the nerve responses from stimulation artefacts and keeps the cells viable for longer. The water bath was cooled with ice which was held from the US path by stainless steel meshing and monitored by a digital thermometer. The bath was insulated with foam and had a stable temperature of between 1-4°C for approximately 6 hours. If longer was required, the ice was replaced between experiments.

The water bath also allowed for the inclusion of a PCD to measure the acoustic

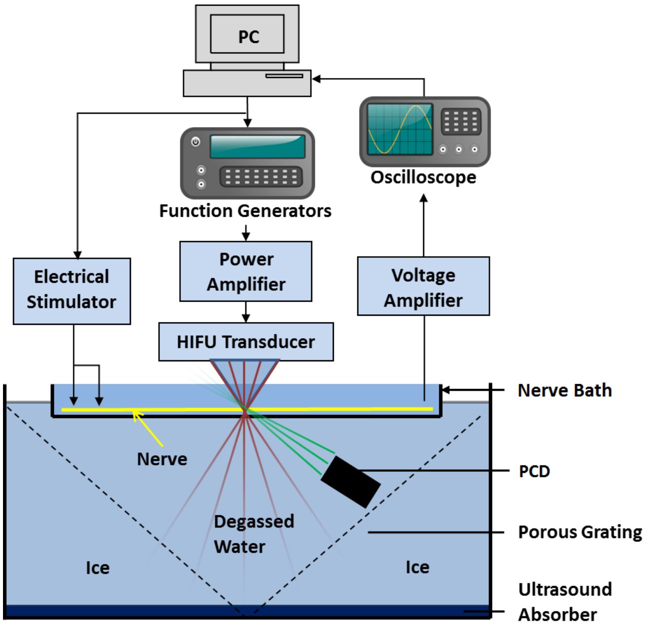

Figure 4.1: Schematic diagram of the experimental setup used to generate alternate electrical and US stimuli recordings. In the moving focal point experiments the nerve bundle can be moved freely under the US focus while remaining in contact with the recording and stimulating electrodes.

signals emitting from the cavitating bubbles, for meaningful modelling (Figure 4.6) of the acoustic field [Soneson, 2009] and for hydrophone field measurements of the stimulatory US to be made (Figure 4.12) *in situ*. The focused PCD was fixed in place at an angle to overlap the foci of the two transducers on the nerve and avoid receiving the direct signal from the driving transducer (Figure 4.1).

Using the free space acoustic field measurements, solid ultrasound coupling cones similar to the one described in section 3.1.2 were designed for each transducer that both sealed in degassed water for near field transmission and mechanically fixed the focal point along the central axis, 5 mm beyond the end of the cone. A flat mylar film (12 μm thick) was used to replace the latex sheath in the previous design. This sealed the truncated end of the cone, allowing mechanical interlocking with the nerve bath and preventing the variable focal height possible with the previous design. Both the lateral and axial targeting resolutions were found to be much more accurate than attempts to use the water bag and laser targeting mechanisms used in the literature [Foley et al., 2008, Min et al, 2011a] or the latex sheath used in the skin nerve experiments (Section 3.1). The seal around the transducer allowed it to be used in any orientation and meant that the volume of water used was kept to a minimum, making the coupling cones lighter than the one used in the rat saphenous experiments. Clear polished perspex was used to allow observation and elimination of bubbles on the transducer surface that may occur during fitting.

Finally, the capability for electrical stimulation was included in the nerve bath to provide positive control stimulation of the nerve bundle. Silver was used as the electrode material to provide a low resistance connection to the nerve bundle and high resistance to interference from the ionic ringers solution. Noise arises from the electrode-electrolyte interface and is reduced by chloriding the surface of the silver, which forms an AgCl layer. Ag/AgCl electrodes also possess the advantages of low polarization and predictable junction potential [Hu et al., 2016].

The Moving Focal Point (MFP) experiments were designed to test different locations along the same nerve bundle, allowing investigation of location specific effects of the stimulus.

The Fixed Focal Point (FFP) was designed to test the conditions necessary to stimulate the same tissue location repeatedly. This also eliminated changes in the relative distance between the focal area and the PCD, preventing absolute amplitude levels from varying between US exposures and therefore allowing comparison of cavitation signals between experiments. This also allowed a much smaller nerve bath design for ease of handling separate, electrically isolated sections and a more accurate focal location that was locked in all dimensions. The fixed nerve position also allowed analysis of the decline in CAP amplitude over time and its association with US exposure (Section 4.8.1).

4.1.1 Moving Focal Point

In these experiments, the PA 409 transducer (0.67 MHz, table 3.1.2) was used exclusively. The nerve bath used was designed with a slot cut into the acrylic wider than the beam profile of the transducer at the focal point (Figure 4.6(a)) to allow ultrasound to pass through, preventing reflection or absorption by the chamber that might amplify or change the effects on the nerve. This slot interlocked with a spacer that in turn fitted the end of the US coupling cone, ensuring a fixed lateral focal location while allowing longitudinal movement of the the nerve bundle to expose different points along the bundle. Only 0.67 MHz ultrasound was used in this experiment.

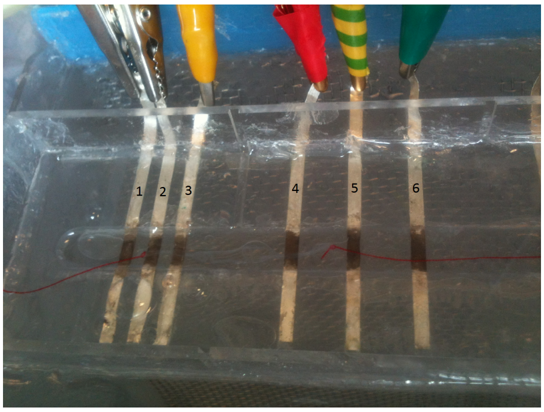

Figure 4.2: Photo of the nerve bath with a nerve in place, marked by the red thread tied to each end of the nerve. Attached to the numbered electrodes are: 1) Stimulation reference 2) Stimulation active 3) Earth 4) Recording A 5) Recording B 6) Earth.

Mylar film was used to cover the slot, providing a 2 mm deep trench to hold the nerve bundle, isolated from the water bath. The downward curvature of the thin film ensured that the nerve bundle was located centrally in the channel by gravity. Plan photographs of the nerve bundle *in situ* were taken and processed after three experiments to test lateral deviation from the central axis of the nerve chamber, which was measured to be less than 1 mm at all points (mean = 0.56 mm σ = 0.32). Chlorided silver foil (0.15 mm thickness) strips were placed at intervals over the mylar film and fixed into the bath acrylic to be used as stimulation and recording electrodes (Figure 4.2). Electrode thickness was chosen to be less than one tenth the wavelength at 0.67 MHz in water (2.3 mm).

Once constructed the bath was tested for interference with the US field through measurement of the focal intensity directly behind the mylar film (within 1 mm) in three separate locations no significant difference was found with unobstructed measurements ($<$0.1% reduction). However, measurements made behind three different foil electrodes showed a significant reduction in acoustic intensity of approximately 25%.

This result led to a further investigation of ultrasound impedance by thin silver foil (Figure 4.3) at several different amplitudes of single 0.67 MHz ultrasound pulses. Sheets of foil were placed in the focal region of the ultrasound, between the hydrophone and transducer. To avoid this unwanted absorption/reflection by the silver, the US was

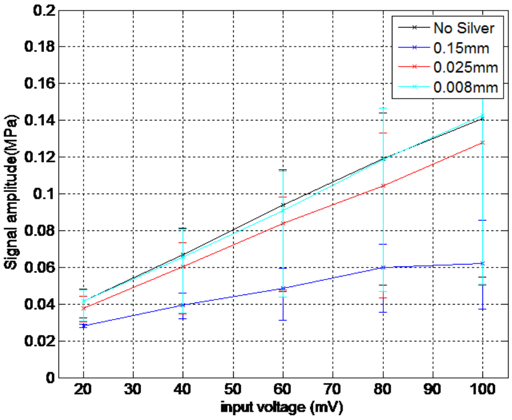

Figure 4.3: Measurements of absolute acoustic pressure taken 10 mm beyond the focal maximum by a Precision Acoustics plane tipped fibre-optic hydrophone. Measurements were made in degassed pure water at 22.6°C at 5 different acoustic amplitudes and three different grades of silver electrode thickness.

targeted only in the spaces between electrodes.

To reduce short circuiting between the different electrodes, white mineral oil was used to fill the nerve bath, acting as US transmission media that was electrically insulating (sterile filtered,0.85 g/ml, Z = 1.26 MRayls). Only a thin sheath of ringers was left around the nerve to keep it alive for the duration of the experiment. The oil was chosen as it has a similar acoustic impedance to water resulting in very little defocusing and energy lost due to reflection (8%, calculated using equation 4.2). Its slightly lower density than water also meant that the nerve bundle would sink and remain in contact with the electrodes.

The PCD shown in figure 4.1 was only included in a subset of these experiments with fixed intensities to allow comparison between the acoustic response of exposure sets. Acoustic data was analysed as per the method described in section 4.7.

4.1.2 Fixed Focal Point

The nerve bath (Figure 4.5) was designed to interlock with the coupling cones, holding the transducer's focal point in a fully fixed position relative to the location of the nerve bundle. To analyse the lateral targeting error of each transducer and coupling cone, three thermo-chromatic gels were exposed with CW ultrasound until a white colour change occurred in the focal region (Figure 4.4). Photos were taken in plan view of the chamber and analysed using MATLAB to determine the centre point of the colour change and its lateral deviation from the centre line of the chamber. Deviation was found to be a maximum of 160 (σ = 67), 84 (σ = 11) and 89 μm (σ = 40 μm) for 0.67, 1.1 and 2 MHz respectively. This corresponds to an uncertainty in acoustic peak pressure at a target point of 5, 15 and 70% respectively. But as the nerve is 1 mm wide at least, some part of it will be exposed to the focal maximum despite lateral targeting error.

The nerve bath itself was separated into three electrically isolated sections, allowing efficient electrical stimulation and recording from the nerve. To aid this, the two ends of the nerve bath performing the electrical stimulation and recording were filled with mineral oil. Crab ringers solution was used in the central, earthed chamber. The use of ringers solution as the acoustic coupling media has the advantage of reducing the US reflection off the bath and nerve surface and increasing the longevity of the nerve bundle when compared to the MFP experiments.

All electrodes were made from thinner (0.025 mm) silver chloride coated silver electrodes than those used in section 4.1.1. Thin mylar film was used as an acoustic window, separating the water in the cone from the nerve bath and the ringers in the nerve bath from the water bath underneath (Figure 4.1). The width of the acoustic window in the nerve bath was 10 mm, allowing the primary focus and at least one side lobe to pass unobstructed with every transducer used (Figure 4.6). To reduce atmospheric electrical noise, the entire setup was contained within a copper mesh Faraday cage.

Though the sections of the bath containing oil and water were physically separated except for the nerve gates, droplets of oil were occasionally seen in the water compartment. At 0.84 g/ml the mineral oil does produce reflections in the US path which were considered to be a source of error. Therefore given the characteristic acoustic impedance of 1.26 compared to 1.48 MRayls of water [Casarotto et al., 2004] and the equation for normal pressure reflection at a boundary (Equation 4.2), the reflection coefficient can be calculated at 0.08, or 8% reflection.

4.2 Equipment Details

The equipment used in the current setup shown in figure 4.1 is detailed here. US stimulus waveform was produced by two Agilent 33220A function generators, one gated by the other to produce the pulsed protocol which was then amplified by an E&I 1020L

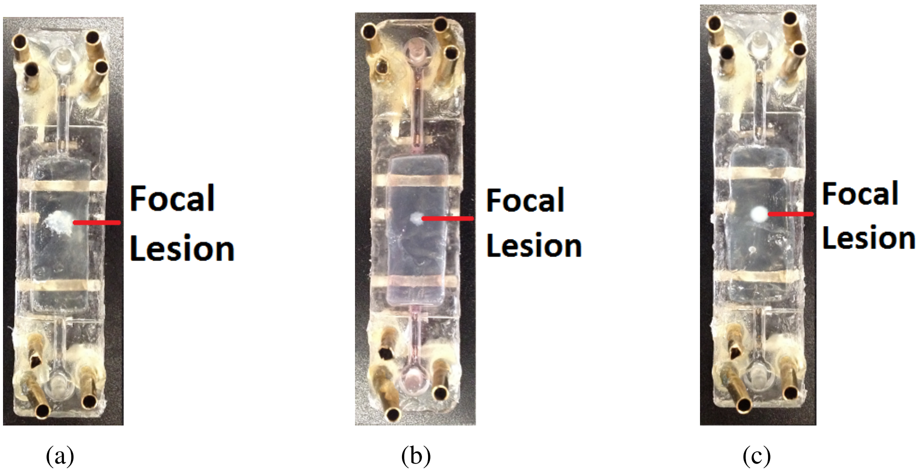

Figure 4.4: Visualisation of the size and position of of the focal points produced by each ultrasound transducer within the nerve bath (a) 0.67 MHz (b) 1.1 MHz (c) 2 MHz. Temperature induced colour changes were produced in an polyacrylamide gel. 10 s continuous wave exposures with different focal intensities were used with each transducer to achieve a good visualisation of the focal area.

200 W class AB linear power amplifier with 55 dBm gain. Details of the US transducers used are shown in table 3.1.2. Electrical stimulus was produced using a Digitimer DS3 constant current isolated stimulator. Electrical recordings from the nerve were taken using a WPI DAM50 differential amplifier at 100× Direct current gain. A simple high pass filter RC circuit (1.6 kΩ resistor, 10 μF capacitor) was built and inserted between the oscilloscope and bio-amplifier. Recording of the scattered acoustic signal was performed using an Ultran XL50 5.8 MHz focused ultrasound transducer as a PCD, the signal of which was amplified by a SRS inc. Model 445A, four channel voltage amplifier providing a 5 times gain (max 25 times). Electrical and acoustic data was plotted on a Lecroy HDO6054 500 MHz oscilloscope and saved on a PC. Synchronisation of US stimulation, electrical stimulation, and signal acquisition was performed using a National Instruments 9402 4 channel I/O module and 9171 cDAQ chassis.

Electrical transducer input power measurements were made using a Sonic Concepts 22A RF wattmeter. Foam used to absorb US and prevent reflections from the tank walls or bottom was Precision Acoustics AptFlex F48 PU foam.

Ringers solution was kept kept no longer than 3 weeks without replacement and was an aqueous solution of 525 mM/l NaCl, 13.3 mM/l KCl, 12.4 mM/l CaCl2, 24.8 mM/l MgCl2 and 5 mM/l dextrose. A spray bottle was kept cool for the extraction procedure using an ice bucket.

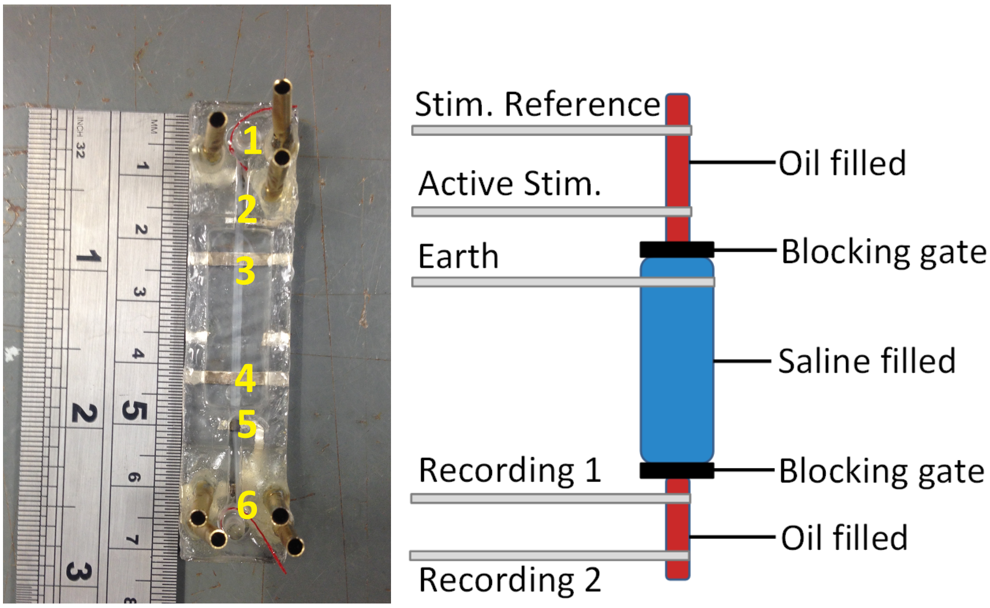

(a) (b)

Figure 4.5: (a) Photo of the nerve bath with a nerve bundle in place. The red thread visible at either end of the chamber ligates each end of the bundle. Attached to the numbered electrodes are: (1) Stimulation reference (2) Stimulation active (3) Earth (4) Earth (5) Recording A (6) Recording B. (b) Schematic diagram of the nerve bath with electrodes and important features labelled.

4.3 Nerve Bundle Characterisation

Five extracted crab nerve bundles were fixed in 3% glutaraldehyde (0.05 M sodium cacodylate buffer pH 7.2-7.4) directly after extraction. The bundle was then sectioned and fixed in araldite resin using a methylene blue/azure II/ basic fuchsin stain for light microscopy examination. Axon fibre density was estimated using a digitally applied, randomly positioned 50 μm square, counting only the axons with more than 50% of their area within the square. This was repeated three times for each of the 5 nerve bundles. neuron density was calculated to be 136/100 μm^2 (σ = 27) and mean axon diameter was 8.6 μm (σ = 6.5). Total number of axons per bundle was calculated to be 1017 (σ = 202)(Figure 4.7), using the product of the cross-sectional area of each nerve bundle and the cell density.

By stimulating three nerve bundles electrically only (without US), the mean baseline rate of decline in CAP amplitude was determined for both the oil submerged MFP experiments (Figure 4.8(b)) and the ringers submerged FFP experiments (Figure 4.8(c)). As expected, the nerves submerged in ringers solution took much longer to decline to undetectable CAP amplitude levels (>60 minutes).

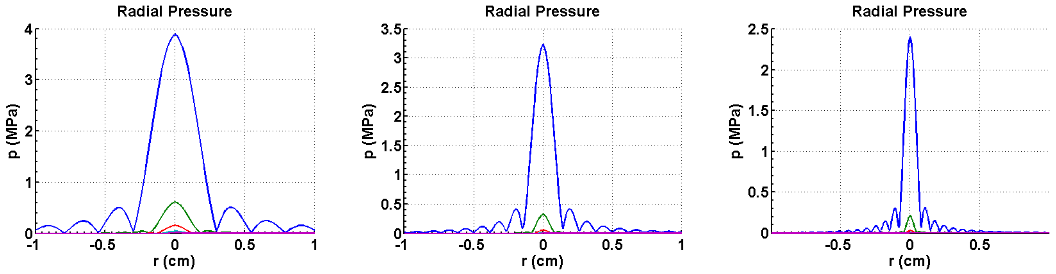

(a) (b) (c)

Figure 4.6: KZK models of the radial peak positive pressure profiles generated by the 0.67 (a), 1.1 (b) and 2 MHz (c) transducers respectively. Modelling technique described in section 4.6. Driving power was set to the maximum input used to generate the forces in table 4.2. Dark blue, green, red, light blue and purple traces show the 1st to 5th harmonic respectively. [Soneson, 2009]

4.3.1 Light Microscopy

Observation of the nerve bundles *in situ* was also performed by light microscopy to characterise the average dimensions of the bundle (diameter = 1.34 mm, σ = 0.21 mm) and of the microbubbles that were introduced on the surface of the nerve bundle during submersion in acoustic coupling media (Figure 4.9). 10 nerves were examined in this way and in the 0-1 minute period post nerve submersion in the bath, a mean of 11 bubbles (σ=8.8) with a mean diameter of 78 μm (σ = 54) were seen over 2 cm of nerve. Assuming even distribution, a mean of 2 bubbles will be located within the US focus on every nerve bundle (3.5 mm FWHM) at the start of each experiment. However, due to the high standard deviation in observed bubble numbers, 33% of extracted nerve bundles will not have bubbles present in the US focus. These microbubbles are introduced by the extraction process as the bundle is submerged into the ringers solution/mineral oil bath.

Three nerves were also observed by microscopy in between ultrasound stimulation protocols. Larger ($>$100μm) bubbles were observed to rise to the surface after ultrasound exposure and smaller ones ($<$100μm) dissolved rapidly into the surrounding ringers solution (Figure 4.9(a)). Therefore neither were observed past the first two US exposures in 10 examined nerve experiments with a fixed US focal point. The dissolution of gas into the surrounding media altering the size of bubbles means that there was an unknowable exact size distribution in the population of bubbles attached to the nerve surface upon US exposure in the MFP experiments and in the first 2 FFP

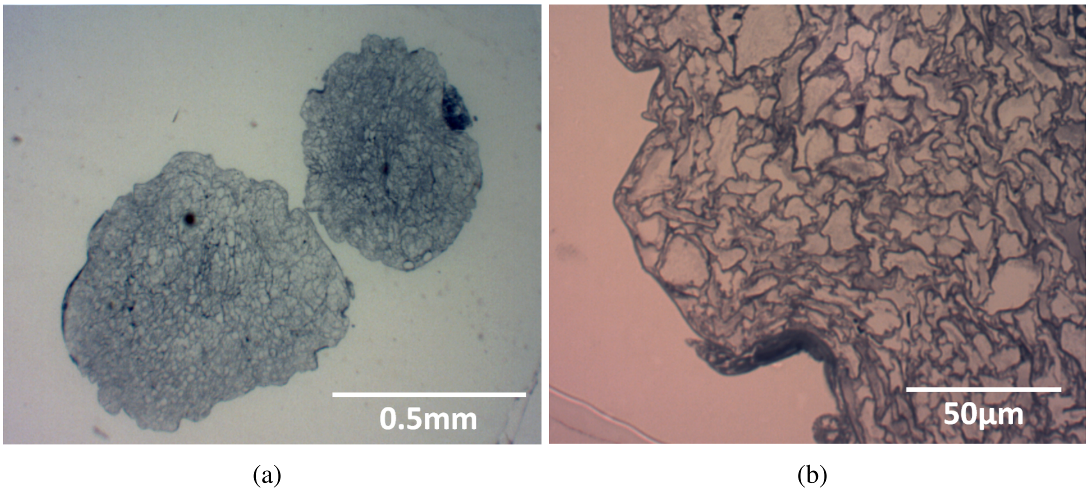

(a) (b)

Figure 4.7: Extracted nerve bundles were fixed in situ in 3% glutaraldehyde (0.05 M sodium cacodylate buffer pH 7.2-7.4) without any exposure to US. The exposed sections were then extracted and fixed in araldite resin using a methylene blue/azure II/ basic fuchsin stain and sectioned for light microscopy. (a) 160× magnification (b) 1280× magnification. Both photos are digitally scaled by a factor of 0.32.

exposures.

4.4 Nerve Preparation Procedure

All nerves were taken from live crabs (*Cancer pagurus*) sourced on the day of use from London markets. Nerves were extracted from the crab leg by stripping away each joint section, removing the shell and muscle from around the nerve bundle. During extraction the nerve was regularly sprayed with chilled ringers solution. The nerve was then ligated at both the proximal and distal ends with red cotton thread. Cutting above the distal ligation, the nerve was detached from the claw, transferred into the nerve bath and wetted with chilled ringers.

In the case of the MFP experiments an extracted nerve of at least 55 mm was laid in the nerve bath with spare nerve length resting past electrode 6, (Figure 4.2) and a small volume of chilled ringers poured over it. Less dense, electrically insulating white mineral oil was then poured over the top of this. The nerve was more dense than the oil and therefore sank and was centralised in the acoustic window by the downward curvature of the mylar film, ensuring good electrode contact.

In the case of the FFP experiments, the nerve was handled by the string attachments and passed through the two blocking gates (Figure 4.5), then pulled straight between them, avoiding causing undue tension in the tissue. This ensured that the nerve

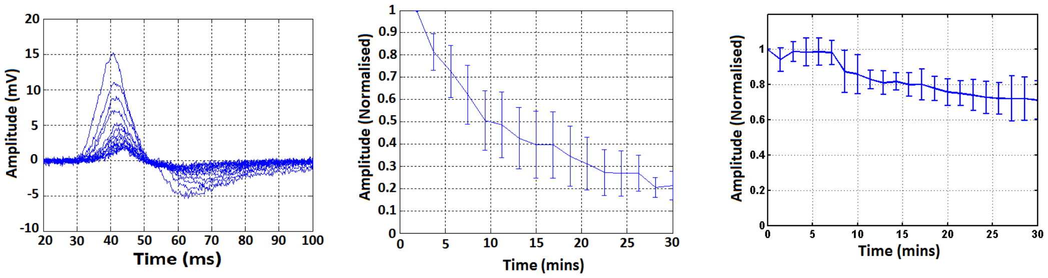

(a) (b) (c)

Figure 4.8: (a): Overlayed time series of electrically induced CAPs (2 mA, 200 μs stimulus). The nerve was stimulated as soon as possible after extraction and every 2 minutes in the experimental setup described in section 4.1.1. (b) and (c): Average peak positive amplitudes over three repeats were recorded using the MFP (b) and FFP (c) apparatus, normalised to the first peak and plotted against time. Error bars represent the standard deviation for each time point.

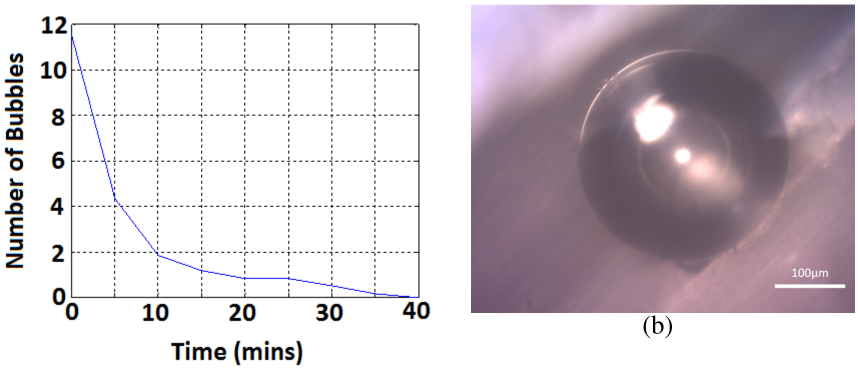

(b)

(a)

Figure 4.9: (a) Observed number of bubbles attached on the surface of a 20 mm section of crab leg nerve bundle prepared as per the protocol in section 4.4 observed over a period of 40 minutes without exposure to any stimulus protocols. Displayed is the mean numbers for 10 observed nerve bundles. (b) A 150× magnified light microscopy image of a large bubble attached to the surface of the nerve bundle.

was located directly under the ultrasonic focus (within ± 0.1 mm) and in contact with both the recording and stimulation electrode pairs. Oil was then added to the two side channels which kept the nerve cool, prevented dehydration and insulating the inter-electrode path. Ringers solution was added to the central chamber. Surface tension in the small aperture of the blocking gates (most of which was occluded by the nerve diameter) prevented the oil and ringers from mixing between the chambers. This factor led to the preferential selection of larger crab specimens with thicker nerves to reduce the electrical short and prevent oil-water mixing.

Stress to an animal can alter nervous conduction properties. Efforts were therefore made to try and keep stress during transit and storage to a minimum although some is no doubt unavoidable. Susceptibility of nervous tissue to mechanical stimulation may depend on many factors in the living crabs prior to extraction which could not be controlled such as levels of muscular activity or general health of the animal.

The nerve bath was transferred to a holder on the surface of the water bath and the US cone fitted on top, ensuring that no bubbles were trapped in the US propagation path using a small endoscopic camera. The nerve bath and all implements were cleaned and sterilised with ethanol before use.

4.5 Electrical and Ultrasound Stimulation Parameters

Based on precedent in the literature for pulsing in successful neurostimulation protocols [Kim et al., 2014a, King et al., 2013, Tufail et al, 2010] and optimisation of the stimulus parameters described in section 3.1.3, a new stimulation protocol was tested for the crab leg nerve experiments.

The primary stimulus protocol used in this study was 80 pulses of the driving frequency at 10 kHz PRF, over an 8 ms TSD (50% DC). Short, 8 ms TSD stimuli were initially chosen to limit the variety of acoustic events that might occur during each stimulus, so that the signal could be processed as a whole, making it easier to link acoustic signatures to responses from the nerve. Short latency also reduced electrical interference from US generation on CAP recordings as the CAP transmission time along the nerve bundle to the electrodes was longer than the pulse duration.

Electrical and US stimulation were paired in these experiments so that every US stimulus was preceded by an electrical stimulus, three seconds apart.

4.5.1 Moving Focal Point

For the MFP experiments, electrical/US stimulation pairs were repeated 5 times in the same location with 3 seconds between stimulus of either modality and separated from the next set of 5 pairs by 60 seconds (Figure 4.10). The pulse average intensity of each set was varied between 3 and 138 W/cm^2 (I_{SPPA}) (Table 4.5.1) and the US nerve bundle moved by 5 mm, away from the recording electrodes during the rest time between each set. Orders of intensities being tested on a single nerve were randomised to prevent systematic error from nerve inhibition or other effects. Each nerve bundle was exposed a total of seven times (in sets of 5) to cover the full range of intensities.

Intensity was kept constant at 138 W/cm^2 in four nerve experiments where the PCD was used to analyse the acoustic response. For these, stimuli continued in new sections of the nerve bundle until the whole length had been exposed or till the nerve electrical response declined below detection threshold.

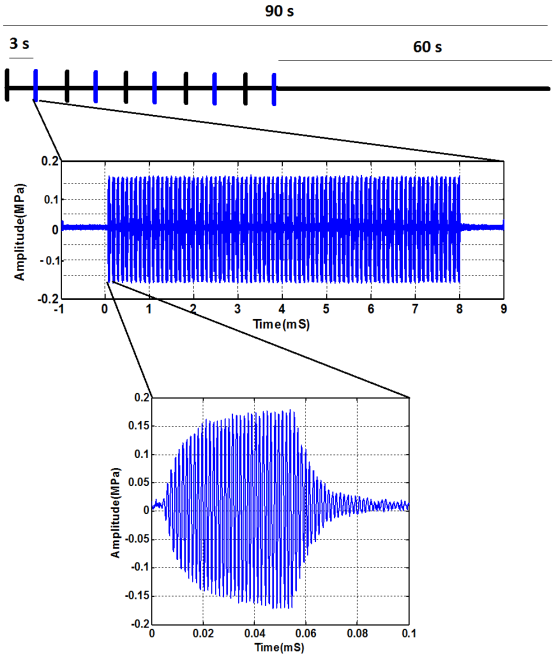

Figure 4.10: Stimulation protocol used in the MFP experiments. Electrical stimulation is marked by vertical black lines, US stimulation by vertical blue lines. Each US stimulus shown on the top timeline is comprised of 80 0.05 ms pulses at 50% DC. The entire stimulus protocol is repeated every 90 s. Pulse train (middle) and single pulse (bottom) were recorded using a plane tipped fibre optic hydrophone placed in the focal region of a 0.67 MHz PA407 HIFU transducer. The ramping up and trailing off of the pulse is due to the transducer's damping properties.

Electrical stimulation was applied via electrode 3 (Figure 4.2) using a 0.2 ms fixed current electrical stimulus. Stimulation amplitude was adjusted before each experiment to achieve saturation. The use of electrically insulating mineral oil as the US coupling media allowed saturation with relatively small current stimulus.

The influence of recovery time on a single stimulation site, with no nerve movement was tested. After a successful US response was observed, the same location was stimulated repeatedly with varying time intervals between sets of 5 stimuli (1, 5, 10 and 20 minutes). The nerve was then moved again by 5 mm and exposed to another set of 5 stimuli.

0.67 MHz

Radiation Force (mN/cm^2)	Pressure (MPa)		I$_{\text{SPPA}}$ (W/cm^2)
0.4	-0.3	0.3	3
2	-0.6	0.6	11
4	-0.8	0.9	25
7	-1.1	1.2	44
11	-1.4	1.5	70
17	-1.6	1.8	101
23	-1.9	2.2	138

Table 4.1: Intensity, pressure and radiation force values of the exposures used in the MFP experiments at 0.67 MHz. Spatial peak negative and positive pressure values were measured using a plane tipped fibre-optic hydrophone. Radiation force values are a summation of numerically modelled absorption and reflective forces (Section 4.6.1).

4.5.2 Fixed Focal Point

The timing between electrical/US stimulation pairs was alternated between 27 and 87 seconds causing the whole pattern to repeat every 120 seconds with an average of one pair per minute as shown in figure 4.11. Each nerve bundle was exposed to 22 of these electrical/US stimulation pairs resulting in a total experimental time of 22 minutes. This paired pulse protocol was designed to reduce possible heating effects and test the effect of recovery time on the acoustic signal and stimulation success.

Electrical stimulation was applied via electrode 2 using a 0.2 ms 20 mA electrical stimulus pulse (Figure 4.5(a)). Stimulation amplitude was adjusted before each experiment to achieve saturation. Full saturation may not have been achieved every time due to varying levels of ringers solution short circuiting between electrode 2 and the earthed central bath. Larger crabs with generally thicker nerve bundles were preferentially selected to reduce this effect, as their nerve bundles better occluded the holes in

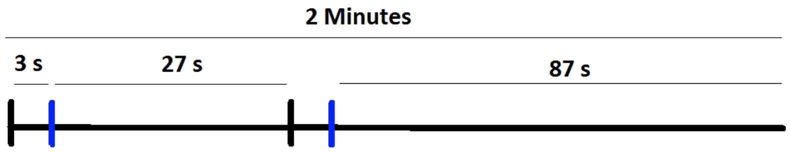

Figure 4.11: Stimulation protocol used in the FFP experiments. Electrical stimulation is marked by vertical black lines, US stimulation by vertical blue lines. Each US stimulus is comprised of a pulse train of 0.05 ms pulses at 50% DC as shown in figure 4.10. The entire stimulus protocol is repeated every 2 minutes 11 times for every nerve experiment.

the blocking gates.

Focal intensity was varied between the values shown in table 4.2. Orders of intensities being tested on a single nerve were randomised to prevent systematic error from nerve inhibition or other effects. The 1.1 and 2 MHz exposure parameters shown in the table were designed to match the radiation forces produced by the 0.67 MHz exposures using the methods described in the section 4.6.1.

	0.67 MHz			1.1 MHz			2 MHz		
Radiation force (mN/cm^2)	Pressure (MPa)		I_{SPPA} (W/cm^2)	Pressure (MPa)		I_{SPPA} (W/cm^2)	Pressure (MPa)		I_{SPPA} (W/cm^2)
1	-0.8	0.8	20	-0.7	0.7	17	-0.7	0.5	12
5	-1.4	1.6	76						
6	-1.6	1.8	100	-1.5	1.7	84	-1.4	1.3	61
9	-1.9	2.2	140						
11	-2.1	2.4	169	-1.9	2.2	143	-1.7	1.8	103
15	-2.4	2.9	230						
18	-2.6	3.2	274	-2.4	2.8	232	-2.1	2.4	167
23	-2.8	3.6	352						
27	-3.1	4.0	419	-2.9	3.6	353	-2.5	3.0	255
31	-3.3	4.3	485						
36	-3.5	4.7	562	-3.3	4.2	475	-2.8	3.6	343

Table 4.2: Intensities, negative and positive peak pressures and radiation forces at three frequencies. Intensities and pressures were chosen to create equal radiation forces across the frequencies used.

Beyond the intensities for the two higher frequencies shown in table 4.2, a range of higher intensities (up to 0.86 kW/cm^2 at 1.1 MHz and 6.7 kW/cm^2 I_{SPPA} at 2 MHz) were investigated using the same protocol to determine if a threshold for stimulation could be found for each driving frequency. Focal intensity was increased by 100 W/cm^2 I_{SPPA} until a response was found or in the case of 1.1 MHz, until input levels were reached that may damage the transducer.

To test the effect of longer exposure durations on the nerve response dynamics at 0.67 MHz, a second set of stimulus experiments, with the same pulse parameters, were performed using 100 ms instead of 8 ms stimulus durations (1000 pulses).

Parameters found in a recent study by Lee et al. (250 kHz fundamental, 500 Hz PRF, 50% DC for 300 ms, with three seconds between each stimulus [Lee et al., 2015]) were also tested at the higher frequency of 0.67 MHz in the current setup to determine if the observed low sensitivity of the peripheral nerves compared to previous CNS studies was due to the pulsing protocol. These parameters were used initially at 0.7 W/cm^2, shown to be effective in Lee's study, and then incrementally increased in the same steps seen in table 4.2 until a response threshold was found. As with all exposure protocols, each stimulus intensity was repeated 22 times on a new nerve bundle.

4.6 Acoustic Modelling and Measurement

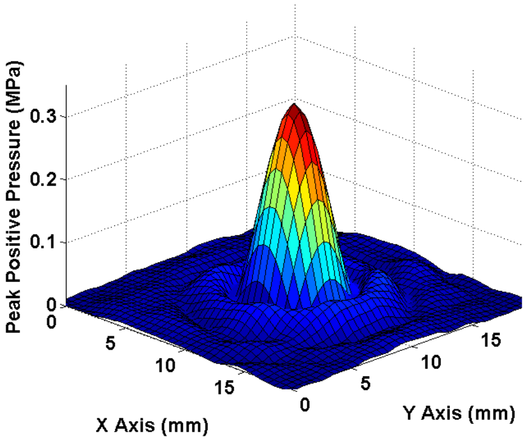

Figure 4.12: 20 × 20 mm scan of the transverse plane of the 0.67 MHz ultrasound field in steps of 0.5 mm at the focal maximum (73 mm from transducer surface). The transducer was driven with 0.4 W input power in continuous wave mode in a degassed and deionised water tank at 23°C. Reflections from tank walls was prevented with ultrasound absorbent foam

At low negative pressure amplitudes (0-2 MPa), intensity was measured by three separate plane tipped fibre-optic hydrophones, taking the mean positive and negative peak pressures for each transducer at different input powers and calculating I_{SPTP} via equation 1.1. These measurements were made *in situ* with the whole experimental setup (Figure 4.1) and the hydrophone tip at the US spatial maximum, aligned with the beam axis and facing the transducer. Higher amplitudes were not directly measured due to the risk of damage to the hydrophones. For each transducer, these low pressure measurements were then used to calibrate acoustic field modelling software [Soneson, 2009] based on the Khokhlov-Zabolotskaya-Kuznetzov (KZK) equation [Hamilton and Blackstock, 1998]:

$$\frac{\partial^2 p_a}{\partial z \partial \tau} = \frac{\partial}{\partial \tau}\left[\frac{\beta}{2\rho_0 c_0^3}\frac{\partial p_a^2}{\partial \tau} + \frac{\delta}{2c_0^3}\frac{\partial^2 p_a}{\partial \tau^2}\right] + \frac{c_0}{2}\triangle_\perp p_a \tag{4.1}$$

where P_a is the acoustic pressure, z is the axial coordinate, τ is the retarded time defined by $t - \frac{z}{c_0}$, β is the nonlinearity coefficient, ρ_0 and c_0 are density and wave speed at equilibrium condition respectively. Parameter δ is the diffusivity of sound which is a quantity that reflects the total effect of viscosity and heat conduction.

The output efficiency parameter within this software was changed till predictions matched the outputs measured at lower pressures to within 1% error. This model takes into account non-linear effects by modelling the propagation of the first 50 harmonics around the fundamental frequency. The model was then used to predict peak pressures of exposures above 2 MPa used in the current study (Table 4.2).

The KZK model has assumptions that limit it's theoretical accuracy to within 20° of the axis [Lee, 1986]. Transducers with f-numbers lower than 1.74 will therefore suffer from lower accuracy using this modelling technique. Though the transducers used in this study do fall into this catagory, validation of the model has been carried out using low f-number transducers [Canney et al., 2008] and the effect is thought to be minor [Lee, 1986]. This validation was carried out at 2 MHz and up to 24,000 W/cm^2 I_{SPPA} [Canney et al., 2008]. Power input measurements to the transducer used in the KZK modelling were calculated given the known input power from the signal generator and fixed 55 Decibels (dB) amplifier gain. These measurements were confirmed using a power meter.

Hydrophone measurements and KZK modelling determined that there was significant non-linear propagation of ultrasound at the power levels used in the current study, increasing at higher amplitudes at all frequencies (Table 4.2). This results in higher positive pressures compared to the peak negative values. To facilitate easy comparison with other papers in the literature, I_{SPPA} will be used throughout the rest of the paper but it should be noted that these are linear approximations and the positive and negatives pressure peaks will be the most accurate metrics, especially at higher amplitudes. These peak pressures are displayed along side peak and pulse average intensity values at all frequencies and driving powers for the crab leg nerve experiments (Table 4.2). The 1.1 and 2 MHz exposure parameters used in the FFP experiments were designed to match the radiation forces produced by the 0.67 MHz exposures using the methods described in section 4.6.1.

Using the same HIFU simulator software, to ensure temperature was a negligible factor a Bio-heat transfer equation was used to determine the temperature rise at the focal maximum at the highest intensities used in this study. The predicted rise was less than 0.1°C in all cases.

Reflections within the water bath were measured to affect the peak focal pressure by less than 5% at any of the amplitudes used in this study, measured by a fibre optic hydrophone positioned *in situ* within the experimental setup shown in figure 4.1.

4.6.1 Radiation Force Calculations

Radiation forces produced by the 0.67 MHz stimulation protocol shown in table 4.2 and 4.5.1 were predicted using equations 2.1 and 2.2.

Adding to this, the radiation forces due to the reflection at the water- or oil-tissue interface were calculated using the equations [Leighton, 1994]:

$$R = \frac{Z_2 - Z_1}{Z_2 + Z_1}, \qquad (4.2) \qquad\qquad F_{ref} = \frac{2 I_{SPPA} R}{c}, \qquad (4.3)$$

where R is the pressure reflection coefficient, Z_1 and Z_2 are the specific acoustic impedances for the US transmission media and tissue respectively, F_{ref} is the radiation force acting on the boundary due to reflection assuming a linear plane wave, perpendicular angle of incidence and a reflecting surface area much larger than the wavelength. The radiation force due to reflection was then added to F_{abs}. The reflective forces were predicted to be relatively stronger for the MFP experiments due to the larger impedance mismatch between oil and soft tissue as a pose to the ringers solution used in the FFP experiments.

Once the radiation forces produced by the 0.67 MHz FFP protocol had been calculated, the process was reversed to find the focal intensities required at 1.1 and 2 MHz that would reproduce the same radiation forces. This resulted in a target intensity range of 17-475 W/cm^2 at 1.1 MHz and 12-343 W/cm^2 at 2 MHz (Table 4.2). Error caused by plane wave and reflective surface assumptions in radiation force calculation will not affect the desired equality of the radiation forces across the frequencies as the errors will be cancelled in the reverse calculations. However, the degree of non-linearity in the field will change with pressure, leading to underestimation of the radiation forces produced by highly non-linear exposures.

The radiation force acting on the liquid path before the nerve was also calculated using equation 2.2 to investigate the potential significance of acoustic streaming effects. Using the highest intensity (I_{SPPA}) in either of the crab nerve experiments and an α_0 value for water of $0.26e^{-3}$ [Duck, 1990] in nepers per meter, the maximum streaming force produced was 1 μN/cm^3 at the focal peak. Given the small scale of this force, the short exposure times (8-300 ms) for which this force is applied and mylar film barriers restricting the free axial distance above the nerve to 4-5 mm, acoustic streaming effects were not considered further.

4.6.2 Bubble Radiation Forces

Total radiation force on the nerve bundle will also be added to by forward forces created by US reflecting and scattering off microbubbles that are introduced onto the nerve surface during submersion in the transmission media. Though these bubbles are loosely attached to the bundle and are therefore not likely to transfer force efficiently to it before dissociating (As observed by light microscopy in section 4.3.1), to determine the maximum possible significance of this effect, the case of a variable initial radius bubble positioned at the US focal maximum that transfers force efficiently to the nerve bundle is considered.

The primary radiation force at the driving frequency of each transducer on a range of bubble sizes can be calculated the equation [Tortoli et al., 2002]:

$$F_{bub} = \frac{\pi P_a^2 2R_0}{\rho c \omega} \frac{\delta_{tot}\omega_0/\omega}{[(\frac{\omega_0}{\omega})^2 - 1]^2 + (\frac{\delta_{tot}\omega_0}{\omega})^2}, \tag{4.4}$$

where F_{bub} is the primary radiation force on a bubble, P_a is the local ultrasound pressure, R_0 is the bubble radius, δ_{tot} is the total damping constant (Including dissipation due to radiation viscoelastic and thermal losses), ω is the US driving frequency,ρ is the fluid density and ω_0 is the resonant frequency of the bubble. A damping constant for soft tissue of 0.27 was used [Leighton, 1994]. This equation assumes that the spherical bubbles are much smaller than the acoustic wavelength. Drag force is not considered due to the assumed immediate transference of force to the nerve bundle. Secondary radiation forces are not considered as these are short range, inter-bubble forces that are not expected to increase the forward radiation pressure regularly [Leighton, 1994].

The resonant frequency of a bubble (ω_0) with radius R_0 can be determined by

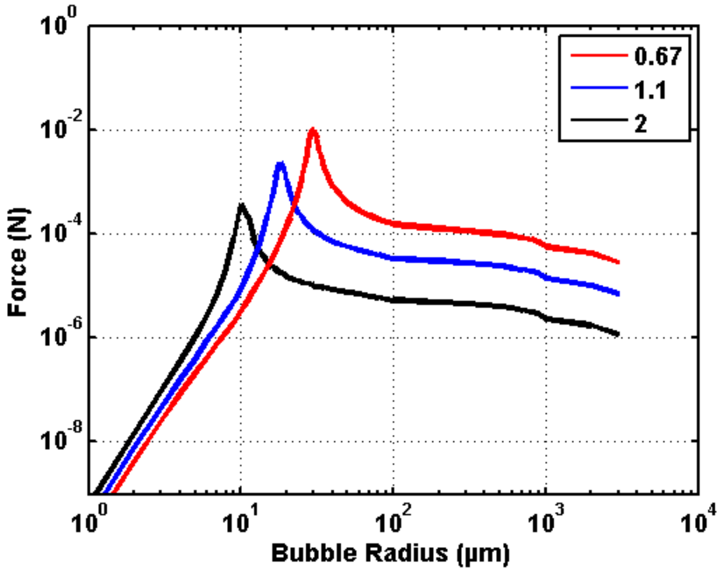

Figure 4.13: Primary radiation forces calculated using equation 4.4 for a range of bubble sizes using the driving frequencies and highest intensities used in the FFP experiments shown in table 4.2. The legend shows the driving frequencies in MHz.

equation 4.5 [Neppiras, 1980]:

$$\omega_0^2 = \frac{1}{\rho_L R_0^2}\left[3\kappa\left(P_0 - P_v + \frac{2\gamma}{R_0}\right) - \frac{2\gamma}{R_0} + P_v - \frac{4\mu^2}{R_0^2 \rho_L}\right] \tag{4.5}$$

where P_0 is hydrostatic pressure, P_v is the vapour pressure, κ is the heat capacity ratio, γ is the surface tension of the bubble (approximated as constant for air water interfaces) and μ is the dynamic viscosity.

Using these equations to model the primary radiation forces with the I_{SPPA} values used in the FFP experiments (Table 4.2) for a range of bubble radii results in the patterns shown in figure 4.13. The maximum potential radiation force generated by the 0.67 and 1.1 MHz exposures on bubbles are larger than those produced by reflection and absorption in the nerve bundle (9.8 and 2.3 mN respectively, compared to 2.2 mN calculated for the approximate dimensions of a nerve bundle (1×1×6 mm) under the US focus).

Given the continuous size range and sporadic location of the bubbles, their influence will vary greatly between exposures. This simple modelling is therefore intended only to explore the range of forces that may be produced and to determine their significance as a potential contributing stimulation mechanism when interpreting the experimental results.

4.7 Passive Cavitation Detection

Acoustic signal data was recorded from the PCD for an identical duration as the electrical nerve recordings. The time section containing the US stimulus was then detected by a 5σ threshold. If the resultant duration deviated from the expected TSD by more than 10%, the threshold was adjusted recursively until a signal with the correct length and time position was found. This accounted for very low amplitude signals. If a signal was not detected, all associated data was ignored during analysis. This data filtering process is described further in section 4.9.

The spectral content of the signal was corrected for the PCD's frequency sensitivity bias using its voltage spike emission spectra to deconvolve the recorded signal, before being analysed by FFT and wavelet decomposition techniques. Aliasing of frequencies above the Nyquist (6.25 MHz) was not expected to have a significant influence on recorded acoustic signals. This is because the signal to noise ratio of cavitation signals are high, meaning that any higher than Nyquist noise should be insignificant and any higher than Nyquist cavitation signals still contribute to the detection of cavitation via the methods described below.

In the case of the 100 and 300 ms exposures, the key 10 ms section of the US stimulus likely to have caused any resultant CAP, was determined by subtracting the expected CAP transmission lag time from the point when the CAP peak was received. A 10 ms section of PCD signal data was analysed around the resulting time point, illustrated by the vertical red lines in (Figure 4.14). In cases where no US stimulated CAP was detected, a random 10 ms time section of PCD data was analysed for comparison.

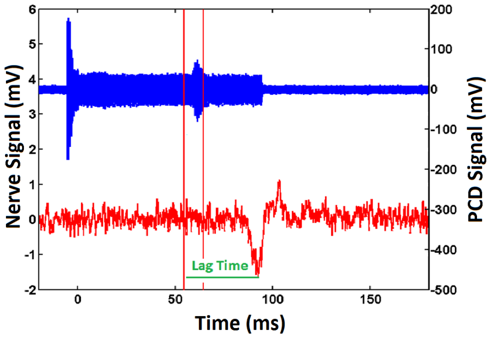

Figure 4.14: Example of a nerve CAP response (red, left axis) to the 0.67 MHz, 100 ms stimulation protocol at 562 W/cm^2, recorded simultaneously with acoustic PCD data (blue, right axis) Vertical red lines show the region of the stimulus pulse expected to have initiated the US CAP.

4.7.1 Frequency Domain Analysis

Cavitation signal in both the MFP and FFP experiments were analysed using techniques similar to those first described by Larry Crum's group in 2002 [Chen et al., 2003, Tu et al., 2006]. The 8 ms PCD signal was extracted and the frequency domain analysed by an FFT. To investigate stable cavitation, narrow frequency bands (0.1 MHz width) over the 2nd to 8th harmonic (Figure 4.15) were integrated and summed with the other inter-harmonics to give the Stable Cavitation Dose (SCD). Before summing, each harmonic was normalized to the mean amplitude of that harmonic across all stimuli on that nerve. Though this method reduces the ability to detect signals that are present throughout all stimuli in an experiment, it increases the ability to detect changes in harmonic amplitudes between stimuli and weights all the harmonics equally, making it well suited to detecting stochastic events anywhere in the frequency spectra.

Inertial Cavitation Dose (ICD) was calculated via the same method but using frequency bands at five half harmonic intervals around the centre receiving frequency of the PCD transducer (5.8 MHz). This avoided interference from the harmonic peaks as much as possible and was used to detect the broadband inertial cavitation signature (4.15).

In the calculations and measurements earlier in this chapter (Table 4.2), it was found that for the exposures used in the FFP experiments, non-linear propagation was much more significant than in the MFP experiments. Since this creates higher harmonics, its contribution to the received acoustic signal can be interpreted incorrectly as stable bubble cavitation. However, sub- and ultra-harmonics can be used to differentiate this from bubble oscillation as they aren't produced by non-linear propagation through the media [Hamilton and Blackstock, 1998]. These signatures are examined when more detailed analysis is required. Also the variability of scattered signal between stimulus attempts will allow differentiation from harmonics produced just through non-linear propagation.

4.7.2 Wavelet Analysis and Statistical Data Handling

Improving upon, and used along side with the FFT methods described above, a new analysis method was developed for the FFP experiments, the theory and advantages of which are described in section 1.1.6.

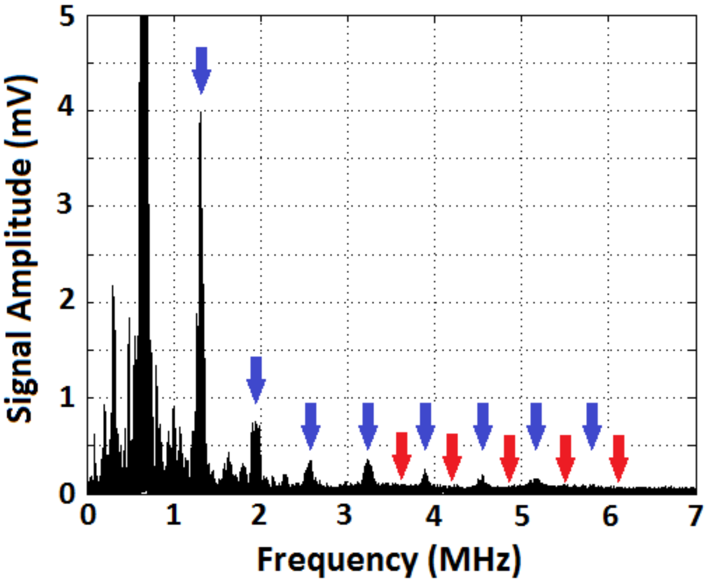

Figure 4.15: FFT of the 8 ms US exposure section taken from PCD recording. Blue arrows point to integer harmonics of the driving frequency that are analysed to determine the SCD. Red arrows indicate the inter-harmonic sections that are analysed to determine the ICD

This technique can be viewed as a bank of filters which decompose the acoustic emission signal into several components in the time domain where each component spans over a specific frequency band. The frequency bands are determined by the Nyquist frequency and the desired number of levels of decomposition. This is implemented by the wavelet transformation where the wavelet function specifies the transfer function of filters in the set. The Nyquist frequency was $f_N = 6.25$ MHz with $M = 5$ levels of decomposition. This gives the decomposed frequency bands the following frequency ranges: $\frac{f_N}{2^{n+1}} - \frac{f_N}{2^n}, n = 0, \ldots, M-2$. The wavelet function we chose is the Daubechies wavelet of order 10 (db10) as it has the right time characteristics for detecting inertial cavitation events and it has been shown to be effective for cavitation analysis in a previous study [Haqshenas and Saffari, 2015]. After performing the discrete wavelet transformation, short Fourier transform (STFT) and statistical analysis of each component of the signal are carried out to identify and characterise different cavitation regimes. Further explanation of the technique and its effectiveness at picking up multiple types of cavitation signals can be found in a previous study by this group [Haqshenas and Saffari, 2015].

In PCD recordings there is a baseline noise amplitude distribution that is added to both by direct signal from the driving transducer and signals from cavitation activity within the focal area. Cavitation adds large amplitude values to the right hand tail of the amplitude probability distribution. This modifies all the moments of the distribution: (Mean, Variance, Skewness, crest factor and Kurtosis). We briefly examined kurtosis, skewness and crest factor as quantifiers of cavitation activity and found that kurtosis was the best predictor of inertial cavitation activity with the highest signal to noise ratio. Kurtosis identifies the proportion of the signal variance due to infrequent extreme deviations such as the short duration high amplitude acoustic signals that inertial cavitation is characterised by. It is described mathematically below [Vaseghi, 2008]:

$$K = \frac{E(x-\mu)^4}{\sigma^4}, \tag{4.6}$$

where E is the expectation operator, x is the time series and μ and σ are the mean value and standard deviation of x respectively. A high kurtosis value will be produced if the probability mass is concentrated around the tails of the distribution, Gaussian noise will give a kurtosis value of approximately 3. Data was analysed in this way to measure cavitation activity (in each frequency band) in a way that could be scaled to large datasets. Signal variance in the time domain was used as a measure of total acoustic energy content within each frequency band and which includes signals from both stable and inertial cavitation.

The standard deviation of the kurtosis of a PCD noise recording (no acoustic emission signal), 0.02 at the highest frequency band and 0.07 at the lowest, was initially used to determine a threshold for detection of inertial events ($> 5\sigma$). It was subsequently found that the signal variation from reflections, pulsing and changing stable oscillation behaviours were sufficient to be reliably above this threshold. The kurtosis threshold was therefore increased until no signals in the lowest amplitude exposures used in the FFP experiments, where no inertial cavitation is expected to occur, were above this level (Figure 5.9).

4.8 Electrical Signal Analysis

Due to the volume of data being processed it was necessary early on to automate detection and quantification of nerve CAPs. This section will detail the data processing applied to the differentially amplified nerve activity recordings from the detection electrodes.

To detect CAPs, the electrical signal was split into 10 ms windows with no overlap and an FFT performed on each. As the extracellular population recording of a CAP is characterised by a slow summation of many signals, a low frequency component (0-5kHz) was used for detection. An amplitude threshold for CAP detection was set at 5 times the standard deviation (σ) of the 0-5 kHz background activity in the frequency domain or 5σ of the total background noise in the time domain. Once a CAP had been detected, a local amplitude maximum was found. The integrated area under the curve of a CAP, 5 ms each side of the peak voltage amplitude was used to measure the response amplitudes for both electrical and US stimulated CAPs.

In the MFP experiments, a boolean presence/absence value was used to replace the CAP amplitude measurement for the purposes of correlation testing as amplitude was primarily linked to the quality of connection between the nerve bundle and recording electrodes, which changed every time the bundle was moved.

The saturated, electrically stimulated CAP response, recorded 3 seconds before each US stimulation, was used as a reference point to normalise the absolute amplitudes recorded from US stimulation. This allowed comparison between nerve experiments and corrected for the decline in CAP amplitude seen over the 20 minute course of an experiment (Figure 4.8).

In cases where it was suspected that nerve responses to US were present but undetected due to less synchronous activation of nerve fibres such as by the 100 ms stimulation protocol, wavelet decomposition techniques described in section 4.7 were also used to process the nerve recording. The recording from the US stimulated nerve was decomposed into 20 levels using the Coiflet5 wavelet function and checked for correlation at each level to the same decomposition of the electrically stimulated nerve recording. The Coiflet5 type of wavelet function was selected following [Sherwood and Derakhshani, 2009]. This was not applied en masse to detect responses as it was not required to detect the large synchronous classical CAPs and was an intensive and time consuming analysis. This method was primarily used in the 100 ms exposure set for the reason mentioned above and because it allowed identification of weak nerve activity in the presence of electrical noise from US generation.

Response latency was measured from the onset of the ultrasound or electrical stimulus to the peak of the resultant CAP and is therefore the median latency of all the fibres in the bundle. This measure includes US travel time, nerve response time and CAP transmission time. Since nerve response time is of interest to the US stimulation mechanism, the other two factors were estimated and subtracted. The US travel time was constant and calculated to be 47 μs and 40 μs for the 0.67 and 1.1/2 MHz transducers respectively. The CAP transmission time along the nerve was estimated on a nerve by nerve basis using the preceding CAP transmission time from the interleaved electrical stimuli and the known relative distances between the electrodes. Subtracting these from the total lag time, an estimate for the nerve response time was calculated for each US induced CAP (Figure 5.7). This method assumes that the stimulation occurs in the centre of the US focal point every time, uniform conduction velocity along the length of the nerve and that the relative position of the CAP peak amplitude does not change with time or different stimulation modalities. These assumptions introduce non-systematic (pseudo-systematic within each nerve experiment) errors which, with a large enough dataset, will not affect the mean but will introduce significant error to individual latency estimations.

Any CAP detected more than 30 ms past the expected time window was excluded. These were used to estimate the probability of false positive results within the expected time window and occurred in less than 1% of the total recordings across all amplitudes.

4.8.1 Damage Analysis

Sensitive analysis of damage to the nerve bundle could not be performed during the MFP experiments as moving the nerve bundle altered the stimulation and reception of CAPs, meaning any decline in CAP amplitude could not be attributed to damage. However, experiments were performed using the MFP setup in three extracted nerves without movement to measure the mean normalised rate of decline when exposed to the maximum intensity US protocol (138 W/cm^2, 0.67 MHz, 10 kHz PRF, 8 ms TSD) compared against the mean rate of decline for three nerve bundles not exposed to US (all other conditions remaining constant). The nerve bundle was also macroscopically examined for signs of damage such as cavitated or thermal lesions after all experiments.

In the FFP experiments, damage to the nerve bundle was detected by two means.

The primary method was to measure proportional reductions in electrical stimulation amplitude from one stimulation to the next. A significant damage event detected by these means was defined as more than a 20% reduction caused by a single US stimulus. This threshold was defined by 1.5 times the maximum point to point decline detected in nerves not exposed to US (Section 4.3).

Smaller scale damage that may have been caused by US stimulation over a longer period was tested for by determining the correlation coefficient of the decline in CAP amplitude with acoustic kurtosis and signal energy at all frequency bands in each nerve experiment. Correlation was also tested for between the same variables, irrespective of US frequency or individual nerve experiments, across all data for each stimulation protocol.

The second method used to detect significant damage events was through identification of after-discharge (repetitive nerve activation) after a successful US stimulation event (Figure 5.18c). After-discharge is known as a sign of poration in the nerve membrane as the charged ions equilibrate causing the membrane to regularly depolarise [Lee et al., 1995]. After-discharge was identified when the standard deviation of the raw electrical signal (100-150 ms after the CAP peak) was more than 1.5 times greater than the background σ measured before CAP initiation.

4.9 Artefacts and Data Filtering

In both the MFP and FFP experiments, artefacts were present in both the electrical and acoustic data sets that were filtered out before statistical analysis or measurements of response reliability were performed. When any artefact described below was detected, electrical and acoustic recordings, and corresponding recordings from the paired electrical or US stimulation, were excluded.

Due to the spiky noise produced by inertial cavitation, the acoustic signals sometimes exceeded the captured voltage range of the oscilloscope, causing peaks to become clipped (flat on top). These signals caused anomalies in the frequency spectrum analysis of the signal which were easily detected.

Sometimes during the course of an experiment a nerve would degenerate until the electrically stimulated CAP was no longer detected. As this would guarantee failure to detect any successful US stimulus, only US stimuli attempts with successful preceding electrical stimulation were included in the analysis. Similarly, if no ultrasound signal was detected by the PCD, the associated data was ignored.

If the US driving signal was detected by the PCD with anomalies, such as a TSD outside the expected range (0.1 times smaller or larger than the expected value), the associated data was excluded. Another such anomaly is DC drift which, despite the high pass filter RC circuit between the amplifier and oscilloscope, was observed very infrequently in both acoustic and electrical recordings.

Depending on the efficiency of the transducer in question, a weak oscillating electrical field potential was generated by the US transducer which generated noise at the driving frequency through induction in the recording electrodes, interfering with recordings from the nerve. Though the noise was greatly reduced by using an earthed ringers bath (Figure 4.1), a temporal and spectral filtering algorithm was designed to prevent such noise being mistaken for CAP responses. Poor earthing of the ringers bath solution in the MFP experiments occasionally caused the driving frequency of the US to be picked up very strongly by the recording electrodes. This was detected as an increased mean absolute electrical signal amplitude lasting for the expected acoustic stimulus duration (8 or 100 or 300 ms) and the associated data excluded.

4.10 Correlation Analysis

Statistical correlation was tested for between many measured parameters such as radiation force and stimulation success to test potential causative links. This analysis was performed using a Pearson Correlation Coefficient function in MATLAB after excluding all the anomalies mentioned in section 4.9.

4.11 Control Experiments

A sham experiment with no air gap and a wet bundle of cotton threads in place of the nerve, replicating the tissue's impedance for the differential voltage amplifier, was used to determine the amplitude of the raw electrical noise from US generation within the transducer. This induction noise was found to be between 0.1-0.5 mv.

Direct stimulation of the nerve via a weak oscillating electric field [Francis et al., 2003] was ruled out by a sham experiment where the US cone was raised, creating a reflecting air gap between the cone and the ringers bath and the primary US stimulation protocol repeated at high intensity. No direct stimulation was observed in this manner across 3 electrically responsive nerves and 66 individual stimuli (8 ms TSD, 0.67 MHz, 10 kHz PRF, 50% DC, 30/90s repetition period).

Chapter 5

Crab Walking Leg Nerve - Results

5.1 Moving Focal point

Out of 19 nerves that were confirmed viable by electrical stimulation post extraction, 10 responded to some level of US stimulation (53%). Of the 19 nerve bundles, across all amplitudes tested including repeat stimuli, only 6% of US stimuli (n = 580) resulted in any observable CAP (Table 5.1.1). It was quickly noticed that predominantly the first US burst of any series of repeats resulted in successful neurostimulation (Figure 5.1), not the subsequent 4 repeats in the same location. If only these first pulses are counted the success rate of US neurostimulation increases dramatically to 28% (n = 116) or 69% at the highest amplitude tested. The lowest US amplitude that resulted in CAP generation was 25 W/cm^2 I_{SPPA}. The Electrical and US stimulated CAPs appear at different times due to the different physical stimulus locations along the nerve bundle, the US focal point being located much closer to the recording electrodes (Figure 4.2)

5.1.1 Recovery Times

In one nerve extraction experiment after a successful US response was observed, without moving the US focus, times between sets of 5 stimuli were varied to 1, 5, 10 and 20 minutes. All subsequent stimuli beyond the first failed to result in an US induced CAP over the whole 37 minutes. US stimulus was immediately successful again upon subsequent movement of the nerve bundle by 5 mm.

5.1.2 Analysis of Acoustic Emission

In the four nerve experiments exposed with a constant 138 W/cm^2 (96 total exposures, 18 successful stimuli), acoustic data was recorded and analysed using the methods

I_{SPPA} (W/cm^2)	Total Exposures	Exposures on Responsive Nerves	Successful US Responses
3	95	85	0
11	95	75	0
25	95	75	1
44	95	90	4
70	95	85	9
101	95	90	7
138	95	80	11

Table 5.1: Total Ultrasound Exposures, exposures on electrically responsive nerves and successful responses to US stimuli in 19 nerves.

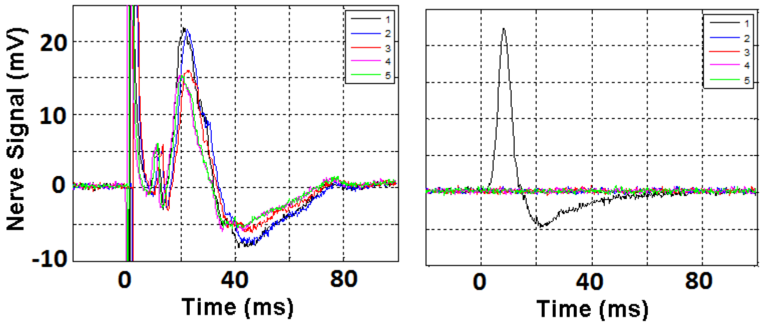

(a) (b)

Figure 5.1: Recorded voltage amplitude profiles involving large CAP activity from a crab leg nerve bundle using alternating electrical and ultrasonic stimulation as per the protocol in section 4.5.1. Five electrical stimulation recordings are grouped in (a) and five US stimulation recordings in (b). All recordings were taken over a 30 s period.

described in section 4.7.1. Higher amplitude harmonics were found to be positively and significantly correlated with US stimulus success compared to unsuccessful stimuli. The degree of correlation in a single nerve experiment between the binary observation of a CAP and the amplitude of the different harmonics can be seen in figure 5.2. The aggregate of this across all recordings with harmonic amplitudes normalised to mean PCD signal amplitude for each nerve is shown in figure 5.3. the amplitude of the half and second harmonic are most significantly correlated to successful CAP generation.

No significant correlation was found between ICD and nerve response in any of the four nerve experiments tested.

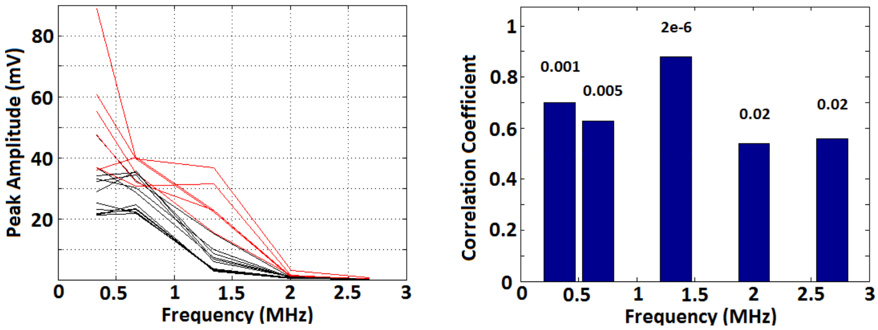

(a) (b)

Figure 5.2: Analysis of harmonic amplitudes from 18 US stimulation events In a single nerve. (a) Peak harmonic amplitudes of the acoustic emission. The 6 successful stimuli (that produced a CAP response) are coloured red. (b) Correlation statistics of the binary presence/absence of a CAP and harmonic amplitudes with P-values displayed above the bars.

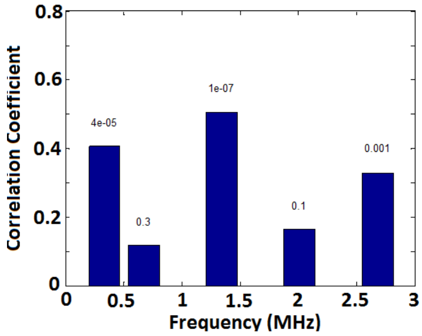

Figure 5.3: Correlation statistics of the binary presence/absence of a CAP and harmonic amplitudes across all acoustic data with P-values displayed above the bars (n=96, 18 successful stimuli).

5.1.3 Damage

No macroscopic damage to the nerve tissue was observed after any experiment. The mean rate of electrically stimulated SNAP response decline of a nerve bundle with and without US exposure (138 W/cm^2 I_{SPPA}) over 30 minutes was not found to be significantly different, as shown in figure 5.4.

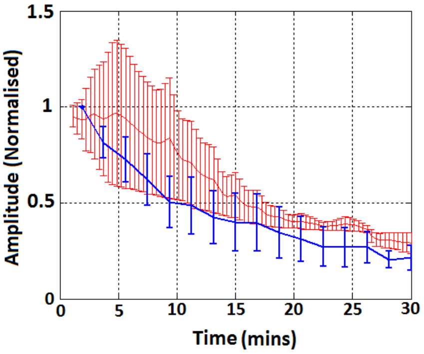

(a)

Figure 5.4: Mean peak positive voltages of electrically stimulated CAPs, with (red), and without interleaved US stimulation (blue). Background nerve decline (without US), also shown in figure 4.8. The highest intensity US exposure protocol used in the moving focal point experiments (138 W/cm^2 I_{SPPA}) was used interleaved with 80 electrical stimuli in 30 minutes.

5.2 Fixed Focal Point

142 nerves responsive to electrical stimulation were exposed to a range of ultrasound parameters which, similar to the MFP experiments, were shown to be capable of eliciting large and synchronous CAP events from the unmyelinated crab leg nerve bundle (Figure 5.5). Responsive nerve bundles could be stimulated multiple times with stimulus reliability varying between 5 and 80%, strongly depending on fundamental frequency and pulse average intensity of stimulation. The lowest threshold for any observation was at 100 W/cm^2 I_{SPPA} for the 8 ms, 0.67 MHz stimulus. Inertial cavitation signals were detected in all successful stimuli. The results from each stimulus protocol variant are presented in this section.

5.2.1 8 ms 0.67 MHz Stimuli

61 electrically responsive nerves across 26 crabs were tested using a range of 11 different US stimulation intensities (Table 4.2). Using the stimulation protocol described in section 4.5.2, overall response reliability was less than 25 % at all intensities (Figure 5.6 a). Responses occur at sporadic times throughout the 22 minutes of an experiment with an increased response probability for the first stimuli, similar to findings described in section 5.1(15% of all experiments responded on the first attempt compared to a mean of 7% for any other time point).

The intensity threshold for the neurostimulation effect was at 100 W/cm^2. Cor-

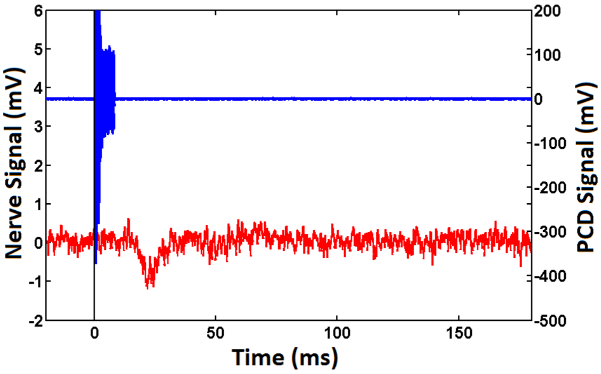

Figure 5.5: Example of a nerve CAP response (red, left axis) to the 0.67 MHz, 8 ms stimulation protocol at 562 W/cm^2, recorded simultaneously with acoustic PCD data (blue, right axis).

relation coefficients between the amplitude of the CAP response and both PCD signal energy and kurtosis, find significant ($P<0.05$, $n=22$) correlation in two nerve experiments at 485 and 562 W/cm^2 across all frequency bands.

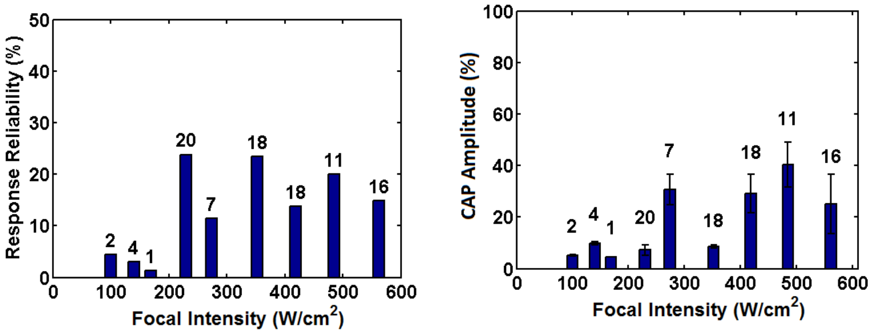

(a) (b)

Figure 5.6: Response success statistics for the 8 ms, 0.67 MHz stimulation protocol. Numbers of successful stimuli at each intensity are displayed above each bar. (a) Total response reliability for all nerves tested at each intensity level. Two nerve experiments with over 50% reliability were excluded as outliers. (b) Mean amplitude of US induced CAPs as a proportion of the electrically induced CAP amplitude.

Mean response lag time was 3.16 ms (n=106) once estimated CAP transmission time for each response had been subtracted. The combined effect of the assumptions in this estimation (Section 4.8) resulted in significant error, with a number of responses occurring before the beginning of the stimulus (Figure 5.7(b)). This resulted in a high latency standard deviation of 4.28 ms. A closer estimate of the true response latency variability was determined by the mean intra-nerve standard deviation, calculated at 2.87 ms, as the errors due to prior assumptions were consistent within the same nerve.

Latency did not vary significantly with US stimulation intensity.

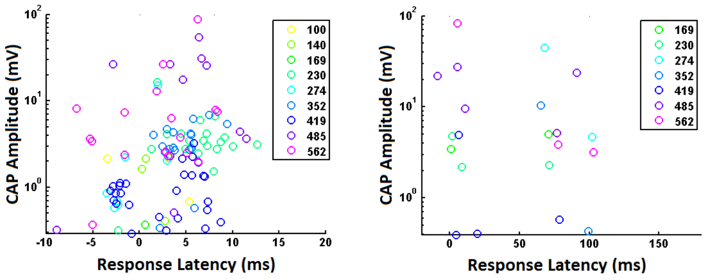

(a) (b)

Figure 5.7: Heatmaps of US CAP responses resulting from the 0.67 MHz, 8 ms stimulation protocol, colour and corresponding legends note the intensity of stimulation in W/cm^2. (a & b) Latency of ultrasound responses, measured from the onset of ultrasound stimulus to the peak of the CAP response, estimated CAP conduction time has been subtracted. Colour and corresponding legends note the intensity of stimulation in W/cm^2. (a - 8 ms TSD, b - 100 ms TSD).

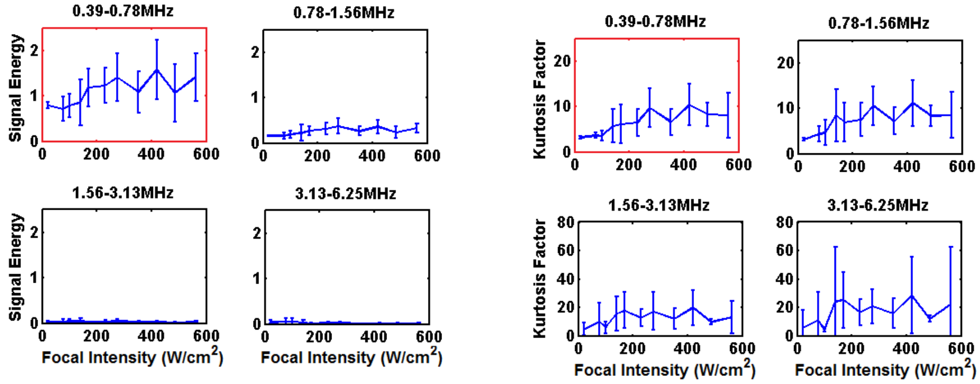

(a) (b)

Figure 5.8: Mean and standard deviation error bars of (a) signal energy and (b) time domain kurtosis in four frequency bands decomposed from PCD recordings of the 8 ms, 0.67 MHz US stimulation protocols. The frequency band containing the US driving frequency is highlighted in red.

The majority of the signal energy for the 0.67 MHz protocol lies in 0.39-0.78 MHz band, covering the primary driving frequency. This signal component will primarily be generated by refraction of the driving signal from the nerve bundle in the focal area and by scattering by bubbles. Amplitude variation of this component, shown by high error bars in figure 5.8 (a), therefore indicates a change in refraction or re-radiation of the driving signal from the focal region by impeding or resonating structures such as bubbles.

Inertial cavitation was found to be ubiquitous at pulse average intensities past 100 W/cm^2, with broad frequency band (1.56-6.25 MHz) inertial events (kurtosis>6) occurring in more than 70% of US stimuli (Figure 5.9). This matches with the threshold for successful US stimulation also seen at 100 W/cm^2. These broadband events are not as prevalent in the lower bands (0.39-1.56 MHz) (Figures 5.9 and 5.8(b)) because of the greater influence of continuous signals such as the primary and secondary harmonics on the spikedess of the temporal signal. The majority of inertial cavitation events are not associated with any resultant nerve activity, which is discussed further in section 6.2.1.1.

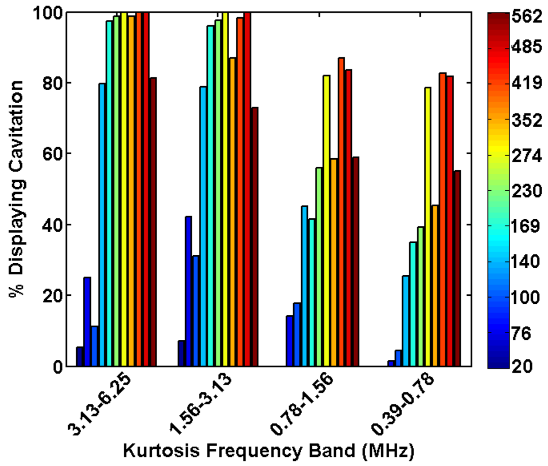

(a)

Figure 5.9: Percentage of US stimuli (8 ms,0.67 MHz protocol) showing above threshold kurtosis (>6) in four frequency bands at each stimulus intensity. The colour-map on the right is in units of W/cm^2

5.2.2 100 ms, 0.67 MHz Stimuli

19 electrically responsive nerves across 6 crabs were tested using the same range of US stimulation intensities (Table 4.2) as used in the 8 ms protocol. The threshold intensity for CAP generation (first detected response at 169 W/cm^2) as well as the response reliability profile are close to findings in the 8 ms experiments (Figures 5.6 and 5.10(a) and (b)). The pattern of inertial cavitation activity measured by kurtosis and its standard deviation matches well with the response threshold and more generally with the pattern of response reliability and response amplitude (Figure 5.10). In particular, the threshold intensity level for US responses, 169 W/cm^2 is also the first to show significant standard

deviation of kurtosis in either of the lower frequency bands, shown by the error bars in figure 5.10(c). This is an indicator of signal variation between exposures as would be found with cavitation with variable initial nuclei.

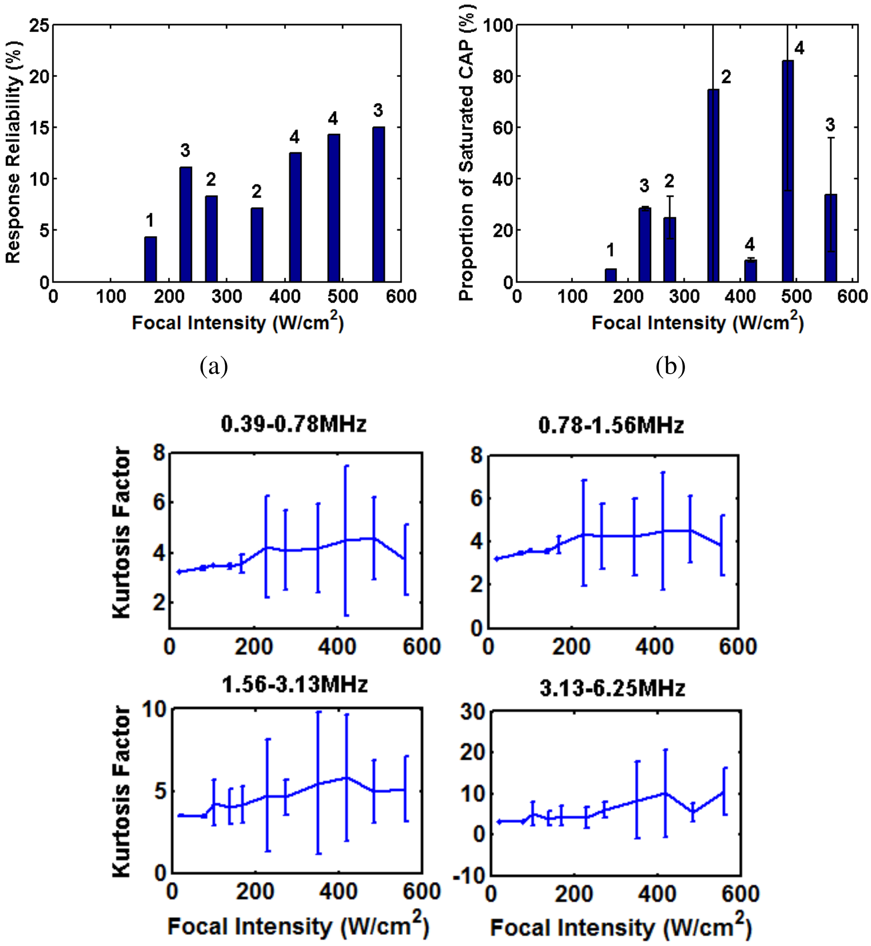

(a) (b)

(c)

Figure 5.10: (a and b) Response success statistics for the 100 ms, 0.67 MHz stimulation protocol. Nerves that did not respond to electrical stimuli were excluded. Numbers of successful stimuli at each intensity are displayed above each bar (a) Mean response reliability for all nerves tested at each intensity level. (b) Mean Amplitude of US induced CAPs as a proportion of saturated electrical stimulus recording taken before each US stimulus. (c) Mean acoustic signal kurtosis of four frequency bands across all intensities. Error bars show standard deviation.

This apparent coherence was tested by correlation coefficients within each nerve experiment. Significant positive correlation between cavitation measures (kurtosis and signal energy) in key PCD time sections and nerve response amplitude was found in 5 individual nerve experiments (56% of US responsive nerve experiments) across all frequency bands. All 100 ms exposures were then aggregated to determine the correlation between cavitation and response amplitude, irrespective of US driving intensity and separate nerve experiments. Significant positive correlation was found between kurtosis of acoustic signals and nerve response amplitude across all frequency bands as shown in figure 5.11. This strongly implicates the involvement of inertial cavitation, typified by temporally short, broad frequency band signals, in the successful stimulation events.

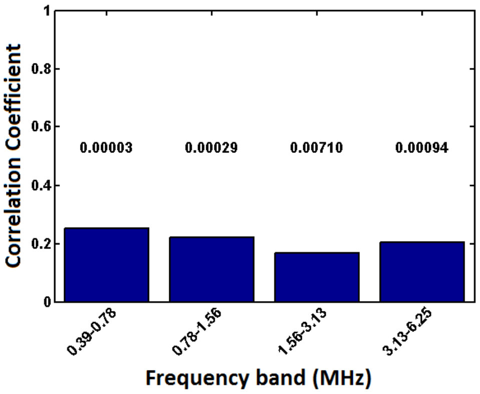

Figure 5.11: Correlation between acoustic signal kurtosis in four frequency bands and nerve response amplitude across all experiments in the 100 ms exposures. P values are displayed above each bar (N=304).

Similar to the 8 ms exposures, ubiquitous cavitation activity detectable in all frequency bands was found over 169 W/cm^2 shown in figure 5.10(c). However, Analysis of the kurtosis of separate time sections showed that the majority of the inertial activity was restricted to the first 10 ms time bin (Figure 5.12). Sporadic events did occur after the initial burst of cavitation such as shown in figure 4.14, at a much lower event frequency, demonstrated by the much lower mean kurtosis values seen in figure 5.10(c) compared to 5.8(b).

5.2.3 300 ms 0.67 MHz Stimuli

Reproductions of the intensities and pulse parameters found in CNS stimulation literature [Lee et al., 2015] at 0.67 MHz were unable to generate CAP responses in the crab nerve bundle. Incrementally increasing the intensity of stimulation resulted in a threshold for CAP generation at 169 W/cm^2.

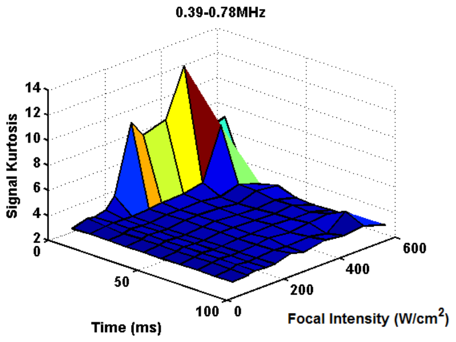

(a)

Figure 5.12: Mean values of PCD signal kurtosis of the lowest frequency band over 100 ms, split into 10 ms divisions and a range of stimulation intensities (I_{SPPA}).

5.2.4 1.1 and 2 MHz Stimuli

58 electrically responsive nerves across 11 crabs were tested using a range of 5 different US stimulation intensities (Table 4.2). US stimulus intensity levels for these frequencies were chosen to reproduce the radiation forces due to tissue absorption and reflection (Table 4.2). At these intensity values no nerve responses were observed.

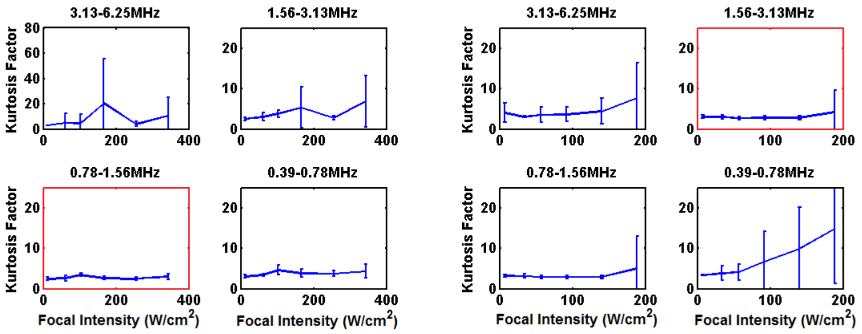

(a) (b)

Figure 5.13: Mean values and standard deviation error bars of time domain kurtosis in four frequency bands decomposed from PCD recordings of the 8 ms, 1.1 MHz (left) and 2 MHz (right) US stimulation protocols. The frequency band containing the US driving frequency is highlighted in red.

Occasional high kurtosis events were seen with 1.1 and 2 MHz exposures (Figure 5.2.4), though, as expected, the acoustic signal energy in frequency bands other than driving was near zero (<0.1% of total signal energy at all points) with very low standard deviation between experiments. Therefore the cavitation activity present was considered negligible.

At higher amplitudes, no CAPs were measured for stimulation at 1.1 MHz (up to 0.86 kW/cm^2). At 2 MHz the threshold for stimulation was found at 6.7 kW/cm^2 where responses were again associated with inertial acoustic events as shown in figure 5.14.

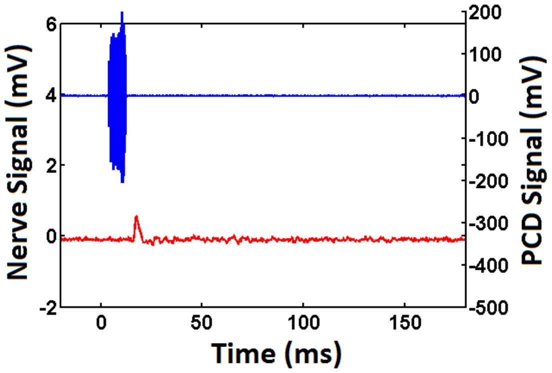

Figure 5.14: Example of a nerve CAP response (red, left axis) to the 2 MHz, 8 ms stimulation protocol at 6.7 kW/cm^2, recorded simultaneously with acoustic PCD data (blue, right axis).

5.2.5 Individual Case Analysis

Though correlation coefficients show a strong association between inertial cavitation and nerve activation, they could mask individual cases where stimulation occurs without cavitation. To test for this possibility, individual nerve experiments with weak or negative correlation between US stimulated CAP amplitude and acoustic kurtosis or signal energy were investigated in more depth. The ubiquitous cavitation activity that dominated throughout the 8 ms recordings meant that inertial cavitation was always found preceding a stimulus even in experiments showing poor correlation. In the 100 ms exposures, several stimuli were identified that were poorly correlated to kurtosis or signal energy values. Two of these are shown in figure 5.15.

In most cases such as the example in figure 5.15(d), standard spectrographic analysis of the entire signal was sufficient to detect signature broadband cavitation events within the anticipated region. Poor correlation in these cases was due to particularly high amplitude acoustic events throughout the rest of the experiment (22 US exposures). The lowest intensity example of successful stimulation with 100 ms exposures did not have any obvious signs of cavitation using standard spectrographic analysis (Figure 5.15(a) and (b)). However, using wavelet decomposition and windowed kurtosis, inertial events were found in the 195-391 kHz signal component within the expected time section (Figure 5.16). Sub-harmonic emission is generated by non-linear bubble pulsation [Leighton, 1994] and could arise from large bubbles (that have a lower reso-

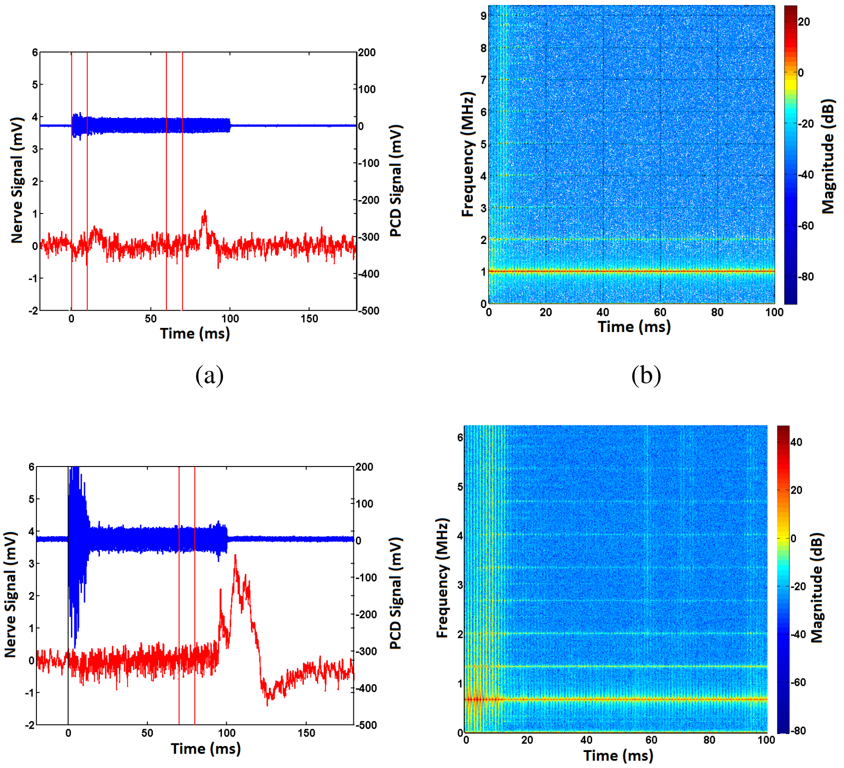

(a) (b)

(c) (d)

Figure 5.15: Two examples of US stimulation with the 0.67 MHz, 100 ms protocol ((a & b) 169 W/cm^2 (c & d) 485 W/cm^2) that had poor correlation with cavitation activity. **Left** - PCD recordings (blue trace, right axis) and electrical nerve responses (red trace, left axis). Vertical red lines show the region of the stimulus pulse expected to have initiated the US CAP. **Right** - Spectrographic analysis of the raw 100 ms PCD recording of the US stimulus.

nant frequency than the driving US) oscillating at their resonant frequency [Neppiras, 1980, Wijngaarden, 2012], such as those introduced by the extraction process (Figure 4.9). The faintness of these low frequency events is due to the very low sensitivity of the PCD at such frequencies.

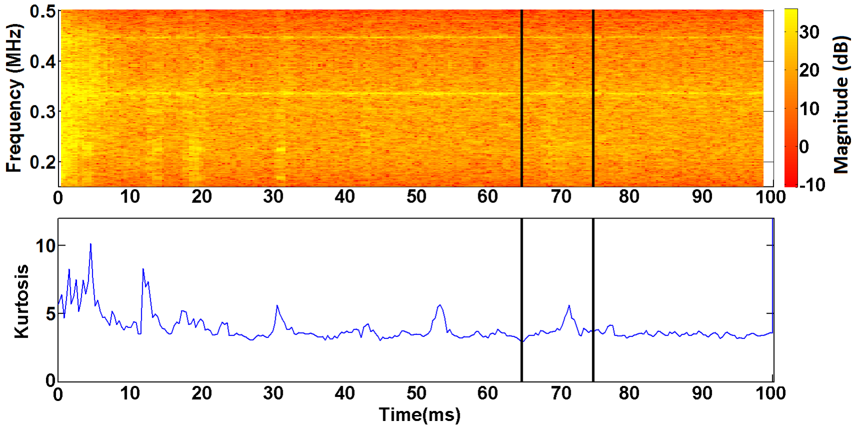

Figure 5.16: Spectrographic and kurtosis analysis of the 0.2-0.39 MHz component of a 100 ms, 0.67 MHz protocol stimulus at 169 W/cm^2, shown in figure 5.15 (a) & (b). The signal was decomposed into frequency bands via the wavelet analysis method. Vertical black lines indicate the estimated window when the CAP was initiated.

5.2.6 Hypersensitive Examples

Two nerves exposed using the 8ms, 0.67 MHz protocol were found to be hyper-responsive, showing response reliabilities of between 65-80% (n=22), occurring at 352 and 230 W/cm^2 respectively. Considering the mean response reliability of this protocol across all intensities was 11.6%, these nerve experiments were treated as outliers and investigated separately.

Though the mean signal energy content of PCD data from either hypersensitive experiment was not significantly different from other experiments at the same intensity, the time domain kurtosis was on average 0.8 and 0.63 times the mean value of the different frequency bands at 230 and 352 W/cm^2 respectively across all frequency bands. The variance of kurtosis between different exposures in each experiment was also found to be low compared to three other experiments at the same intensities (0.46 and 0.68 times the mean signal energy variance and 0.48 and 0.55 the mean kurtosis variance across all energy levels respectively). The same was also found for the variance of the (frequency domain) harmonic amplitudes within each 8ms stimuli measured by spectrographic analysis (0.72 and 0.66 times mean variance of signal amplitude of the 2nd, 3rd and 4th fundamental harmonics compared to three other experiments at the same intensities) (Figure 5.17).

Compared to harmonic emissions measured for other experiments at the same intensity, the two hyper-responsive nerve experiments showed approximately 50%

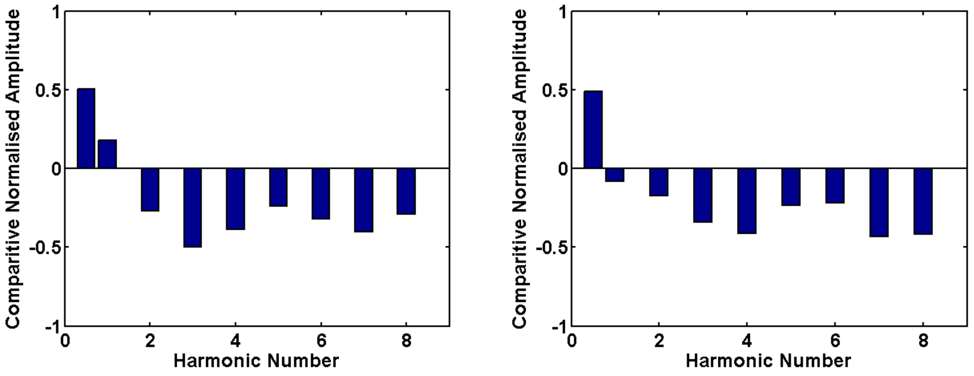

(a)

(b)

Figure 5.17: Mean frequency domain amplitude (n=22) of 1 sub harmonic ($f_0/2$) and 8 harmonics (f-f_8) of the hypersensitive nerve experiments normalised by the sum of all the harmonic amplitudes excluding f_0 as a proportion of the mean harmonic amplitude of three other experiments (n=66) at each intensity (a) 230 W/cm^2 (b) 352 W/cm^2.

greater sub-harmonic content as a proportion of the total signal (Figure 5.17). This which can indicate the oscillation of large bubbles [Neppiras, 1980, Wijngaarden, 2012]. Given the likelihood of large micro-bubbles being introduced by submersion of the nerve, described in section 4.3.1, and the consistency of the harmonic emission in these two studies, the source of the harmonic emission pattern is thought to be persistent large bubbles under the US focus. Bubbles in these cases could have been trapped in close proximity or inside the nerve bundle in these two experiments, thereby repeatedly stimulating the nerve bundle through a stable oscillation mechanism.

5.2.7 Damage

US was found to damage the exposed nerve bundles sporadically. The lowest intensity example of after-discharge in the 0.67 MHz 8 ms protocol, at 230 W/cm^2, is shown in figure 5.18(c). Two other after-discharge events in separate nerve experiments were observed above this intensity threshold (at 485 and 562 W/cm^2), all three were concurrent with reduced electrically stimulated CAP amplitude.

Each of the damage events causing after-discharge were examined spectrographically. Large broadband noise signatures marking inertial cavitation events (Figure 5.18(d)) were seen preceding all these instances of significant damage (proportional decline of $>20\%$). The cause was therefore deemed likely to be inertial cavitation induced membrane rupture.

Significant positive correlation ($P<0.05$, n=22) between decline of the electrically

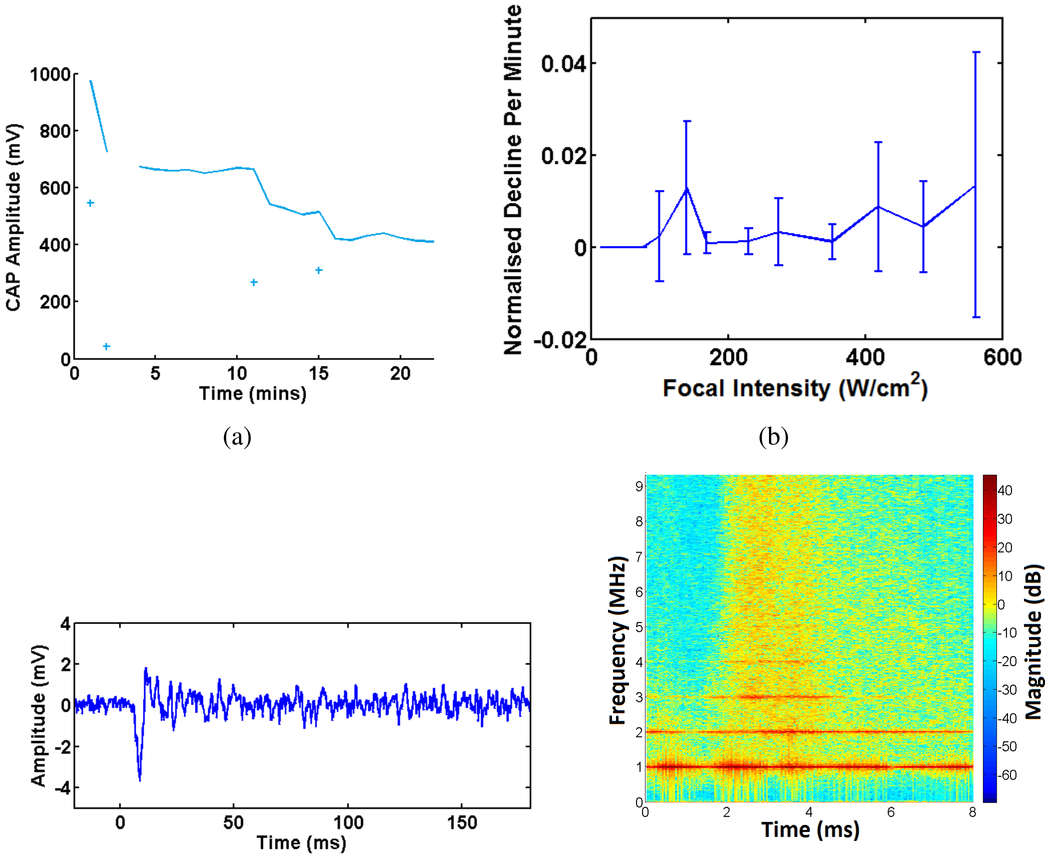

(a) (b)

(c) (d)

Figure 5.18: (a) Example of electrically stimulated CAP amplitude (line) and US stimuli (+) over 22 stimuli on a single nerve. This example was exposed using the 0.67 MHz, 8 ms stimulation protocol at 562 W/cm^2. (b) Mean decline over time of the electrically stimulated CAP amplitude of the 0.67 MHz, 8 ms stimulated nerves, normalised to the amplitude of the first stimulus with standard deviation error bars. (c) Example of after-discharge due to nerve damage using the 0.67 MHz, 8 ms stimulation protocol at 230 W/cm^2. (d) spectrographic analysis of the PCD signal of the first damage causing ultrasound event in (a)

stimulated CAP and acoustic kurtosis & signal energy was seen in two of the three after-discharge occurrences mentioned above and in three more nerve experiments shown in figure (5.19(a)). Positive correlation is also found in 3/19 nerve experiments in the 100 ms exposures (Figure 5.19(b)). Occurrence of damage by any of these measures was observed in 4% of total nerve experiments at any intensity or frequency. No significant damage as a result of US exposure occurred at either 1.1 or 2 MHz.

Degradation of the electrically stimulated CAPs in nerves not exposed to US (Section 4.3) across 22 minutes (Mean normalised decline per minute = 0.009, σ=0.013) was not significantly different from mean decline of US exposed nerve bundles where

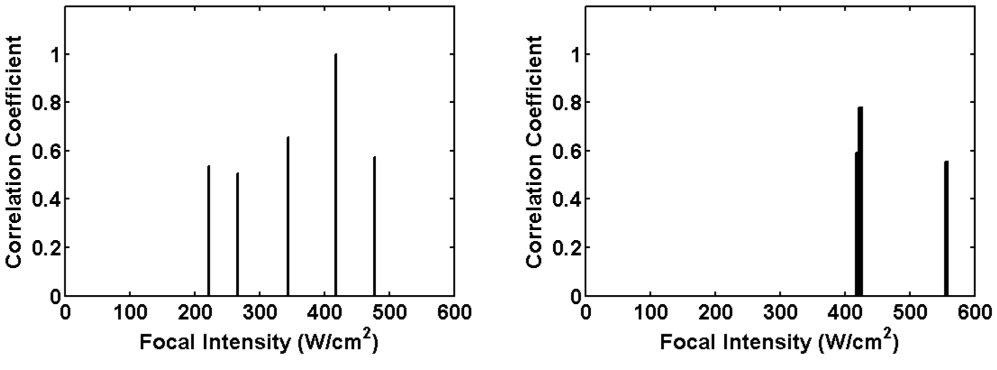

(a) (b)

Figure 5.19: Significant ($P<0.05$) correlation coefficients between damage (proportion of amplitude reduction from one electrical stimulation to the next) and acoustic kurtosis from (a) 8 ms and (b) 100 ms US stimulation irrespective of frequency band in which correlation occurred. Bars represent individual nerve experiments. In cases with correlation present across multiple frequency bands, the highest correlation coefficient is displayed.

signs of major damage events as above were not seen at any intensity. The rate of decline in CAP amplitude over the 22 minutes also did not significantly change between exposure intensities (Figure 5.18(b)). No significant correlation between damage and either signal energy or kurtosis was found when measured across all data for each stimulation protocol, irrespective of US frequency or individual nerve experiments.

Chapter 6

Discussion

Our results demonstrate that US stimulation can elicit *de-novo* action potentials in both mamalian and crustacian peripheral nerves. Unmyelinated axonal tissue alone is found to be sufficient to generate action potentials in response to ultrasound stimulation. Examining the nature of this response allows several insights into the underlying mechanisms, which, in the present case, the author demonstrates to be cavitational.

The lowest threshold at which responses were seen in any of the experiments conducted here, was an order of magnitude greater than pulse average intensities used in some studies achieving successful stimulation in rat brain tissue [Kim et al., 2014a,b, 2012, Tufail et al, 2010, Yoo et al, 2011a]. These studies use lower frequency ultrasound (300-350 kHz) which has indeed been shown to be a critical factor by the current study and others [Gavrilov et al., 1977, Kim et al., 2014a, King et al., 2013, Lee et al., 2014, Muratore et al., 2009] and may acount even for this large discrepancy in the pulse average intensity threshold. From investigations repeating the pulsing parameters of an applied study in the human brain (Section 5.2.3) [Lee et al., 2015], pulse protocol does not appear to play a role. The potential for the mechanism observed here to be the same as in many *in vivo* brain studies cannot be ruled out, though until further research tests this link, the mechanisms should be treated as distinct. Subsequent discussion will therefore focus on the characterisation of the currently observed stimulation phenomenon.

The intensity thresholds found in this study are much closer to those reported by Gavrilov's group and others targeting peripheral nerve structures [Gavrilov et al., 1996, Legon et al., 2012, Mihran et al., 1990, Tych et al., 2013, Wright and Davies, 1989], re-enforcing the apparent divide in threshold US amplitude between neuromodulation of the CNS and the Peripheral Nervous System (PNS) (Figure 2.2). The extent of the separation in required intensities between these two paradigms demonstrate the importance of identifying in different tissue types, the specific US effects and their thresholds. This could then be used to develop a fuller understanding of the US-tissue interaction and targeted ultrasound therapies, including but not limited to neurostimulation.

6.1 Rat Saphenous

These preliminary experiments demonstrated several important mechanistic features of the US-nerve interaction which were used to drive the design of the crab leg nerve experiments but also represent several distinct findings.

The first of these is that direct US neurostimulation can be observed in mammalian peripheral nerves. the second is that observed stimulation cannot function through synapse or cell body related mechanisms such as vesicular fusion as these structures are not present in the preparation. The stimulus effect is therefore acting directly on the axons in the nerve bundle or on the nerve endings in the skin, directly underneath the bundle. There are several different populations of sensory neurons that innervate onto the skin through the Saphenous nerve, many of which have high concentrations of MS ion channels in their terminals. During these experiments it was noted that reliability and amplitude of SNAP responses varied greatly between stimulus location. This same observation was made by Gavrilov's group and others in several different studies eliciting different sensations in the skin [Dickey et al., 2011, Gavrilov and Tsirulnikov, 2012]. In the case of skin stimulation Dickey et al., found that the success of the effect was directly correlated to the density of mechanoreceptors. It is therefore possible that MS ion channels contained in sensory nerve endings in the skin are the mode for US induced stimulation in these experiments.

Though all of the US forces increase with increasing power, only the peak pressure varies in the same linear fashion as the observed response reliability (Table 3.3). This suggests that response success is dependant on peak pressure directly, or on a secondary pressure dependant effect instead of intensity dependant forces such as heating or radiation force. In relation to the potential mechanisms proposed in section 2.3, the candidates are direct pressure effects (Section 2.3.3) or cavitation effects (Section 2.3.4).

The unreliability of the observed response even at very high amplitudes or pulse lengths indicates that there is some stochastic process either in the propagation and absorption of the ultrasound within the tissue or in the effects that it elicits on the cell. One possibility to explain this could be cavitation resulting from the presence of small gas bubbles or other cavitation nuclei in the tissue which may move and change between stimuli. The synthetic interstitial fluid that filled the bath was in fact constantly gassed with oxygen for the health of the sample, the gas saturation of which would make cavitation likely.

Although inertial cavitation appears not to be necessary for a stimulatory effect [Tufail et al, 2011, Tyler et al, 2008, Yoo et al, 2011a], it is possible that it was responsible for stimulation in these experiments due to higher peak pressures than used for *in vivo* studies. A similar cavitation hypothesis was proposed by Dinno et al. [Dinno et al., 1989] and supported by others [King et al., 2013, Lee et al., 2014, Muratore et al., 2009, Tych et al., 2013]. Dinno's group showed that entirely degassing the tissue bath media eliminated an electrophysiological effect of US similar to the one observed in the present study.

Given the stochasticity of the proposed mechanism, pulse length was expected to be a strong determinant of response success, but in fact had a low saturation point. In a similar result to a previous parametric study [Kim et al., 2014a], sub 1 ms pulse lengths were shown to have a strong effect on response reliability, with a much lesser effect at lengths over 1 ms (Figure 3.4), in keeping with the prevailing opinion in the literature [Gavrilov and Tsirulnikov, 2012, Tyler et al, 2008, Yoo et al, 2010]. As only one data point was taken below 1 ms, more data is required to reliably identify the importance and cause of this pulse length dependence.

Though the discoveries made in these experiments fit with a cavitational mechanism, they are limited in their conclusive power due to the multiple tissue types under the US focus and uncontrolled, reflective acoustic environment. The next section will detail the results of the crab nerve experiments, designed to address these issues and test the predictions made here.

6.2 Crab Leg Nerve

6.2.1 Ultrasound Force Mechanism

In the moving focal point experiments, US responses were seen at much lower intensities compared to results from the rat saphenous, but were observed to primarily stimulate only on the first pulse train fired. The application of repeat stimuli often only succeeded to generate a CAP when the nerve was moved so that a new section was under the US focus (success rate increases to 67% from 29% when considering only US stimulus on fresh nerve sections). Recovery times of up to 20 minutes also seemed to have no effect in creating a new CAP, which indicates that the conditions within the nerve bundle required for US stimulus are permanently changed upon US application, or take a longer time than tested to regenerate. Given that inhibition of electrically induced CAPs from a US exposed bundle was not seen compared to base rate (Figure 5.4), the lack of further US induced CAPs is not thought to be due to mechanical damage or any condition of the nerve which is involved in normal CAP conduction.

It is possible in both the MFP and FFP experiments that analysis of damage through changes in the electrically induced CAP could fail to detect damaging events if they affected a population that was not effectively electrically stimulated or recorded from within the bundle. However, this is deemed unlikely and therefore would not significantly affect datasets with large numbers of repeats such as these.

Without mechanical damage as a source of this inhibition the author proposes that the mechanism of the observed stimulation in this experiment involves the bubbles that were observed on the nerve bundle described in section 4.9, which are knocked off or destroyed/dissolved during the first US stimulation. As well as explaining the location specific inhibition seen in the MFP experiments, it could also explain the location specific sensitivity changes observed in the skin-nerve preparation. Though the first stimulation was also preferred in the FFP experiments (15% compared to 7% for any other time point in the 8 ms dataset), the effect is smaller, thought to be due to the influence of saline versus oil transmission media on the attachment of the bubbles to the bundle. The two nerve experiments that displayed particularly high response reliability in the FFP experiments described in section 5.2.6 were thought to be due to one of these introduced microbubbles that was stabilised within the nerve bundle.

Cavitation involving these large introduced bubbles cannot be the only mechanism however, as occasional responses were seen at a lower rate from repeats in the same location on the nerve in the MFP experiments, and at a more comparable rate in the FFP experiments. This difference of stimulation success rates in the same location between MFP and FFP experiments is expected with a cavitational mechanism due to the higher negative pressures used in the FFP experiments. This makes cavitation in absence of the introduced bubble nuclei more likely as smaller, less effective nuclei can be affected.

This probabilistic response is seen throughout the experiments, where large events that involved many axons in the bundle occur infrequently. This points to a correspondingly probabilistic cause that occurs on a scale affecting a large proportion of the fibres in the bundle or not at all, consistent with a large cavitating bubble occurring outside of nerve fibres. If the mechanism of stimulation was on a small scale such as the intra-membrane bubble model [Krasovitski et al., 2011], the many isolated events that act at the individual cell level would be expected to produce a reliable response when aggregated to the level of the entire bundle.

The same argument against cellular scale probabilistic effects can be applied to discount other consistent forces as a mechanism, such as the radiation force. In a system where nothing is being changed between US exposures, radiation force as a result of tissue absorption and reflection should remain constant as well as any effects on the nerve it elicits, but this is not what was observed. Second to this, the radiation forces produced in the 0.67 MHz exposures were calculated and reproduced at 1.1 and 2 MHz (Table 4.2) and found to be ineffective at generating responses from the nerve. Indeed these modelled forces are lower than compressional experiments in the literature shown to generate mechanical stimulation of axons [Rivera et al., 2000], though conductance changes from weak compression may contribute to the overall effect [Julian and Goldman, 1962b, Olesen et al., 1988]. Even when the intensity of the 2 MHz stimulus was increased to produce intensities up to 6.7 kW/cm^2 (703 mN/cm^2), responses were only found at this highest intensity and the pattern remained as occasional activations of large numbers of fibres which were associated with inertial acoustic events (Figure 5.14).

Also consistent with a cavitational mechanism given random initial nuclei sizes, in the FFP experiments it was found that any part of the pulse train had an equal chance to stimulate the nerve bundle. In the proposed cavitational mechanism, the random response delay would be caused by the time required to grow bubbles from particular nuclei up to resonant sizes. This is supported by the 3.16 ms mean latency value, well within 1 standard deviation of the expected 4 ms value (Centre of the TSD) assuming instantaneous activation upon a cavitation event. The dynamics of the current observed phenomena also does not match with studies that find only the onset or offset of US stimuli to be effective [Dalecki et al., 1995, Gavrilov et al., 1977, King et al., 2013, Krasovitski et al., 2011, Menz et al., 2013, Plaksin et al., 2014] which would be consistent with radiation force or intra-membrane bubble mechanisms. This high variance in stimulation latency is also seen in the 100 ms exposures (Figure 5.7(b)), where it is again clear that responses are not significantly associated with the start or end of the stimulus. This cavitation hypothesis is also fully supported by the PCD data.

6.2.1.1 PCD Data

In the MFP experiments PCD recordings showed strong evidence for the occurrence of stable but not inertial cavitation through correlation to the harmonics of the driving frequency. Furthermore, higher amplitude sub harmonics (Figure 5.3) rules out non-linear propagation through the media as only higher harmonics are produced by this phenomenon. Broadband acoustic events as measured by the ICD, though detected, were not significantly correlated to successful stimulation in any of the MFP nerve experiments. A similar pattern of acoustic data to this was also found in a limited set of two nerve preparations in the FFP experiments that show greater response reliabilities (>50%). In these, signs of inertial cavitation were much lower and the relative amplitude of half harmonic emissions were much greater than other nerve preparations exposed at the same intensities. The lack of correlation of responses and SCD in these two experiments is thought to be due to the highly consistent signal that does not show much variance even when no response is seen. It is not known what caused the unreliability in these cases, though it could be determined by small changes in the relative position of the bubble and nerve, or more complex differences in oscillatory behaviour where the received harmonic signal amplitude stays the same. Both in these and the MFP experiments therefore, stable oscillation of bubbles in the vicinity of the nerve bundle are thought to be responsible, rather than the inertial cavitation mechanism that is preferred through the rest of the FFP stimulation data. Although these micro-bubbles were probably introduced as an artefact of the extraction process (Figure 4.9), it demonstrates that the introduction of commercial micro-bubble nuclei could greatly increase the efficacy and potentially reduce the threshold of US neurostimulation as recently shown in a *c.elegans* model [Ibsen et al., 2015].

In the FFP experiments, both the 8 ms and 100 ms datasets saw a plateauing of kurtosis and signal energy after 230 W/cm^2 (Figures 5.8 and 5.10). This is likely to be caused both by the non-linear scaling of peak negative pressures with intensity (Table 4.2) and resulting saturation in the occurrence, but not amplitude of cavitation events. Concurrently with this observation, response reliability also saturates around this intensity (Figure 5.6 and 5.10), further supporting the link between stimulation and inertial cavitation in these experiments.

Across all US stimuli in the FFP experiments, inertial cavitation was most often observed with no resultant nerve response. The reason for this is that the focal area (6×3.5 mm FWHM) and potential volume in which cavitation is likely to occur, was much larger than the volume occupied by the nerve bundle (1-2 mm diameter). Cavitation therefore may not be occurring in close proximity to the nerve. Further evidence for this theory is found in the pattern of cavitation activity in the 100 ms exposures where inertial activity is much lower after the first 10 ms of any US stimulus (Figure 5.12). This pattern implies that cavitation nuclei present before the start of the stimulation are either destroyed or moved from focus by acoustic streaming or by direct bubble radiation forces. This reduces the acoustic activity during the remainder of the exposure, but then the nuclei regenerate or return before the beginning of the next pulse. This implicates free floating nuclei rather than those statically associated with the nerve bundle as these would not regenerate or re-attach to the bundle after submersion. The majority of the cavitation nuclei in the FFP experiments are therefore likely to be free floating in the nerve bath ringers solution or water bath underneath, the activation of which will not affect nerve activity.

This affected the 8 ms much more than the longer exposures as the non-proximal cavitation activity is found throughout the exposure, but only in the first 10 ms of longer stimuli. Significant positive ($P<0.05$) correlation was seen in two individual 8 ms exposed nerve experiments despite this. In the 100 ms experiments, the lower average background activity over the whole time period allowed the much smaller dataset to find highly significant correlations between US stimulated CAP amplitude and PCD signal kurtosis in individual nerve experiments ($P<0.05$) and across the whole dataset ($P<0.005$) (Figure 5.11).

Correlation coefficients can mask infrequent stimulation events that may occur without any sign of cavitation. A key finding of the FFP experiments therefore, is that, through detailed individual PCD signal analysis, broad frequency band inertial cavitation events were detected in the expected time section preceding 100% of successful US neurostimulation events in both the 8 and 100 ms datasets. These arguments combined leads the author to conclude that bubble activity is necessary to the stimulation effect and that both inertially and stably cavitating bubbles can each elicit direct induction of action potentials in axonal tissue under different circumstances.

6.2.1.2 Radiation Force Analysis

While the evidence for the involvement of cavitation in the stimulation effect is strong, an alternate stimulatory force mechanism exists in the form of nerve compression resulting from primary ultrasonic radiation force on the bubbles. The calculations in section 4.6.2 give a peak radiation force of 9.8 mN acting on a resonant size bubble (20 μM for 0.67 MHz), well within the size range identified to be present in section 4.3.1. This is much larger than the sum of attenuation and reflective forces (2.2 mN spatial average over the focal area) and is concentrated with a much smaller contact area on the nerve. When F_{abs} is calculated over an aproximate bubble contact area (half the bubble surface area), it is found to be almost 1000 times smaller than F_{bub} (9 nN). Therefore, in the ideal case of bubbles resting on the top surface of the nerve that transfer force efficiently to the bundle, not only is the total force greater, it is also significantly more concentrated, vastly increasing tissue compression and stretch associated with the displacement gradient.

The author believes that this radiation force did not play a stimulating role where inertial events were involved because the magnitude of the forces acting on the nerves would be potentially much greater from a collapsing bubble. However it may still play a critical role in pushing bubbles into close proximity to the nerve, or may contribute to stimulation where no inertial cavitation was seen such as in the MFP experiments.

Considering this as a cellular stimulation mechanism versus other stable and inertial cavitation effects is speculative without significant modelling work to determine the relative force strengths of different mechanisms or known membrane stretch thresholds for poration or ion channel gating. The next step in this research will therefore be to determine the exact role and behaviour of the bubbles responsible for stimulation, which is discussed further in section 6.3.

6.2.2 Damage

In the FFP experiments, damage was found to occur as a result of US exposure in several cases, strongly correlated to inertial cavitation at all intensities. The lowest instance of damage occurred close to the threshold for stimulation (230 W/cm^2), which raises concerns as to the safety of US stimulation at these intensities. However, given the lack of damage in the majority of exposures in both the FFP and MFP experiments and the scope for optimisation and refinement of the stimulation parameters, it is hoped that the risk of damage can be eliminated in future. It is also as yet unclear how a full, *in vivo* situation will affect both the success of the stimulation effect and the occurrence of damage but the latter should be examined in more depth *in vitro* before applying the current technique to animal models.

Though the damage induced by extraction is likely to result in inflammation and consequent mechanical sensitivity [Dilley et al., 2005, Tych et al., 2013], the short timescale of the experiment should prevent cellular alteration of this kind from changing the response to US. however, the damaged ends of torn fibres, previously inervating the crab muscle that surrounded the nerve bundle may have altered the bundle's sensitivity to US. As these open ended fibres represent a small proportion of the total at the stimulation site, increased sensitivity of damage fibres cannot account for the very large, approaching saturated responses that were observed. Both these possibilities are therefore not thought to contribute to the current stimulation effect.

6.2.3 Biological Mechanism

Given the nature of the causative US forces discussed above and the presence of axonal tissue alone, the biological mechanism involved in reaching threshold membrane depolarisation has been narrowed down to two options. The first option involves the opening of ion channels by membrane stretch induced by cavitational or bubble radiation forces. The second is general ionic flux and resultant depolarisation through a microporation effect caused by cavitation mechanisms [Wan et al., 2015].

Large scale perforation resulting from inertial cavitation is likely to have been the cause of after-discharge (Figure 5.18(c)) and other occurrences of damage to nervous function. Smaller scale, reversible micro-poration from jetting effects, such as observed in sonoporation studies[Ohl et al., 2006, Zhou et al., 2008], may therefore be the mechanism behind the inertially induced stimulation effect though more work will be required to satisfactorily differentiate between this and membrane stretch effects.

6.3 Future Work

This research area is still in very early stages, with a lot of fundamental research still needed to fully understand the US neuromodulation phenomenon. This section will identify the research aims and experiments where the author perceives the greatest value to advancing the current understanding of US neurostimulation. This section will begin with plans for continued work using the current crab leg nerve model, followed by arguments for other avenues of research.

6.3.1 Further Work Using the Current Model

The research group intends to continue work on the current crab leg nerve bundle after implementing several improvements to the protocol. Firstly, to address the issue of weak sub harmonic detection, multiple transducers should be used with overlapping frequency ranges to increase the range of sensitive acoustic signal detection. The addition of multiple fixed position transducers would also allow location mapping of cavitation events, making it much easier to determine the proximity of an event to the nerve axon. Also, to decrease the probability of cavitation occurring away from the nerve, the cold water bath should be fully degassed prior to each experiment. Lastly, circulation and bubbling of ringers solution in the central chamber of the nerve bath should be performed to maintain consistent cavitation probabilities and keep the nerve alive for longer.

New techniques will also be employed to fully characterise the neurostimulation effect observed in this study. One of the first additions to the current work should be an analysis of controlled cavitation nuclei to increase the reliability of the effect and decrease its threshold. Blood brain barrier opening using microbubbles and 1.5 MHz US for example can be achieved without any cellular damage at 0.3-0.45 MPa peak rarefactonal pressure [Tung et al., 2010]. This will also reduce the variability of different cavitation events occurring both within and between stimuli, making stimulatory bubble activity much easier to differentiate and control. Furthermore, the targeted delivery of the nuclei would serve to accurately control the location of activity. Degassing of the nerve bath ringers solution could also be performed as a negative control.

High speed imagery employed simultaneously with current electrical and acoustic recording will be used to characterise the range and location of stimulatory bubble activity, linking specific modes of activity such as stable or inertial cavitation to successful stimulus or to different CAP response waveforms. This technique will also be combined with mathematical models of observed bubble activity to identify threshold forces acting on the nerve membrane for stimulation effects. This understanding of cellular level thresholds will truly open up this field and allow theoretical models to be used to design and optimise stimulation and modulation protocols.

Recording potentials directly from single neurons can provide a lot of advantages over population recordings. Some of these are more accurate analysis of changes in response time, AP amplitude and response waveform. The latter of these could be used to asses the variability in the action potential response with different modes of cavitation to gain information on electrical response dynamics at the stimulation site and therefore the mechanism of AP initiation. Most importantly though, it will be essential for analysis of single cell stimulation force thresholds when used in combination with high frequency photography. Either micro-electrodes or whole cell patch clamping could be used for this [Zhou et al., 2008].

The current study was only concerned with the observation of US stimulation of *de novo* action potentials. This approach ignores effects of the US-nerve interaction that are sub threshold or that only become apparent when interacting with existing nerve activity. Attempts to study sub-threshold effects with the current *in vitro* model were prevented by concerns about US interaction with the electrodes if they were placed under the focus (Section 4.1.1). The thinnest grade of silver (8 μm) did not impede the US at 0.67 MHz (Figure 4.3) but was made too brittle by the chloriding process to use.

Improvements in the chloriding process therefore or different choice of electrode material may make examination of sub-threshold electrical effects at the US focus possible. This would also eliminate the effects of CAP conduction on the recorded waveform, allowing much more accurate measurement of response latency and and waveform. This electrode could also be used to stimulate for investigation of combined, same site electrical and US stimulation. Same site stimulation is planned by the author to be used with a threshold tracking technique [Bostock et al., 1998] to analyse the short and long term changes to the electrical stimulation response, picking up effects on the nerve which are potentially much more subtle and far below the US intensity threshold for direct stimulation by US. Alternatively Transcranial Magnetic Stimulation could be used to stimulate in conjunction with US exposure to analyse sub-threshold US effects, though this introduces new problems to do with magnetic coil positioning.

To differentiate between the two current possibilities of the cellular response (sonoporation or stretch effects on ion channels), a highly localised administration of ion channel blockers could be performed under the US focus. Firstly, a general block of all ion channels could be used to test if direct membrane effects such as sonoporation are the cause. If ion channels instead are essential to the nerve's sensitivity to US, specific channel blockers could be employed to determine the relative thresholds and importance of each in the stimulation effect. This block could be performed before adding ringers solution to stop the spread of the blocking toxins, and the blocking solution withdrawn after a time before the addition of ringer's solution. Tight block localisation would be essential to allowing CAP conduction away from the depolarisation site. Alternatively, sensitive same-site electrical recording could be used to detect local potential changes, bypassing the need for CAPs to detect depolarisation.

6.3.2 Cell Constructs

It is the research group's intention to return to test the applicability of the current technique to mammalian peripheral nerves but with a controlled acoustic environment as used with the crab nerve model. An ideal way to test on peripheral, central and potentially any nerve model would be to use neuronal cell constructs such as demonstrated in [Georgiou et al., 2013] as an *in vitro* analogue of nervous tissue which retains applicability to *in vivo* observations and allows a highly controlled acoustic environment.

Such a setup has been recently described by Carugo et al. [Carugo et al., 2015]. The constructs would also improve upon using *ex vivo* tissue by eliminating the variability between experiments due to extraction quality and innate biological variability between individual animals. The ability to grow different cell types within these constructs also grants the potential to examine differential effects between cell types and investigate real sensitivity differences that would advance both the understanding of the biological effect and direct application of the technique.

This cellular model can be used as a basis for studying individual mechanosensitive channels through transfection into cell lines which, as recently demonstrated in nematode worms [Ibsen et al., 2015], can sensitise cells to US stimulation. by analysing the US force threshold of a range channels in an *in vitro* analogue of brain tissue and then tracking the expression of these channels within the brain, different brain areas could be selectively stimulated with tailored ultrasound parameters and focusing patterns.

6.3.3 Peripheral Neurostimulation

With further study and optimisation the technique used in the current study has potential as a method of direct, non-invasive, targeted neurostimulation. Stimulation of peripheral nerve axons in this way could have a wide range of useful clinical applications such as sacral nerve stimulation for incontinence, sensory feedback from prosthetics or localisation of nerve damage as envisaged by Gavrilov et al. [Gavrilov, 1984].

Currently the outlook for clinical applications of the stimulus observed here is complicated by the difficulty of causing caviation in soft tissue [Gateau et al., 2011], low response reliability and potential for inertial caviation and the associated chance of damage in soft tissue. As highly reliable stimulation resulting from stable cavitation has also been identified (Figure 5.17), this mode could be utilised alongside microbubble or other cavitation nuclei to elicit *in vivo* neurostimulation more reliably and with safer, less chaotic force mechanisms. This method would however reduce the non-invasive advantage that US neurostimulation promises, though focused US could also be investigated as a way of growing bubble nuclei before stimulating the grown population [Ter Harr et al., 1986].

Chapter 7

Conclusions

It is hoped that future studies by this group and others will soon elucidate separate mechanisms and thresholds of possible US neuromodulation effects. This will require a shift in the focus of the literature towards achieving a cellular level mechanistic understanding of the various US bioeffects. A cornerstone of this progression will be accurate and universally comparable US metrics, in the form of positive and negative peak instantaneous pressures through either *in situ* measurement or modelling techniques.

Reported here, in a step towards this goal, are successful parameters for ultrasonic neurostimulation in the peripheral crab leg nerve bundle, demonstrating that the constituents of unmyelinated axonal tissue are sufficient to generate *de-novo* action potentials in response to US stimulus. The threshold for this stimulation was much higher than similar procedures performed on CNS models but in good agreement with other PNS focused studies. Low intensity stimulation parameters shown to be successful *in vivo* in the literature were unsuccessful at generating any response from the nerve bundles. Given the difference in threshold intensities and physical environment, the current observed stimulation phenomenon is assumed to have a distinct US force mechanism.

In characterising the observed stimulation phenomena, lower intensity (25-138 W/cm^2) ultrasound was found to be able to stimulate nerves in the presence of large microbubbles on the nerve surface through a stable cavitation or bubble dependant radiation force mechanism. At higher intensities (100-562 W/cm^2), inertial cavitation activity was found to be highly correlated to successful US stimulation and was observed preceding every example of stimulation. These intensities were able to stimulate the same nerve location multiple times but resulted in occasional nerve damage over 230

W/cm^2.

This work represents the first directly observed, ultrasound induced action potentials within peripheral axons and provides the first clear evidence for the involvement of cavitation in an ultrasound stimulation mechanism. With further work into protocol refinement and control of cavitation nuclei, this US stimulation mechanism has potential for beneficial application to both clinical and research applications. Future work by the group will aim to determine the exact cellular level forces required to generate stimulation in this and other models.

Bibliography

Alberts B, Johnson A, Lewis J, Raff M, Roberts K, Walter P. Molecular Biology of the Cell, 2002.

Altland OD, Dalecki D, Suchkova VN, Francis CW. Low-intensity ultrasound increases endothelial cell nitric oxide synthase activity and nitric oxide synthesis. Journal of thrombosis and haemostasis: JTH, 2004;2:637–643.

Andersen AP, Mørch KA. Cavitation nuclei in water exposed to transient pressures. Journal of Fluid Mechanics, 2015;771:424–448.

Andersen SSL, Jackson AD, Heimburg T. Towards a thermodynamic theory of nerve pulse propagation. Progress in Neurobiology, 2009;88:104–113.

Arieli R, Marmur A. Decompression sickness bubbles: are gas micronuclei formed on a flat hydrophobic surface? Respir Physiol Neurobiol, 2011;177:19–23.

Bachtold M, Rinaldi P, Jones J, Reines F, Price L. Focused ultrasound modifications of neural circuit activity in a mammalian brain. Ultrasound in Medicine & Biology, 1998;24:557–565.

Barry PH. Volume flows and pressure changes during an action potential in cells of Chara australis - II. Theoretical considerations. The Journal of membrane biology, 1970;3:335–71.

Belova V, Gorin DA, Shchukin DG, Möhwald H. Selective Ultrasonic Cavitation on Patterned Hydrophobic Surfaces. Angewandte Chemie International Edition, 2010;49:7129–7133.

Bjelkmar P, Niemelä PS, Vattulainen I, Lindahl E. Conformational changes and slow dynamics through microsecond polarized atomistic molecular simulation of an integral Kv1.2 ion channel. PLoS computational biology, 2009;5:e1000289.

Bostock H, Cikurel K, Burke D. Threshold tracking techniques in the study of human peripheral nerve. Muscle & Nerve, 1998;21:137–158.

Broun G, Gavrilov L, Zhadan G, Ilinskii O, Tsirul'nikov E. Effect of focused ultrasound on the electroreceptor system of skates and certain fish and amphibian tissues. Zh. Evol. Biokhim, 1980;16:352–358.

Canney MS, Bailey MR, Crum LA, Khokhlova VA, Sapozhnikov OA. Acoustic characterization of high intensity focused ultrasound fields: a combined measurement and modeling approach. The Journal of the Acoustical Society of America, 2008;124:2406–2420.

Carugo D, Owen J, Crake C, Lee JY, Stride E. Biologically and Acoustically Compatible Chamber for Studying Ultrasound-Mediated Delivery of Therapeutic Compounds. Ultrasound in Medicine & Biology, 2015;41:1927–1937.

Caruso MM, Davis DA, Shen Q, Odom SA, Sottos NR, White SR, Moore JS. Mechanically-induced chemical changes in polymeric materials. Chemical Reviews, 2009;109:5755–5798.

Casarotto RA, Adamowski JC, Fallopa F, Bacanelli F. Coupling agents in therapeutic ultrasound: acoustic and thermal behavior 1,2. Archives of Physical Medicine and Rehabilitation, 2004;85:162–165.

Chandran J, Aravind UK, Aravindakumar CT. Sonochemical transformation of thymidine: A mass spectrometric study. Ultrasonics Sonochemistry, 2015;27:178–186.

Chandrapala J, Zisu B, Palmer M, Kentish S, Ashokkumar M. Effects of ultrasound on the thermal and structural characteristics of proteins in reconstituted whey protein concentrate. Ultrasonics Sonochemistry, 2011;18:951–957.

Chapman I, MacNally N, Tucker S. Ultrasound-induced changes in rates of influx and efflux of potassium ions in rat thymocytes in vitro. Ultrasound in Medicine & Biology, 1980;6:47–49.

Chen B, Grinnell A. Integrins and modulation of transmitter release from motor nerve terminals by stretch. Science, 1995;269:1578–1580.

Chen WS, Brayman AA, Matula TJ, Crum LA. Inertial cavitation dose and hemolysis produced in vitro with or without Optison. Ultrasound in Medicine & Biology, 2003;29:725–737.

Chen WZ, Qiao H, Zhou W, Wu J, Wang ZB. Upgraded nerve growth factor expression induced by low-intensity continuous-wave ultrasound accelerates regeneration of neurotometicly injured sciatic nerve in rats. Ultrasound Med Biol, 2010;36:1109–1117.

Cho H, Shin J, Shin C, Lee SY, Oh U. Mechanosensitive ion channels in cultured sensory neurons of neonatal rats. J. Neurosci., 2002;22:1238–1247.

Choi J, Lim S, Cho K, Kim D, Jang D, Kim I. The effect of focused ultrasonic stimulation on the activity of hippocampal neurons in multi-channel electrode. In: 2013 6th International IEEE/EMBS Conference on Neural Engineering (NER), 2013. pp. 731–734.

Choubey A, Vedadi M, Nomura Ki, Kalia RK, Nakano A, Vashishta P. Poration of lipid bilayers by shock-induced nanobubble collapse. Applied Physics Letters, 2011;98:023701.

Christensen A, Corey D. Trp channels in mechanosensation: direct or indirect activation? Nat Rev Neurosci, 2007;8:510–521.

Chu PC, Liu HL, Lai HY, Lin CY, Tsai HC, Pei YC. Neuromodulation accompanying focused ultrasound-induced blood-brain barrier opening. Scientific Reports, 2015;5:15477.

Church C. Prediction of rectified diffusion during nonlinear bubble pulsations at biomedical frequencies. J. Acoust. Soc. Am., 1988;83:2210–2217.

Cohen L. Time-frequency Analysis. Prentice Hall PTR, 1995.

Colucci V. Focused ultrasound effects on nerve action potential in vitro. Ultrasound in Medicine & Biology, 2009;35(10):pp.1737–1747.

Cowin SC, Doty SB (Eds.). Tissue Mechanics. Springer New York, New York, NY, 2007.

Crick F. Do dendritic spines twitch? Trends in Neurosciences, 1982;5:44–46.

Crisci A, Ferreira A. Low-intensity pulsed ultrasound accelerates the regeneration of the sciatic nerve after neurotomy in rats. Ultrasound Med Biol, 2002;28:1335–1341.

Crum LA. Bjerknes forces on bubbles in a stationary sound field. The Journal of the Acoustical Society of America, 1975;57:1363–1370.

Dai S, Xu C, Tian Y, Cheng W, Li B. In vitro stimulation of calcium overload and apoptosis by sonodynamic therapy combined with hematoporphyrin monomethyl ether in C6 glioma cells. Oncology Letters, 2014;8:1675–1681.

Dalecki D, Child SZ, Raeman CH, Carstensen EL. Tactile perception of ultrasound. The Journal of the Acoustical Society of America, 1995;97:3165–3170.

Deffieux T, Younan Y, Tanter M, Aubry JF, Wattiez N, Pouget P. Transcranial ultrasound neuromodulation of the contralateral visual field in awake monkey. In: Ultrasonics Symposium (IUS), 2013 IEEE International, 2013a. pp. 1–4.

Deffieux T, Younan Y, Wattiez N, Tanter M, Pouget P, Aubry JF. Low-intensity focused ultrasound modulates monkey visuomotor behavior. Current biology: CB, 2013b;23:2430–2433.

Della Rocca G. The science of ultrasound therapy for fracture healing. Indian J Orthop, 2009;43:121–126.

Dickey T, Tych R, Kliot M, Loeser J, Pederson K, Mourad P. Intense focused ultrasound can reliably induce sensations in human test subjects in a manner correlated with the density of their mechanoreceptors. Ultrasound Med Biol, 2011;38:85–90.

Dilley A, Lynn B, Pang SJ. Pressure and stretch mechanosensitivity of peripheral nerve fibres following local inflammation of the nerve trunk. Pain, 2005;117:462–472.

Dinno M, Dyson M, Young S, Mortimer A, Hart J, Crum L. The significance of membrane changes in the safe and effective use of therapeutic and diagnostic ultrasound. Phys Med Biol, 1989;34:1543–1552.

Doherty JR, Trahey GE, Nightingale KR, Palmeri ML. Acoustic Radiation Force Elasticity Imaging in Diagnostic Ultrasound. IEEE transactions on ultrasonics, ferroelectrics, and frequency control, 2013;60:685–701.

Duck FA. Physical properties of tissue: a comprehensive reference book. Acad. Press, London, 1990.

Duck FA. Medical and non-medical protection standards for ultrasound and infrasound. Progress in Biophysics and Molecular Biology, 2007;93:176–191.

Duval E, Adichtchev S, Sirotkin S, Mermet A. Long-lived submicrometric bubbles in very diluted alkali halide water solutions. Physical Chemistry Chemical Physics, 2012;14:4125, arXiv: 1201.4253.

Ebisawa K, Hata KI, Okada K, Kimata K, Ueda M, Torii S, Watanabe H. Ultrasound enhances transforming growth factor beta-mediated chondrocyte differentiation of human mesenchymal stem cells. Tissue Engineering, 2004;10:921–929.

Eisenberg B. Bubble Gating Currents in Ionic Channels. arXiv:0802.0308v1 <http://arxiv.org/abs/0802.0308v1>. in the arXiv of physics <http://arxiv.org>, 2008;arXiv:0802.0308v1 <http://arxiv.org/abs/0802.0308v1>.

El-Bialy T. Therapeutic ultrasound applications in craniofacial growth, healing and tissue engineering. Rejuvenation Research, 2007;10:367–371.

El Hady A, Machta BB. Mechanical surface waves accompany action potential propagation. Nature Communications, 2015;6:6697.

Fan Z, Kumon RE, Park J, Deng CX. Intracellular Delivery and Calcium Transients Generated in Sonoporation Facilitated by Microbubbles. Journal of controlled release : official journal of the Controlled Release Society, 2010;142:31.

Farny CH, Holt RG, Roy RA. Temporal and spatial detection of HIFU-induced inertial and hot-vapor cavitation with a diagnostic ultrasound system. Ultrasound in Medicine & Biology, 2009;35:603–615.

Fatemi M, Ogburn P, Greenleaf J. Fetal stimulation by pulsed diagnostic ultrasound. J Ultrasound Med, 2001;20:883–889.

Foley J, Little J, Vaezy S. Effects of high-intensity focused ultrasound on nerve conduction. Muscle Nerve, 2008;37:241–250.

Foster K, Wiederhold M. Auditory responses in cats produced by pulsed ultrasound. J. Acoust. Soc. Am., 1978;63:1199–1205.

Francis JT, Gluckman BJ, Schiff SJ. Sensitivity of Neurons to Weak Electric Fields. The Journal of Neuroscience, 2003;23:7255–7261.

Frey B, Janko C, Ebel N, Meister S, Schlücker E, Meyer-Pittroff R, Fietkau R, Herrmann M, Gaipl US. Cells under pressure - treatment of eukaryotic cells with high hydrostatic pressure, from physiologic aspects to pressure induced cell death. Current Medicinal Chemistry, 2008;15:2329–2336.

Fry W. Electrical stimulation of brain localized without probes-theoretical analysis of proposed method. Acoust Sot Am, 1968;44:919–931.

Fry W, Wulff V, Tucker D, Fry F. Physical factors involved in ultrasonically induced changes in living systems:i. identification of non-temperature effects. Acoust Sot Am, 1950;22:867–876.

Galkin V, Orlova A, Egelman E. Actin filaments as tension sensors. Current Biology, 2012;22:R96–R101.

Garrison SR, Dietrich A, Stucky CL. TRPC1 contributes to light-touch sensation and mechanical responses in low-threshold cutaneous sensory neurons. Journal of Neurophysiology, 2012;107:913–922.

Gateau J, Aubry JF, Chauvet D, Boch AL, Fink M, Tanter M. In vivo bubble nucleation probability in sheep brain tissue. Physics in Medicine and Biology, 2011;56:7001–7015.

Gavrilov L. Use of focused ultrasound for stimulation of nerve structures. Ultrasonics, 1984;22:132–138.

Gavrilov L, Gersuni G, Ilyinski O, Tsirulnikov E, Shchekanov E. A study of reception with the use of focused ultrasound. i. effects on the skin and deep receptor structures in man. Brain Research, 1977;135:265–277.

Gavrilov L, Tsirulnikov E. Focused ultrasound as a tool to input sensory information to humans. Acoustical Physics, 2012;177:1–21.

Gavrilov L, Tsirulnikov E, Davies I. Application of focused ultrasound for the stimulation of neural structures. Ultrasound Med Biol, 1996;22:179–192,.

Gavrilov L, Tsirulnikov E, Shchekanov E. The use of focused ultrasound for stimulating the organ of hearing. Akust zhurn, 1975;21:706–710.

Georgiou M, Bunting SCJ, Davies HA, Loughlin AJ, Golding JP, Phillips JB. Engineered neural tissue for peripheral nerve repair. Biomaterials, 2013;34:7335–7343.

Graps A. An introduction to wavelets. IEEE Computational Science and Engineering, 1995;2:50–61.

Hameroff S, Trakas M, Duffield C, Annabi E, Bagambhrini Gerace M, Boyle P, Lucas A, Amos Q, Buadu A, Badal J. Transcranial ultrasound (tus) effects on mental states: A pilot study. Brain Stimul., 2012.

Hamill O. Mechanosensitive Ion Channels. Academic Press, 2011.

Hamilton MF, Blackstock DT. Nonlinear Acoustics. Academic Press, 1998.

Haqshenas SR, Saffari N. Multi-resolution analysis of passive cavitation detector signals. Journal of Physics: Conference Series, 2015;581:012004.

Harvey EN. The effect of high frequency sound waves on heart muscle and other irritable tissues. American Journal of Physiology, 1929.

Horridge G, Chapman R. Sheaths of the motor axons of the crab carcinus. Quarterly Journal of Microscopical Science, 1964;3-105:175–181.

Hsieh Cy, Probert Smith P, Mayia F, Ye G. An Adaptive Spectral Estimation Technique to Detect Cavitation in HIFU With High Spatial Resolution. Ultrasound in Medicine & Biology, 2011;37:1134–1150.

Hu J, Stein A, Bühlmann P. Rational design of all-solid-state ion-selective electrodes and reference electrodes. TrAC Trends in Analytical Chemistry, 2016;76:102–114.

Hu Y, Wan JMF, Yu ACH. Cytomechanical Perturbations during Low-Intensity Ultrasound Pulsing. Ultrasound in Medicine & Biology, 2014;40:1587–1598.

Hu Y, Zhong W, Wan J, Yu A. Ultrasound can modulate neuronal development: Impact on neurite growth and cell body morphology. Ultrasound Med Biol, 2011;39:915–925.

Hua S, Gottlieb P, Heo J, Sachs F. A mechanosensitive ion channel regulating cell volume. Am J Physiol Cell Physiol, 2010;298:C1424–C1430.

Hughes S, El Haj A, Dobson J, Martinac B. The influence of static magnetic fields on mechanosensitive ion channel activity in artificial liposomes. European biophysics journal: EBJ, 2005;34:461–468.

Ibsen S, Tong A, Schutt C, Esener S, Chalasani SH. Sonogenetics is a non-invasive approach to activating neurons in Caenorhabditis elegans. Nature Communications, 2015;6.

Iida K, Luo H, Hagisawa K, Akima T, Shah PK, Naqvi T, Siegel R. Noninvasive low-frequency ultrasound energy causes vasodilation in humans. Journal of the American College of Cardiology, 2006;48:532–537.

Janicak P, Nahas Z, Lisanby S, Solvason H, SM S. Durability of clinical benefit with transcranial magnetic stimulation (tms) in the treatment of pharmacoresistant major depression: assessment of relapse during a 6-month, multisite, open-label study. Brain Stimul., 2010.

Janssen AJEM. Bilinear time-frequency distributions. In: Byrnes JS, Byrnes JL, Hargreaves KA, Berry K (Eds.), Wavelets and Their Applications. No. 442 in NATO ASI

Series. Springer Netherlands, 1994. pp. 297–311, dOI: 10.1007/978-94-011-1028-0_13.

Jin F, Li J, Ye X, Wu C. Effects of pH and ionic strength on the stability of nanobubbles in aqueous solutions of alpha-cyclodextrin. The Journal of Physical Chemistry. B, 2007;111:11745–11749.

Johns L. Nonthermal effects of therapeutic ultrasound: The frequency resonance hypothesis. J Athl Train, 2002;37:293–299.

Juan E, González R, Albors G, Ward M, Irazoqui P. Vagus nerve modulation using focused pulsed ultrasound: Potential applications and preliminary observations in a rat. International Journal of Imaging Systems and Technology, 2014;24:67–71.

Julian FJ, Goldman DE. The Effects of Mechanical Stimulation on Some Electrical Properties of Axons. The Journal of General Physiology, 1962a;46:297–313. URL `http://www.ncbi.nlm.nih.gov/pmc/articles/PMC2195257/`

Julian FJ, Goldman DE. The Effects of Mechanical Stimulation on Some Electrical Properties of Axons. The Journal of General Physiology, 1962b;46:297–313.

Jung YJ, Kim R, Ham HJ, Park SI, Lee MY, Kim J, Hwang J, Park MS, Yoo SS, Maeng LS, Chang W, Chung YA. Focused low-intensity pulsed ultrasound enhances bone regeneration in rat calvarial bone defect through enhancement of cell proliferation. Ultrasound in Medicine & Biology, 2015;41:999–1007.

Kamimura H, Wang S, Chen H, Wang Q, Aurup C, Acosta C, Carneiro A, Konofagou E. Pupil dilation and motor response elicitation by ultrasound neuromodulation. In: Ultrasonics Symposium (IUS), 2015 IEEE International, 2015. pp. 1–4.

Kamkin A, Kiseleva I. Mechanosensitivity of the Nervous System, 2009.

Kandel ER, Schwartz JH, Jessell TM. Principles of Neural Science, 4th Edition. McGraw-Hill Medical, 2000.

Kato M, Hayashi R, Tsuda T, Taniguchi K. High pressure-induced changes of biological membrane. Study on the membrane-bound Na(+)/K(+)-ATPase as a model system. European journal of biochemistry / FEBS, 2002;269:110–118.

Kim H, Chiu A, Lee SD, Fischer K, Yoo S. Focused ultrasound-mediated non-invasive brain stimulation: examination of sonication parameters. Brain Stimulation, 2014a;7:748–756.

Kim H, Lee SD, Chiu A, Yoo S, Park S. Estimation of the spatial profile of neuromodulation and the temporal latency in motor responses induced by focused ultrasound brain stimulation. Neuroreport, 2014b;25:475–479.

Kim H, Taghados S, Fischer K, Maeng L, Park S, Yoo S. Noninvasive transcranial stimulation of rat abducens nerve by focused ultrasound. Ultrasound in Medicine & Biology, 2012;38:1568 – 1575.

King R, Brown J, Newsome W, Pauly K. Effective parameters for ultrasound-induced in vivo neurostimulation. Ultrasound in Medicine & Biology, 2013;39:312–331.

King RL, Brown JR, Pauly KB. Localization of Ultrasound-Induced In Vivo Neurostimulation in the Mouse Model. Ultrasound in Medicine & Biology, 2014;40:1512–1522.

Kinsler LE, Frey AR, Coppens AB, Sanders JV. Fundamentals of Acoustics, 3rd Edition. John Wiley & Sons, 1982.

Krasovitski B, Frenkel V, Shoham S, Kimmel E. Intramembrane cavitation as a unifying mechanism for ultrasound-induced bioeffects. PNAS, 2011.

Lansman J, Hallam T, Rink T. Single stretch-activated ion channels in vascular endothelial cells as mechanotransducers? Respir Physiol Neurobiol, 2011;325:811–813.

Lee ES, Lee JY, Kim H, Choi Y, Park J, Han JK, Choi BI. Pulsed high-intensity focused ultrasound enhances apoptosis of pancreatic cancer xenograft with gemcitabine. Ultrasound in Medicine & Biology, 2013;39:1991–2000.

Lee RC, Aarsvold JN, Chen W, Astumian RD, Capelli-Schellpfeffer M, Kelley KM, Pliskin NH. Biophysical mechanisms of cell membrane damage in electrical shock. Seminars in Neurology, 1995;15:367–374.

Lee W, Kim H, Jung Y, Song I, Chung Y, Yoo S. Image-Guided Transcranial Focused Ultrasound Stimulates Human Primary Somatosensory Cortex. Scientific Reports, 2015;5.

Lee W, Kim H, Lee S, Yoo S, Chung Y. Creation of various skin sensations using pulsed focused ultrasound: Evidence for functional neuromodulation. International Journal of Imaging Systems and Technology, 2014;24:167–174.

Lee Y. Numerical solution of the KZK equation for pulsed finite amplitude sound beams in thermoviscous fluids. Mechanical Engineering. Austin, 1986.

Legon W, Rowlands A, Opitz A, Sato T, Tyler W. Pulsed ultrasound differentially stimulates somatosensory circuits in humans as indicated by eeg and fmri. PLoS ONE, 2012;7:e51177.

Legon W, Sato T, Opitz A, Mueller J, Barbour A, Williams A, Tyler W. Transcranial focused ultrasound modulates the activity of primary somatosensory cortex in humans. Nat Neurosci advance online publication., 2014.

Leighton T. The acoustic bubble. Elsevier., 1994.

Lele P. Effects of focused ultrasonic radiation on peripheral nerve, with observations on local heating. Experimental Neurology, 1963;8:47 – 83.

Lin SY, Corey D. Trp channels in mechanosensation. Current Opinion in Neurobiology, 2005;15:350–357.

Louisnard O, Gomez F. Growth by rectified diffusion of strongly acoustically forced gas bubbles in nearly saturated liquids. Phys Rev E Stat Nonlin Soft Matter Phys, 2003;67:036610.

Macdonald A. Ion channels under high pressure. Comparative Biochemistry and Physiology Part A: Molecular & Integrative Physiology, 2002;131:587–593.

Magee T, Davies A. Auditory phenomena during transcranial doppler insonation of the basilar artery. J Ultrasound Med, 1993;12:747–750.

Marsh D. Energetics of hydrophobic matching in lipid-protein interactions. Biophys J, 2008;94:3996–4013.

Maurer K, Bostock H, Koltzenburg M. A rat in vitro model for the measurement of multiple excitability properties of cutaneous axons. Clinical Neurophysiology, 2007;118:2404–2412.

McLaughlan J, Rivens I, Leighton T, Ter Haar G. A study of bubble activity generated in ex vivo tissue by high intensity focused ultrasound. Ultrasound in Medicine & Biology, 2010a;36:1327–1344.

McLaughlan J, University of Southampton, Fluid Dynamics and Acoustics Group. Commentary on the detection of bubble activity generated in ex-vivo tissue by High Intensity Focused Ultrasound (HIFU) with respect to the generation of therapeutic lesions in tissue for the treatment of cancer. University of Southampton, Institute of Sound and Vibration Research, Fluid Dynamic and Acoustics Group, Southampton, 2010b.

Mehic E, Xu J, Caler C, Coulson N, Moritz C, Mourad P. Increased anatomical specificity of neuromodulation via modulated focused ultrasound. Plos One, 2014;9:e86939, WOS:000330631800016.

Menz M, Oralkan , Khuri-Yakub P, Baccus S. Precise neural stimulation in the retina using focused ultrasound. J. Neurosci., 2013;33:4550–4560.

Mihran R, Barnes F, Wachtel H. Temporally-specific modification of myelinated axon excitability in vitro following a single ultrasound pulse. Ultrasound in Medicine & Biology, 1990;16:297–309.

Min et al B. Focused ultrasound modulates the level of cortical neurotransmitters: Potential as a new functional brain mapping technique. International Journal of Imaging Systems and Technology, 2011a;21(2):232–240.

Min et al BK. Focused ultrasound-mediated suppression of chemically-induced acute epileptic eeg activity. Respir Physiol Neurobiol, 2011b;12:23–23.

Mona P. Ultrasound and model membrane interaction. Drexel University, 2007.

Moore ME, Loft JM, Clegern WC, Wisor JP. Manipulating neuronal activity in the mouse brain with ultrasound: A comparison with optogenetic activation of the cerebral cortex. Neuroscience Letters, 2015;604:183–187.

Morris CE, Juranka PF. Lipid stress at play: mechanosensitivity of voltage-gated channels. Current Topics in Membranes, 2007;59:297–338.

Mortimer A, Dyson M. The effect of therapeutic ultrasound on calcium uptake in fibroblasts. Ultrasound Med Biol, 1988;14:499–506.

Mozhaev VV, Heremans K, Frank J, Masson P, Balny C. High pressure effects on protein structure and function. Proteins: Structure, Function, and Bioinformatics, 1996;24:81–91.

Muratore R, LaManna J, Szulman E, Kalisz M, Lamprecht M. abd Simon M, Yu M, Xu N, Morrison B, Ebbini E. Bioeffective ultrasound at very low doses: Reversible manipulation of neuronal cell morphology and function in vitro. Respir Physiol Neurobiol, 2009:25–29.

Neppiras EA. Acoustic cavitation. Physics Reports, 1980;61:159–251.

Nightingale K, Palmeri M, Nightingale R, Trahey G. On the feasibility of remote palpation using acoustic radiation force. J. Acoust. Soc. Am., 2001;110:625–634.

Norton S. Can ultrasound be used to stimulate nerve tissue? BioMedical Engineering OnLine, 2003;2:6.

Nowicki A, Secomski W, Wójcik J. Linear model with streaming velocities measured by 32-mhz doepler, 1996.

of Ultrasound in Medicine Clinical Standards Committee AI. Aium practice guidelines. J Ultrasound Med, 2015.

Ohl CD, Arora M, Ikink R, de Jong N, Versluis M, Delius M, Lohse D. Sonoporation from Jetting Cavitation Bubbles. Biophysical Journal, 2006;91:4285–4295.

Ohshima H. DLVO Theory of Colloid Stability. John Wiley & Sons, Inc., 2010. pp. 420–430.

Olesen S, Clapham D, Davies P. Haemodynamic shear stress activates a k+ current in vascular endothelial cells. Nature, 1988;331:168–170.

Or M, Kimmel E. Modeling linear vibration of cell nucleus in low intensity ultrasound field. Ultrasound Med Biol, 2009;35:1015–1025.

O'Sullivan J, Murray B, Flynn C, Norton I. The effect of ultrasound treatment on the structural, physical and emulsifying properties of animal and vegetable proteins. Food Hydrocolloids, 2016;53:141–154.

Otter T, Salmon E. Pressure-induced changes in ca2+-channel excitability in paramecium. J. Exp. Biol., 1985;117:29–43.

P. A. Nanobubbles and the hydrophobic attraction. Advances in Colloid and Interface Science, 2003;104:75–91.

Page F. A comparative study of five fresh-water and marine species of thecamoebidae. Transactions of the American Microscopical Society, 1971;90:157–173.

Papadopoulou V, Eckersley RJ, Balestra C, Karapantsios TD, Tang MX. A critical review of physiological bubble formation in hyperbaric decompression. Advances in Colloid and Interface Science, 2013;191–192:22–30.

Papandreou-Suppappola A. Applications in Time-Frequency Signal Processing. CRC Press, 2002.

Parker J, Claesson P, Attard P. Bubbles, cavities, and the long-ranged attraction between hydrophobic surfaces. J. Phys. Chem, 1994;98:8468–8480.

Patel US, Ghorayeb SR, Yamashita Y, Atanda F, Walmsley AD, Scheven BA. Ultrasound field characterization and bioeffects in multiwell culture plates. Journal of Therapeutic Ultrasound, 2015;3:8.

Petrov A, Miller B, Hristova K, Usherwood P. Flexoelectric effects in model and native membranes containing ion channels. Eur. Biophys., 1993;22:289–300.

Plaksin M, Shoham S, Kimmel E. Intramembrane cavitation as a predictive bio-piezoelectric mechanism for ultrasonic brain stimulation. Phys. Rev. X, 2014;4:011004.

Pohl P, Rosenfeld E, Millner R. Effects of ultrasound on the steady-state transmembrane pH gradient and the permeability of acetic acid through bilayer lipid membranes. Biochimica Et Biophysica Acta, 1993;1145:279–283.

Preston RC, Bacon DR, Smith RA. Calibration of medical ultrasonic equipment-procedures and accuracy assessment. IEEE transactions on ultrasonics, ferroelectrics, and frequency control, 1988;35:110–121.

Prieto ML, Oralkan m, Khuri-Yakub BT, Maduke MC. Dynamic Response of Model Lipid Membranes to Ultrasonic Radiation Force. PLoS ONE, 2013;8:e77115.

Rappaport S, Berezhkovskii A, Zimmerberg J, Bezrukov S. Thermodynamics of interleaflet cavitation in lipid bilayer membranes. Phys. Rev., 2013;E:87.

Rivera L, Gallar J, Pozo M, Belmonte C. Responses of nerve fibres of the rat saphenous nerve neuroma to mechanical and chemical stimulation: an in vitro study. J. Physiol., 2000;527 Pt 2:305–313.

Rohr KR, Rooney JA. Effect of ultrasound on a bilayer lipid membrane. Biophysical Journal, 1978;23:33–40.

Roth R, Gillespie D, Nonner W, Eisenberg R. Bubbles, Gating, and Anesthetics in Ion Channels. Biophysical Journal, 2008;94:4282–4298.

Roy P. Output Measurenients for Medical Ultrasound. Springer-Verlag, 1991.

Roy RA, Madanshetty SI, Apfel RE. An acoustic backscattering technique for the detection of transient cavitation produced by microsecond pulses of ultrasound. The Journal of the Acoustical Society of America, 1990;87:2451–2458.

Rudenko O, Sarvazyan A, Emelianov S. Acoustic radiation force and streaming induced by focused nonlinear ultrasound in a dissipative medium. The Journal of the Acoustical Society of America, 1996;99:2791–2798.

Scheven BAA, Shelton RM, Cooper PR, Walmsley AD, Smith AJ. Therapeutic ultrasound for dental tissue repair. Medical Hypotheses, 2009;73:591–593.

Schmidt D, del Mármol J, MacKinnon R. Mechanistic basis for low threshold mechanosensitivity in voltage-dependent K+ channels. Proceedings of the National Academy of Sciences of the United States of America, 2012;109:10352–10357.

Selvín-Testa A, Urbina-Vidal C. Axon-glia relationships in crab nerves. Journal of Neurocytology, 1975;4:23–31.

Semmlow JL. Biosignal and Medical Image Processing, Second Edition. CRC Press, 2011.

Sheltawy A, Dawson R. The polyphosphoinositides and other lipids of peripheral nerves. Biochem. J, 1966;100:12–18.

Sherwood J, Derakhshani R. On classifiability of wavelet features for EEG-based brain-computer interfaces. In: International Joint Conference on Neural Networks, 2009. IJCNN 2009, 2009. pp. 2895–2902.

Shung KK, Smith M, Tsui BMW. Principles of Medical Imaging. Academic Press, 2012.

Siechen S, Yang S, Chiba A, Saif T. Mechanical tension contributes to clustering of neurotransmitter vesicles at presynaptic terminals. Proceedings of the National Academy of Sciences, 2009;106:12611–12616.

Soneson JE. A User-Friendly Software Package for HIFU Simulation, 2009;1113.

Soza G, Grosso R, Nimsky C, Hastreiter P, Fahlbusch R, Greiner G. Determination of the elasticity parameters of brain tissue with combined simulation and registration. Int J Med Robot, 2005;1:87–95.

Star E, Kwiatkowski D, Murthy V. Rapid turnover of actin in dendritic spines and its regulation by activity. Nat Neurosci, 2002;5:500–500.

Sukharev S, Anishkin A. Mechanosensitive channels: what can we learn from “simple” model systems? Trends in Neurosciences, 2004;27:345–351.

Tasaki I. Collision of two nerve impulses in the nerve fibre. Biochimica et Biophysica Acta, 1949;3:494–497.

Tasaki I, Byrne PM. The origin of rapid changes in birefringence, light scattering and dye absorbance associated with excitation of nerve fibers. The Japanese Journal of Physiology, 1993;43 Suppl 1:S67–75.

Tasaki I, Kusano K, Byrne P. Rapid mechanical and thermal changes in the garfish olfactory nerve associated with a propagated impulse. Biophysical Journal, 1989;55:1033–1040.

ter Haar G, Daniels S, Eastaugh KC, Hill CR. Ultrasonically induced cavitation in vivo. The British Journal of Cancer. Supplement, 1982;5:151–155.

Ter Harr G, Daniels S, Morton K. Evidence for Acoustic Cavitation In Vivo: Thresholds for Bubble Formation with 0.75-MHz Continuous Wave and Pulsed Beams. IEEE Transactions on Ultrasonics, Ferroelectrics, and Frequency Control, 1986;33:162–164.

Tortoli P, Michelassi V, Guidi F, Corsi M, Hori M, Ishihara K, Moriyasu F, Takeuchi Y. Dynamic Effects of Acoustic Radiation Force on Microbubbles. In: Halliwell M, Wells PNT (Eds.), Acoustical Imaging. No. 25. Springer US, 2002. pp. 449–456, dOI: 10.1007/0-306-47107-8_63.

Trulsson M, Essick GK. Low-Threshold Mechanoreceptive Afferents in the Human Lingual Nerve. Journal of Neurophysiology, 1997;77:737–748.

Tsirulnikov EM, Vartanyan IA, Gersuni GV, Rosenblyum AS, Pudov VI, Gavrilov LR. Use of amplitude-modulated focused ultrasound for diagnosis of hearing disorders. Ultrasound in Medicine & Biology, 1988;14:277–285.

Tsui P, Wang S, Huang C. In vitro effects of ultrasound with different energies on the conduction properties of neural tissue. Ultrasonics, 2005;43:560 – 565.

Tu J, Hwang JH, Matula TJ, Brayman AA, Crum LA. Intravascular inertial cavitation activity detection and quantification in vivo with Optison. Ultrasound in Medicine & Biology, 2006;32:1601–1609.

Tufail et al Y. Transcranial pulsed ultrasound stimulates intact brain circuits. Neuron, 2010;66:681–694.

Tufail et al Y. Ultrasonic neuromodulation by brain stimulation with transcranial ultrasound. Nat. Protocols, 2011;6(9):1453–1470.

Tung YS, Vlachos F, Choi JJ, Deffieux T, Selert K, Konofagou EE. In vivo transcranial cavitation threshold detection during ultrasound-induced blood-brain barrier opening in mice. Physics in Medicine and Biology, 2010;55:6141–6155.

Tych R, Gofeld M, Jarvik J, Kliot M, Loeser J, McClintic A, Ollos R, Pederson K, Sparks R, Terman G, Mourad P. Neuropathic tissue responds preferentially to stimulation by intense focused ultrasound. Ultrasound Med Biol, 2013;39:111–116.

Tyler W. Noninvasive neuromodulation with ultrasound? a continuum mechanics hypothesis. The Neuroscientist., 2010.

Tyler W. The mechanobiology of brain function. Nat Rev Neurosci, 2012;13:867–878.

Tyler et al W. Remote excitation of neuronal circuits using low-intensity, low-frequency ultrasound. PloS One, 2008;3(10):3511.

Ursell T, Phillips R, Kondev J, Reeves D, Wiggins P. The role of lipid bilayer mechanics in mechanosensation. Respir Physiol Neurobiol, 2007.

Vartanyan IA, Gavrilov LR, Svetlogorskaya ID, Tsirul'nikov EM, Khachunts AS, Ajrapetyan NA. Influence of the stimulus duration of focused ultrasound on the skin perceptibility. Sensornie Sistemi, 1990;4:52–59.

Vaseghi SV. Advanced Digital Signal Processing and Noise Reduction. John Wiley & Sons, 2008.

Velling V, Shklyaruk S. Modulation of the functional state of the brain with the aid of focused ultrasonic action. Neurosci. Behav. Physiol, 1988;18:369–375.

Walczyk W, Schönherr H. Characterization of the interaction between AFM tips and surface nanobubbles. Langmuir: the ACS journal of surfaces and colloids, 2014;30:7112–7126.

Wall P, Tucker D, Fry F, Mosberg J. The use of high intensity ultrasound in experimental neurology. The Journal of the Acoustical Society of America, 1953;25:281–285.

Wan M, Feng Y, Haar G (Eds.). Cavitation in Biomedicine. Springer Netherlands, Dordrecht, 2015.

Weijs JH, Snoeijer JH, Lohse D. Formation of Surface Nanobubbles and the Universality of Their Contact Angles: A Molecular Dynamics Approach. Physical Review Letters, 2012;108:104501.

Wijngaarden L. Mechanics and Physics of Bubbles in Liquids: Proceedings IUTAM Symposium, held in Pasadena, California, 15–19 June 1981. Springer Science & Business Media, 2012.

Winter R, Jeworrek C. Effect of pressure on membranes. Soft Matter, 2009;5:3157–3173.

Wright A, Davies II. The recording of brain evoked potentials resulting from intra-articular focused ultrasonic stimulation: A new experimental model for investigating joint pain in humans. Neuroscience Letters, 1989;97:145–150.

Wright A, Graven-Nielsen T, Davies II, Arendt-Nielsen L. Temporal summation of pain from skin, muscle and joint following nociceptive ultrasonic stimulation in humans. Experimental Brain Research, 2002;144:475–482.

Wright CJ, Rothwell J, Saffari N. Ultrasonic stimulation of peripheral nervous tissue: an investigation into mechanisms. Journal of Physics: Conference Series, 2015;581:012003.

Yang P, Kim H, Lee W, Bohlke M, Park S, Maher T, Yoo SS. Transcranial focused ultrasound to the thalamus is associated with reduced extracellular gaba levels in rats. Neuropsychobiology, 2012;65:153–160.

Yefimov S, van der Giessen E, Onck P, Marrink S. Mechanosensitive membrane channels in action. Biophys. J, 2008;94:2994–3002.

Yoo SS, Kim H, Filandrianos E, Taghados S, Park S. Non-invasive brain-to-brain interface (bbi): Establishing functional links between two brains. PLoS ONE, 2013;8:e60410.

Yoo et al S. Non-invasive suppression of animal-model chronic epilepsy using image-guided focused ultrasound. Proceeding of SMRMESMRMB Joint Annual Meeting in Stockholm, Sweden, 2010;Abrsract 2197.

Yoo et al S. Focused ultrasound modulates region-specific brain activity. NeuroImage, 2011a;56(3):1267–1275.

Yoo et al S. Transcranial focused ultrasound to the thalamus alters anesthesia time in rats. Neuroreport, 2011b;22(15):783–787.

Younan Y, Deffieux T, Larrat B, Fink M, Tanter M, Aubry JF. Influence of the pressure field distribution in transcranial ultrasonic neurostimulation. Medical Physics, 2013;40:082902.

Young FR. Cavitation. Imperial College Press, 1999.

Young R, Henneman E. Functional effects of focused ultrasound on mammalian nerves. Science, 1961;134:1521–1522.

Yount D. Bubble nucleation in aqueous media: implications for diving physiology. Applied Scientific Research, 1982;38:37–44.

Yount DE, Gillary EW, Hoffman DC. A microscopic investigation of bubble formation nuclei. The Journal of the Acoustical Society of America, 1984;76:1511–1521.

Yount n. On the Elastic Properties of the Interfaces That Stabilize Gas Cavitation Nuclei. Journal of Colloid and Interface Science, 1997;193:50–59.

Yujin Zong BL. Detection of Individual Microbubbles Using Wavelet Transform Based on a Theoretical Bubble Oscillation Model., 2006:354–363.

Zhao B, Song Y, Wang S, Dai B, Zhang L, Dong Y, Lü J, Hu J. Mechanical mapping of nanobubbles by PeakForce atomic force microscopy. Soft Matter, 2013;9:8837–8843.

Zhou Y, Cui J, Deng CX. Dynamics of Sonoporation Correlated with Acoustic Cavitation Activities. Biophysical Journal, 2008;94:L51–L53.

Zhou Y, Yan D. Real-time membrane fusion of giant polymer vesicles. J. Am. Chem. Soc., 2005;127:10468–10469.